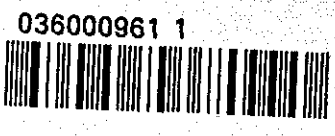

Block Copolymers of Poly(ethylene oxide) and Poly(methyl methacrylate)

by

Keith Redford

A Doctoral Thesis

Submitted in partial fulfilment of the requirements for the award of Doctor of Philosophy of the Loughborough University of Technolology.

July 1991

ACKNOWLEDGEMENTS

I would like to acknowledge the contributions of and thank: Professor John Dawkins for his excellent guidance and supervision of this project; Dr David Brown for his assistance in the SAXS work; Dr Andrew Doroszkowski at ICI paints, Slough both for his hospitality and assistance; and SERC for their financial support under studentship B/83 502 048.

Finally I must thank Glynis, my wife, and Lisa and Paul, my children, for their patience and understanding during the many weekends and evenings consumed in the production of this thesis.

SUMMARY

A series of five AB block copolymers of poly(ethylene oxide) (PEO) and poly(methyl methacrylate) (PMMA) has been synthesised by the coupling of mono-functional homopolymers by an esterification reaction. In this series polymers all contain a PMMA component of number average molecular weight 908 $gmol^{-1}$, as measured by end group analysis, and the PEO components have number average molecular weights of 596, 689, 979, 2023 and 2884 $gmol^{-1}$, as measured by proton nuclear magnetic resonance spectroscopy.

Aqueous "solutions" of these copolymers have been prepared both by direct mixing and via methanol, a solvent for both blocks of the copolymer. Cloud points for these copolymers have been determined and range from 275K to 368K for the lowest and highest PEO blocks respectively. Small angle X-ray scattering (SAXS) of aqueous solutions has been interpreted in terms of a core - shell model and dimensions determined for both. Radii of gyration for the micellar cores have been shown to vary very little with variations in copolymer composition, concentration and temperature up to the cloud point. Fringe thicknesses show a dependence on PEO block length and relating measured fringe thicknesses to calculated chain conformations indicates that the the chain conformation is best described as an unperturbed chain. The measured fringe thickness is not altered by concentration or temperature up to the cloud point. Above the cloud point it is not possible to interpret the SAXS data in terms of a core shell micellar model. Significant differences in the SAXS data have been observed depending upon the mode of addition of copolymer to water. This can be interpreted as differences in micellar

structure

With the exception of the lowest molecular weight copolymer all of the copolymers could be used as steric stabilisers for the aqueous emulsion polymerisation of methyl methacrylate. Polymerisations were only successful if the copolymer was introduced to the aqueous phase either via methanol or via the monomer. Direct addition of copolymer to water resulted in low polymerisation rates and unstable/flocculated products. Emulsions produced have been shown to be stable at pH levels where the electrophoretic mobility was zero, ie. the emulsions were sterically stabilised with no contribution from ionic / dipole interactions.

CONTENTS

4.RESULTS

1. INTRODUCTION

1.1 OBJECTIVES AND SCOPE OF THIS THESIS

This study was initiated as a result of communications between ICI Paints Division, Slough, and Loughborough University. Interest had been shown in the application of graft copolymers of poly(ethylene oxide) (PEO) and poly(methyl methacrylate) (PMMA) for the steric stabilisation of free radical emulsion polymerisation in water. Early investigations into these systems had not shown too promising results. It was proposed that a study of well defined AB block copolymers of PEO and PMMA may yield a valuable insight into the mechanisms of stabilisation for these copolymers.

The work covered in this thesis covers the synthesis of a range of AB block copolymers and detailed characterisation of their compositions and molecular weights. The solution behaviour of these copolymers is investigated with particular emphasis on the determination of micellar dimensions. Finally the potential for these copolymers to stabilise the emulsion polymerisation of methyl methacrylate monomer is investigated.

1.2 BACKGROUND

1.2.1 Stabilisation in non-aqueous media.

When preparing a polymer dispersion in non polar organic media it is not possible to utilise electrostatic effects in the same way as ionic surfactants are used in water. This is a consequence of the dielectric constant of the the dispersing media. An alternative mechanism for stabilisation must be

employed.

A dispersion of polymer particles in an organic medium can be stabilised by the presence of suitable block or graft copolymers. The medium must serve as a selective solvent for one component of the copolymer. The non-solvated component of the copolymer associates with the surface of the polymer particle and the solvated component forms a thin protective layer extending out into the medium. This form of stabilisation is known as steric stabilisation[1].

The steric stabilisation of colloidal particles in organic media has been well documented in the literature with reviews by among others Vincent[1], Osmond and Waite[2], and Napper[3]. Also extensive studies, using block copolymers of polystyrene with poly(dimethyl siloxane) and poly (ethylene-co-propylene), have been undertaken in this group at Loughborough University under the supervision of Dawkins, (Ph.D theses by Taylor[4] and Shakir[5] plus post doctoral work by Maghami[6]).

1.2.2 Stabilisation in aqueous media.

As was mentioned above ionic stabilisation may be utilised to stabilise a polymer dispersion in water. The hydrophobic part of the surfactant molecule associates with the polymer and the ionic (hydrophilic) component is exposed to water. This gives an ionic sheath around the polymer. Studies of the change in potential energy as two such particles approach show that there are two minima in the curve. If the particles come close enough together to enter the first minimum the particles tend to remain connected. Energy is required to separate them again. In this state the particles are said to be loosely flocculated. If the particles come closer together they enter the primary minimum and are irreversibly flocculated. This means that an ionically stabilised dispersion is in a

metastable state and the more energetically favoured state is the flocculated state.

Equivalent studies of steric stabilisation show that there are no minima in the potential energy curve. Thus, as two sterically stabilised particles approach each other the repulsive force between them just increases.

Comparing these two simplified descriptions of the two stabilisation mechanisms, it is clear that the steric system should produce a more robust dispersion. Stability of the dispersion should be independent of pH and ion concentration in the aqueous phase.

1.2.3 The Hydrophobic hydrophilic balance

If a copolymer is to be used as a steric stabiliser in an emulsion polymerisation, the potential to stabilise the final particle is not the only requirement. The copolymer must fulfill all of the stability requirements during nucleation and growth of the polymer particle. Using the pictorial model of Harkins[7,8,9,10], the surfactant, during the initial stages of a polymerisation, should be present in the form of micelles. This requires that the hydrophilic /hydrophobic balance of the molecule favours aggregation of the hydrophobic components of the surfactant molecules. The second requirement is that, during the growth of a polymer particle, the surfactant in micelles that do not contain polymer can pass through the aqueous phase to the growing particle. This surfactant confers stability on the expanding surface. For the transfer of surfactant to occur the hydrophilic/hydrophobic balance must be such that individual surfactant molecules can be found as discrete molecules and that the formation of micelles is reversible. Kinetic considerations must also be considered: this transfer of surfactant must proceed at a rate great enough to maintain the stability of the particle at all times during the polymerisation.

The above observations indicate that for an AB block copolymer there will be a "window" in a plot of A block length vs B block length where the molecule described will function as a stabiliser. The limits of this window will be defined by the solubility and micelle forming characteristics of the polymer. Establishment of the existence of this "window" for the PMMA-b-PEO system will form the ultimate target of this thesis.

2. THEORY

2.1 COPOLYMER SYNTHESIS

There are a number of methods available to the synthetic chemist to produce AB and ABA block copolymers. Authors have employed anionic and cationic polymerisation[11-16], free radical polymerisation and condensation reactions to produce copolymers.

2.1.1 Anionic polymerisation.

AB and ABA block copolymers may be produced by anionic polymerisation methods. Under conditions of extreme purity the first monomer is polymerised. If, under the polymerisation conditions, the selected monomer shows no termination reactions and no chain transfer reactions the polymerisation will proceed until all of the monomer has been used[17,18]. Each polymer chain will be terminated in an anion (with a metal counter ion). As such, all of the polymer chains remain active even after the monomer supply is exhausted. After the completion of the first stage a second monomer is added. This monomer polymerises on the ends of the existing polymer chains. The criteria for selecting a monomer that does not exhibit termination steps or chain transfer reactions is equally important for this second monomer. Care must be exercised in selecting the order in which the two monomers are used because crossover reactions can be selective[19]. The anions or anion pairs of electronegative monomers will not add less electronegative monomers. As an illustration, when making a block copolymer of styrene and methyl methacrylate it is necessary to polymerise the styrene first.

Di- or mono-functional chains may be produced depending on the

initiator, ie. an initiator, such as n-butyl lithium produces a mono-functional polymer chain and would produce an AB copolymer in a two stage reaction. Use of sodium naphthalide which creates radical anions which subsequently dimerise to produce dianions, will produce a BAB copolymer in just two stages. In this case the `A' monomer must be the least electronegative of the two monomers otherwise the crossover reaction will not occur. Tri-block copolymers with the more electronegative monomer in the centre can be produced by producing a di-block copolymer with the more electronegative monomer being polymerised second followed by a coupling with dichlorodimethylsilane[19].

In the case where the initiation step is much faster than the propagation step anionic polymerisation produces polymer material with very low polydispersities, ie. polydispersities approaching 1.0. This makes it an ideal technique for producing well defined materials for study.

Suzuki, Murakami, Tsuji, and Takegami[16] have used the di-sodium salt of poly(ethylene oxide) (PEO) to polymerise methyl methacrylate (MMA) and hence produce an ABA (PMMA-b-PEO-b-PMMA) copolymer. The nucleophilicity of the sodium salt of PEO is not very high but, in the presence of the crown ether dicyclohexyl-18-crown-6, they have shown that polymerisation occurs. With this method it is simple to define the block size of the PEO block but as a consequence of the difficulty in attaining the purity requirements the block length of the PMMA is difficult to control. In the published work they report a degree of trans-esterification yielding graft copolymer and contamination by homopolymer.

Anionic polymerisation can also be used to produce α functional and α,ω functional homopolymers for use in subsequent condensation reactions.

2.1.2 Free radical polymerisation

2.1.2a Terminally functional homopolymers

Free radical polymerisation may be utilised to produce terminally functional polymers and oligomers for subsequent use in condensation reactions.

Mono-functional

The use of functional initiators such as 4,4′-azobis-(4-cyano-pentanoic acid) yield terminally, mono-functionalised polymers. When a functional chain transfer reagent is used in conjunction with the initiator a method for molecular weight control is also introduced. In 1963 ICI published a patent[20] for the polymerisation of 2-ethylhexyl acrylate with 4,4′-azobis-(4-cyano-pentanoic acid) and thioglycollic acid. They demonstrated that by alteration of the initial composition of the reaction the molecular weight could be controlled.

Bifunctional

A free radical polymerisation of a vinyl monomer M initiated by an initiator R-R is expressed by equation 2.1 if no chain transfer occurs and all termination occurs by combination.

$$R{-}R + nM \longrightarrow R{-}M_{n/2}\cdot + R{-}M_{n/2}\cdot \longrightarrow R{-}M_n{-}R \qquad (2.1)$$

For most examples this ideal situation is not realised. In most cases chain transfer reactions and competitive termination reactions result in the average number of initiator fragments per polymer molecule being less

than two.

If the initiator used has very high transfer to initiator, or a part of the initiator easily undergoes primary radical termination, a polymer with two initiator fragments can be produced. The equation representing this yields the same result as equation 2.1 above.

With careful selection of initiator it is possible to synthesise monofunctional or α,ω-bifunctional oligomers or polymers by a free radical mechanism. Otsu and Yoshida[21] in 1982 introduced the term iniferter for this type of initiator system. The term was derived from initiator/transfer agent (inifer) and initiator terminator (initer). Since, in practice, it is impossible to distinguish these two processes they combined the two terms to give the iniferter term. The term inifer was taken from the terminology for cationic polymerisation proposed by Kennedy[22] in 1979. With an iniferter the two end groups of the polymer chain are clearly defined. The chain is initiated by one unit derived either from an initiator fragment or from a chain transfer agent (in the iniferter case these two are indistinguishable). The other end is derived from the other half of the initiator fragment or chain transfer agent. The chain transfer constant of these iniferters is of the order 0.5 to 0.7. This is so high that if you use them in conjunction with a conventional free radical initiator it is difficult to identify any of the original initiator fragments in the polymer[23].

2.1.2b Living free radical polymerisation

The concept of living free radical polymerisation has been developed from the iniferter concept. If a system is selected such that the termination step is reversible the possibility of a living system is obtained. The polymer or oligomer retains the potential re-initiation even after termination.

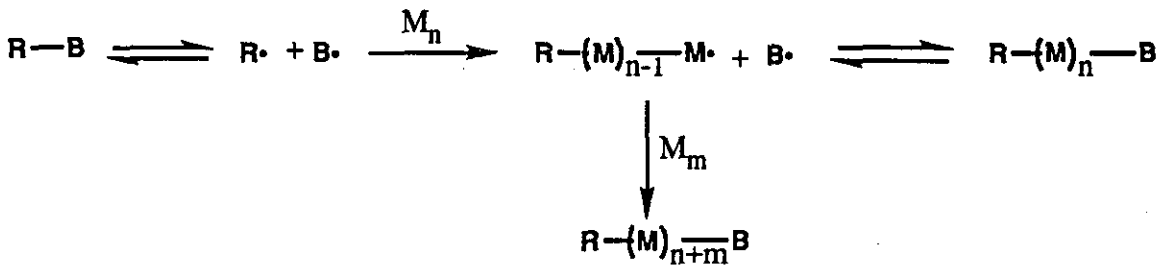

(2.2)

One system of this type that is reported in the literature is the UV polymerisation of methyl methacrylate (MMA) and styrene monomers with the initiator N,N-diethyldithiocarbamate[24].

The limiting case for this process is where the addition of monomers occurs by stepwise addition, ie. one monomer unit at a time. In this situation the resultant polymer would begin to emulate the kinetics of living ionic polymerisations.

The kinetics of these systems resemble those of an addition polymerisation. Molecular weight is seen to increase with time[25,26]. If the polymerisation is halted by cooling and the polymer removed and purified it is possible to add a second monomer and continue the polymerisation. Redford and Clark[26] have produced copolymers of styrene and methyl methacrylate by this method with block molecular weights between 10,000 and 200,000 and polydispersities of around 2.5. This work is currently unpublished and forms part of ongoing research.

These methods do not require the same degree of purity as the anionic polymerisation methods. As a consequence they may prove to be of commercial significance over the next few years. For more academic work the products, being significantly contaminated with homopolymer, are less interesting. There is also a question as to the stability of these polymers; as yet, no literature has appeared concerning this topic.

2.1.2c Mechanical-chemical initiation.

When a homopolymer is subjected to high shear conditions chain cleavage may occur. If a second monomer is present polymerisation is initiated at these cleavage points. Control of block length and homopolymer contamination are both very difficult. Grafting and crosslinking are both said to occur as side reactions.

One commercial copolymer produced by this method was a copolymer of poly(vinyl chloride) (PVC) with n-butyl acrylate[27]. The n-butyl acrylate plasticises the PVC giving a visco-elastic material at room temperature. The polymerisation was performed by cold mastication at 15°C.

More recently the application of ultrasonic radiation has been utilised to generate the chain cleavage. It is difficult to distinguish whether the mechanism of cleavage is a thermal phenomena or as a result of local, microscopic regions of high shear. The result is the same. As an example Fujiwara and Goto[28] have recently employed the technique to produce block copolymers of PVC with methyl methacrylate.

2.1.2d Macro initiators.

Carboxyl terminated polymers can be converted to peroxy esters. If the triphenyl derivative is produced, the compound decomposes to yield two free radicals; the polymeric radical which can propagate further and a triphenyl radical which is too stable to initiate polymerisation.

Polymers terminated by primary alcohol groups may be used as macro initiators[29,30,31]. A complex is formed between the Ce^{4+} and the alcohol which decomposes to yield Ce^{3+} and a free radical as in equation 2.3.

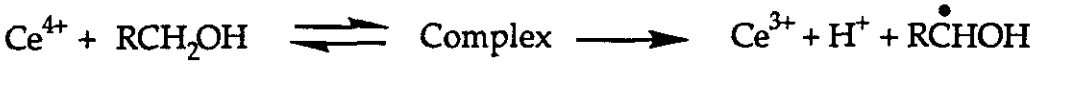

(2.3)

Mino and Kaizerman[32] showed that thiols, aldehydes and amines also act as reducing agents in these conditions.

2.1.3 Condensation reactions.

If two pre-polymers are synthesised with suitable terminal groups AB di- and ABA tri-block copolymers may be produced by coupling reactions. AB di-block copolymers require both pre-polymers to be just α functional and an ABA tri-block copolymer requires that the B block be α, ω functional and the A block just α functional. The coupling reaction can be any condensation reaction eg. Acid + Alcohol, Amine + Epoxy, Isocyanate + Alcohol .....

The advantage of this approach, for a project of this type, is the possibility of fractionation and characterisation of the two component blocks in isolation before the coupling reaction is performed. The pre-polymers may be produced by any suitable method. It is difficult to avoid contamination of the block copolymer with homopolymer. Purification steps must be performed on the final polymer.

2.2 COLLOID STABILITY

For a dispersion of polymer particles in a liquid media to remain as discrete particles and not clump together (flocculate), the forces attracting the particles to each other must be outweighed by repulsive forces. In aqueous media a common method of conferring stability has been to adsorb ionic surfactants, eg. anionic or cationic surfactants, on the particle surfaces. In organic media, media of low polarity, this mechanism is not viable. One solution to the problem has been to use "dissolved" polymer chains attached to the surface of the particles as a barrier against flocculation. It is this principle that will be discussed here in the context of conferring stability to a non-charged colloid in aqueous conditions.

2.2.1 The forces of attraction

The forces of attraction between two adjacent particles are usually referred to as Van der Waals forces. The first model applied to describe these forces was attributed to Keesom[33]. It concerned the interaction between permanent dipoles in separate molecules. A statistical analysis showed that a collection of random, mobile dipoles would orientate themselves to give the maximum sum of the attractive force between all of the particles. As a consequence of thermal motion this model predicts a decrease in attractive force with increasing temperature. A second source of attraction was recognised by Debye[34]. He recognised that a permanent dipole in one molecule would induce a dipole in a second molecule. This second dipole would be in the correct orientation to cause attraction. For a molecule that can be polarised in any orientation this effect becomes independent of temperature as the dipole re-orientates itself to compensate for the thermal motion.

Both of the above models did not account for the attraction of non-polarisable atoms such as helium atoms. London[35] showed that the attraction mechanism in this case was a quantum mechanical effect independent of any permanent or induced dipole-dipole interactions. The London attraction can be described as being a consequence of small fluctuations in the electrical field of an atom. The Heisenberg uncertainty principle requires that the electrical field of any atom is subject to fluctuations. These fluctuations can be considered to form transient dipoles. The behaviour of two adjacent atoms is to couple the oscillations such that the fluctuations of each tends to occur in phase with each other. This coupling reduces the free energy of the system, thus results in an attractive force. With this model every atom can simultaneously attract every other atom within a system.

The London attraction is a second order effect and has been shown to follow the relationship[35]

$$V_A = -L/r^6 \qquad (2.4)$$

where the London interaction constant L is $(3/4)\ Z^{1/2}\ h\nu_v\ a_o^2$, Z is the number of electrons in the outer shell, h is Planck's constant, ν_v is the characteristic frequency of the oscillations and a_o is the static polarisability of the molecules concerned.

Hamaker[36,37] showed that the above model for a gaseous system could be applied to condensed bodies. He considered all possible interactions between the attracting elements of the bodies. He proceeded by replacing the sum of all the pair-wise interactions by a double integral, the solution of which produced:

$$V_A = A \,.\, H \qquad (2.5)$$

where A is the Hamaker constant and H a geometrical function.

The Hamaker constant (A) has the dimensions of energy and is a function of the strength of attraction of two elements (π), the London interaction constant (L) and the number of elements per unit volume (q). The relation has the form:

$$A = \pi^2 q^2 L \qquad (2.6)$$

Two values for the Hamaker constant that are relevant in the context of this thesis are[2]:

Poly(methyl methacrylate) - 6.3×10^{-20}J
and water - 4.38×10^{-20}J

The Hamaker equation suggests that the attraction should occur over distances of the order 10's of nanometers. If we consider longer range effects, the electromagnetic interaction between two dipoles is not instantaneous but proceeds at a finite speed, the speed of light. Vervey and Overbeek[38] noted that when the separation between particles is significant when compared to the wavelength of the fluctuation frequency there is a reduction in the attraction force. This effect is known as the "retardation effect". Casimir and Polder[39] quantified the retardation effect and showed that the inverse sixth power relationship changes to an inverse seventh power at distances greater than the effective wavelength. This effect can greatly reduce the attraction generated by medium sized particles at separations down to 10nm[2]. This becomes more important when the medium between the particles is not a vacuum but has a finite dielectric constant.

Modification of the Hamaker approach to a system where the condensed bodies are within a dispersion medium brings the model closer to the real

system of interest. The addition of a dispersion medium of finite dielectric constant has two effects: firstly the transmission of the London force is no longer through a vacuum but via solvent molecules; and secondly the condensed bodies now have an attraction to the surrounding medium. Both effects serve to reduce the attractive force and move the distance at which the retardation effect becomes important closer to the particle. The secondary medium effect causes the derivation of an effective Hamaker constant A_{12} where:

$$A_{12} = [A_1^{1/2} - A_2^{1/2}]^2 \qquad (2.7)$$

A_1 is the Hamaker constant for the particles and A_2 for the medium. The effective Hamaker constant is always about an order of magnitude smaller than the original constants. For poly(methyl methacrylate) in water the effective Hamaker constant can be calculated to be:

$$[(6.3 \times 10^{-20})^{1/2} - (4.38 \times 10^{-20})^{1/2}]^2 = 1.74 \times 10^{-21} J \qquad (2.8)$$

The system under study in this work is a composite particle with a layer of a second polymer (with a different Hamaker constant) shielding the inner core from the dispersion medium. This outer layer will have a lower Hamaker constant than the particle core thus reducing the effective constant even further.

The model from which the Hamaker equation is derived is based on the interaction of microscopic elements. As such it incurs errors on scaling up to macroscopic systems. An alternative approach has been employed by Lifshitz[40,41]. His model considers the bodies to be ideal materials with the same dielectric properties throughout. This approach takes into account retardation and medium effects eliminating the need for subsequent correction. The mathematical treatment is complex in comparison to the

Hamaker approach. The results obtained by the Lifshitz approach are comparable to those from the Hamaker method. As a consequence the use of the Hamaker method is still preferred by most workers[2].

2.2.2 The forces of repulsion.

For a colloid to be stable, ie. not to spontaneously flocculate, a mechanism must be provided to negate the attractive forces described above. Traditionally in aqueous media electrostatic charge stabilisation has been utilised. Particles with the same charge repel each other hence conferring stability on the system. Quantitative theories have been developed to describe these effects based on the theories of Derjaguin, Landau, Verwey and Overbeek (D.L.V.O. Theory) [38,42]. The nature of this stabilisation is well understood and is well documented both experimentally and theoretically in the literature.

For colloids in non-aqueous media the solution to this problem has been to surround the particles with a layer of "soluble" polymer by a mechanism known as steric stabilisation. The soluble polymer is firmly anchored to the the surface of the particle. The concept of steric stabilisation is less well understood and documented than electrostatic stabilisation. Vincent[1], Osmond & Waite[2] and Napper[43] have reviewed and compared the relevant theories.

As two surfaces, each covered with a layer of soluble polymer, approach each other to a distance less than the combined thicknesses of the polymer layers, they begin to interact. Under most circumstances this interaction will be in the form of a repulsive force. Many attempts have been made to describe the nature and magnitude of these interactions. The problem is usually dealt with in terms of the change in free energy of the system.

The basic model for the two particles is illustrated as figure 2.1. The "soluble" polymer chains are anchored firmly at one end to the particle surface and the other end is free to move about in solution.

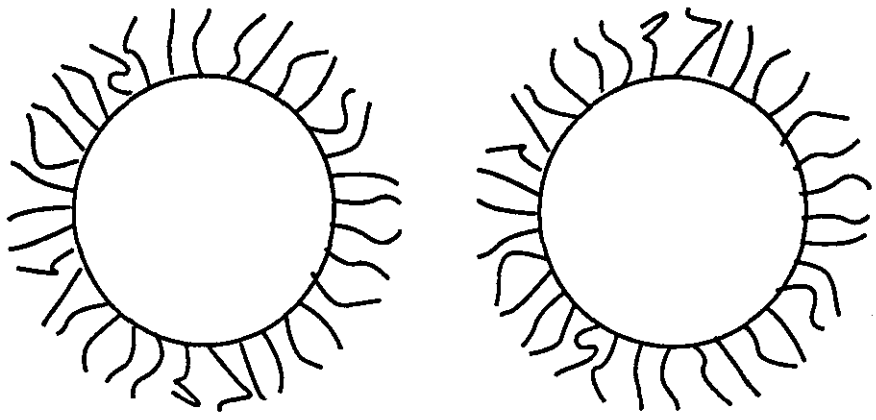

Figure 2.1 Pictorial representation of two sterically stabilised particles.

A number of models have been employed to predict the behaviour of absorbed layers on the surfaces of approaching particles. Fischer[44] suggested that the repulsive force was produced as a result of the overlap of the two layers. He assumed no compression of chains and no redistribution of chains over the particle surface.

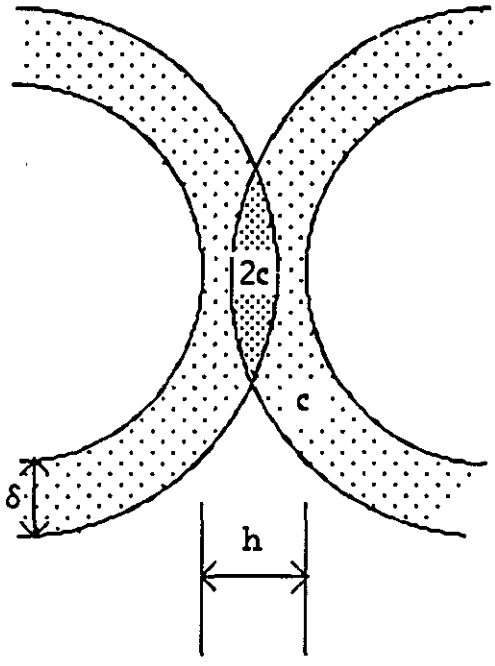

Figure 2.2 Model representing steric repulsion by the overlapping of "dissolved" polymer (Ref. Ottewill and Walker[45])

From the geometry of the system and the application of the Flory-Krigbaum[46] theory of dilute polymer solutions, the change in free energy (ΔG_m) can be evaluated as a function of the overlap. The following equivalent forms of the expression have been utilised in the literature:

by Fischer[44]

$$\Delta G_m = A' \cdot B \qquad (2.9)$$

by Ottewill & Walker[45]

$$\Delta G_m = A' \frac{\Psi_1 - K_1}{V_1} \qquad (2.10)$$

by Napper [47,48]

$$\Delta G_m = A' \frac{(1 - \theta/T)\,\Psi_1}{V_1} \qquad (2.11)$$

where $A' = (4/3)\,\pi kTC^2\,(\delta - h/2)^2\,(3a + 2\delta + h/2)$

and C = concentration of segments in adsorbed layer,

a = radius of particle,

h = surface to surface separation,

δ = adsorbed layer thickness,

Ψ_1 = entropy parameter,

K_1 = enthalpy parameter,

V_1 = partial molar volume of solvent,

B = second virial coefficient,

All three of these expressions contain the same geometric term and are equivalent in the thermodynamic term. In a good solvent they predict that work must be done to create an overlap in the polymer layers, ie. there will be a repulsive force. In theta conditions there will be no change in free energy as the two polymer layers overlap and in a poor solvent energy will be liberated by the overlap, ie. there would be observed spontaneous flocculation.

This model has two significant defects, firstly the assumption that the adsorbed polymer layer has a uniform concentration leads to an over-estimate of the interaction on approach of the two particles and secondly the model does not account for the redistribution of polymer chains as the two layers interact. The model completely breaks down when h becomes less than δ because the adsorbed layer would then have to penetrate the particle core.

Doroszkowski and Lambourne[49] proposed a model allowing for the redistribution of polymer chains. Here the polymer chains were irreversibly attached to the particle surface. As the particles approach the polymer segments are redistributed over the toroidal volume of interaction as shown in figure 2.3. The repulsion can be calculated either

from the force produced or from the free energy of mixing.

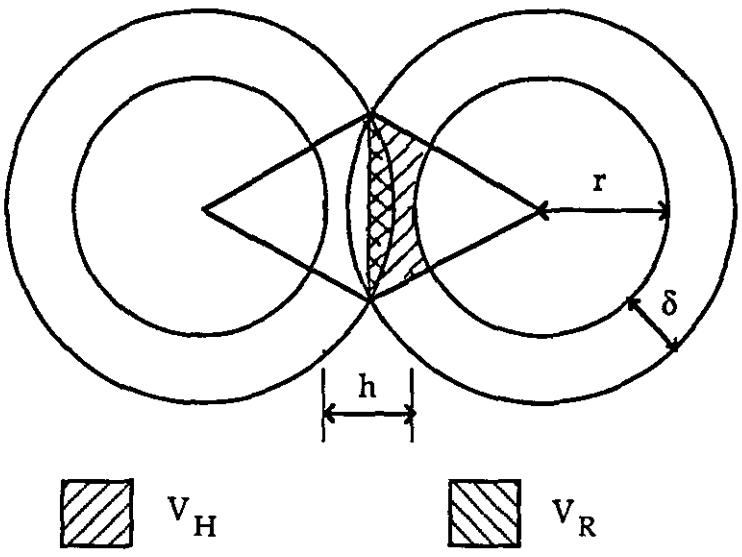

Figure 2.3: Model representing steric repulsion by overlap allowing for the redistribution of polymer chains. After Doroszkowski and Lambourne[49].

Considering the first method, the segmental osmotic pressure and the total force on the plane of contact was calculated and integrated with respect to the distance of approach. This yields the total repulsive potential function with respect to separation distance[50]. For the second method the principle of Flory[51] was applied to the more general model[52]:

$$V'_1(C'_1) + V'_2(C'_2) \rightarrow V'_3(C'_3) \qquad (2.12)$$

where V′ represents the volume and C′ the segment concentration. For the situation where $V'_1 = V'_2$ and $C'_1 = C'_2$ the expression below was obtained.

$$\Delta G_m = C'_3 (C'_3 - C'_1) V'_3 \left(\frac{\Psi_1 - \kappa_1}{V'_1} \right) kT \qquad (2.13)$$

From the relevant volumes and concentrations for the model shown in figure 2.3 above, the following expression for the energy of repulsion was obtained.

$$\Delta G_m = 2kT\left(\frac{\Psi_1 - \kappa_1}{V'_1}\right)C_0^2\left(\frac{V_H + V_R}{V_H}\right)V_R \qquad (2.14)$$

where C_0 is the initial average concentration of polymer in the stabilising layer. The values for V_H and V_R are derived from the geometry of the model and are given by:

$$V_H = (\pi/3)\,(\delta - h/2)\,(r + h/2)\,(2r + \delta + h/2) - (2r^3/(r + \delta) \qquad (2.15)$$

$$V_R = (\pi/3)\,(\delta - h/2)^2\,(3r + \delta + h/2) \qquad (2.16)$$

This model gives good results when compared with values determined by the compression of monolayers of sterically stabilised particle dispersions on a force balance [49].

2.2.3 The attraction repulsion balance.

According to the DLVO treatment[38,42] the forces of repulsion generated by charge stabilisation are of the same order as the attractive forces. Addition of the two forces yields a plot of the potential as a function of inter-particle distance. A plot showing the general shape of this curve is shown as figure 2.4. The curve contains two minima where the net force is attractive. Thus the electrostatic system is thermodynamically unstable. The coagulated or flocculated state is energetically preferred. The presence of a primary maximum in the curve that is sufficiently large when compared to the thermal kinetics of the system confers a quasi-stability to the system. As

long as the kinetic energy of the particles does not enable them to pass over this energy barrier to be exceeded the system remains stable. The secondary minimum at larger separations can result in a loose flocculation but in many systems the kinetic energy of the particles is sufficient to maintain stability.

For the sterically stabilised system the repulsive energy is much greater than the attractive energy. As a consequence, the resultant repulsive energy rises rapidly on approach of two particles and there are no minima in the curve. A sketch of this curve is shown in figure 2.5. The absence of minima from this curve implies that a sterically stabilised system should be more robust than the ionic system. The sterically stabilised system should be thermodynamically stable.

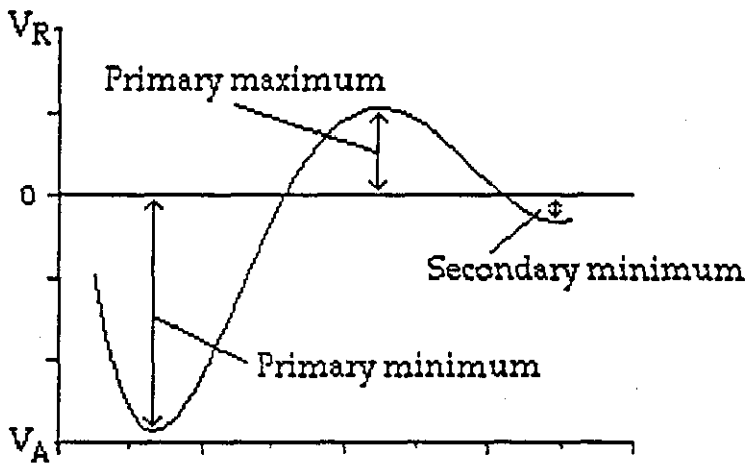

Figure 2.4: The potential energy curve for a charge stabilised dispersion

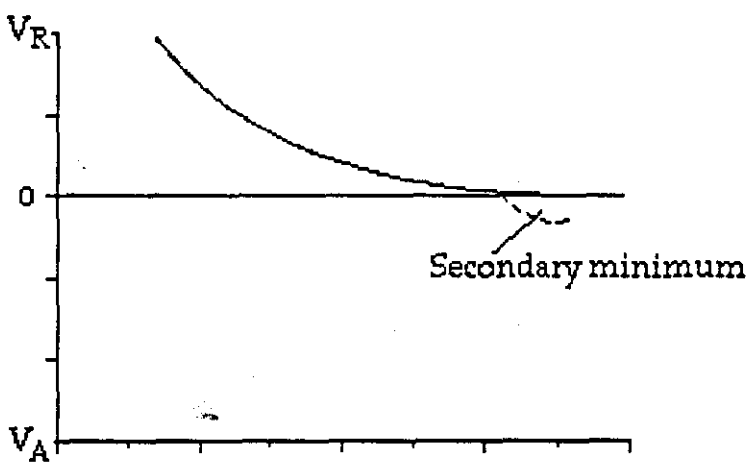

Figure 2.5: The potential energy curve for a sterically stabilised dispersion

2.3 MICELLE FORMATION

Amphipathic molecules always consist of one part which is amphihilic (hydrophilic) and one part that is amphipathic (hydrophobic) to water. In a solution of such molecules there are strong interactions between the solvent and the molecule that result in expulsion of the hydrophobic component. This produces the tendency for the aggregation of molecules into micelles. The free energy of the hydrophilic component increases during this process whilst the free energy of the hydrophobic component decreases. As a consequence of the reduction of the interfacial area between the hydrophobic component and the water the total free energy is also reduced. The driving force behind micellar formation is the reduction in the free energy. The shape and size of the micelles produced is determined, again, by the minimalisation of the free energy.

The concentration at which micelles begin to form is known as the critical micelle concentration (CMC). A typical CMC value for an ionic surfactant is of the order 10^{-3} mol/ℓ. As an example the value quoted for sodium dodecyl sulphate is 8.1×10^{-3} mol/L [53].

There are two fundamental differences between an anionic and a non-ionic surfactant; firstly the size of the hydrophilic portion of the molecule with respect to the hydrophobic part is much greater in a non-ionic surfactant; secondly there is an absence of charge on the molecule in the case of the non-ionic surfactant. This absence of charge results in a much lower CMC for a non-ionic surfactant. With the ionic surfactant the formation of a micelle involves the bringing together of many like charges. This contributes a positive term in the free energy equation, ie. raises the total free energy. A typical CMC for a non-ionic surfactant is of the order 10^{-4} Mol/l.[54]

Surfactants in solution can form many structures; spherical, cylindrical, disc shaped, hollow spheres (vesicles) and stacked bi-layers. The preferred structure for a given system will be the structure that provides the optimum surface area of interface for each surfactant molecule. Israelachvili[55] has shown how the sum of the contributions to the interfacial free energy per molecule, given by the hydrophobic attraction and the head group repulsion as a function of head group area, yields a minimum which he calls the optimal area, a_0. This plot is reproduced as figure 2.6.

If there are two alternative structures satisfying the above criteria, entropy will favour the structure with the smallest aggregation number[55]. It has been demonstrated experimentally by Price, Chan, Hudd and Stubbersfield[56] that a metastable micellar form can be produced under certain conditions and not until sufficient thermal energy is available does it transform to the stable form. They studied a polystyrene-b-polyisoprene block copolymer in N,N´-dimethylacetamide. They showed, by electron microscopy, that the copolymer produced either "worm-like" or spherical micelles depending on the thermal history. The "worm-like" micelles were the metastable form in this case.

There are geometric constraints that prevent surfactant molecules from packing into specific structures of particular size. If the hydrophobic part of the molecule has a fully extended length of l_c it can not pack into a sphere of $R>l_c$. Given a surfactant where the hydrophobic component has a volume v and has an optimum area a_0, the energy will reach a minimum in a spherical micelle of radius R and aggregation number M when[55]:

$$M = 4/3\ \pi R^3 / v = 4 \pi R^2 / a_0$$

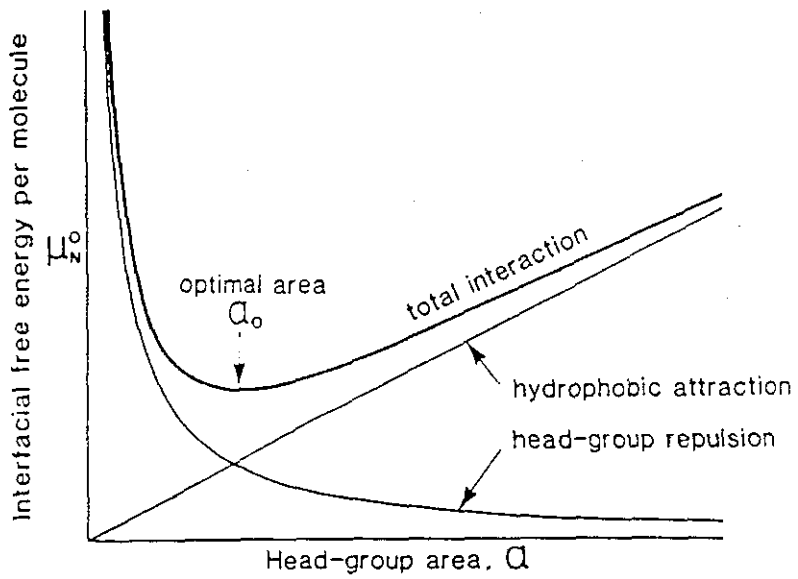

Figure 2.6: Attractive and repulsive interactions occurring at the interface in a micellar structure. Taken from Israelachvili [55].

ie. $R = 3v/a_0$ (2.17)

It follows that if l_c is less than $3v/a_0$ the molecules will not be able to pack into a sphere. Rearrangement yields the statement: if the product v/a_0l_c is greater than 1/3 the molecules will not be able to pack into a sphere. A similar argument for a cylinder yields the requirement that $R=2v/a_0$. Thus if the product v/a_0l_c is greater than 1/3 but less than 1/2 the molecules will be able to pack into cylinders. If the product is greater than 1/2 but less than 1 the surfactant will produce bilayers or vesicles and, if greater than 1, inverted micelles.

2.4 PARTICLE SIZE DETERMINATION BY SMALL ANGLE X-RAY SCATTERING

X-ray scattering can be utilised in a number of ways to provide morphological information to the polymer chemist. Wide angle X-ray scattering (WAXS) has been utilised to quantify crystallinity and, with the application of pole diagrams, to monitor orientation. At large angles information relating to small dimensions is registered. As the angle of scattering decreases the magnitude of the structure under study increases. The magnitude of the structure resulting in the scatter for crystalline material is related to the scattering angle by the Bragg equation.

$$n\lambda = 2d \sin \theta \qquad (2.18)$$

where n is the order of diffraction, λ is the wavelength of the X-rays, d is the interplanar distance and 2θ is the scattering angle. Small angle X-ray scattering (SAXS) is the technique used for the study of scattering in the range $2\theta = 0.05°$ to 4°. For CuK_α X-rays with a wavelength $\lambda = 1.54$Å this corresponds to dimensions from ca. 10Å up to 800Å. This makes SAXS ideal for the study of particles dispersed in a matrix, ie crystal lamellar in semi-crystalline polymers, incompatible polymer blends and micelles in solution.

It might be considered to use longer wavelength radiation than the CuK_α X-rays to increase the angle of scattering. Unfortunately the longer wavelength X-rays are strongly absorbed by matter, thus greatly decreasing the intensity of the scattered radiation. In practice there is a gap in the useful electromagnetic spectrum from approximately 2Å up to the far ultraviolet light[57].

2.4.1 Corrections for SAXS camera geometry.

The ideal geometry for a SAXS camera, from a mathematical viewpoint, would be a pinhole collimated camera. However the intensity of X-rays from pinhole collimation is so low as to generate practical problems. The practical solution is to use slit collimation. The slit collimated camera can be considered to be equivalent to a large number of pinhole collimated beams stacked on each other. The resultant scattering pattern is thus the interference pattern constructed from all of the pinhole patterns. The effect on a relatively sharp maximum in the original scattering curve is not only to broaden it but to displace it to lower angle by 10-20% [58]. As a consequence, either the theory must be modified to take into account the slit optics of the camera or the data must be treated to construct the curve that would have been obtained from the pinhole optics.

Guinier[59] proposed the relation for an infinitely high X-ray beam of zero width:

$$I(h) = \frac{1}{\pi}\int_0^{\infty} \frac{d\tilde{I}\left(\sqrt{h^2+t^2}\right)}{d\sqrt{h^2+t^2}} \frac{dt}{\sqrt{h^2+t^2}} \qquad (2.19)$$

where $\tilde{I}$ is the slit smeared intensity, I is the non-smeared intensity, h is a quantity related to the scattering angle ($h = 4\pi \sin\theta/\lambda$), and t an integration variable of the same dimensions as h. This relation can be simplified by substituting m for $\sqrt{h^2+t^2}$ and writing m_j for h.

$$I(m_j) = -\frac{1}{\pi}\int_{m_j}^{\infty} \frac{d\tilde{I}(m)}{dm} \frac{dm}{\sqrt{m^2-m_j^2}} \qquad (2.20)$$

The method adopted for performing this desmearing during this study was that proposed by Dijkstra, Kortleve and Vonk[58]. Firstly the curve was modelled by a Fourier series in the form:

$$\tilde{I}_f(m) = \frac{1}{2}A_o + \sum_{n=1}^{n_{max}} A_n \cos\left[2\pi n \frac{m-m_{min}}{2(m_{max}-m_{min})}\right] \qquad (2.21)$$

in which the coefficients A are found from

$$A_n = \frac{2}{m_{max}-m_{min}} \int_{m_{min}}^{m_{max}} \tilde{I}(m) \cos\left[2\pi n \frac{m-m_{min}}{2(m_{max}-m_{min})}\right] dm \qquad (2.22)$$

where, m_{min} and m_{max} are the smallest and largest values for m for which values of $\tilde{I}(m)$ are given or assumed. The quality of the fit between $\tilde{I}_f(m)$ and $\tilde{I}(m)$ depends on the ratio between the number of terms (n_{max}) and the number of points at which $\tilde{I}(m)$ is measured. If this ratio is too low the fit will be poor and if this ratio is too high the fit will follow irrelevant details in the curve, ie will trace the statistical scatter in the data.

The Fourier series, unlike the real data, is symmetric around m_{min} and m_{max}. To accommodate this it is beneficial for the gradient of $\tilde{I}(m)$ to be zero at m_{min} and m_{max}. This is, in practice, achieved by extrapolating the data by a few points at each extreme of the data set.

The integration is performed according to equation 2.20 after replacement of the upper limit to m_{max} and the lower limit by m^1, where m^1 is the first real data point not m_{min}. Equation 2.20 is not well suited for numerical integration as the integral becomes infinite at the lower limit. To avoid

this Dijkstra, Kortleve and Vonk[58] employ a semi-numerical method where the function is divided into small intervals of $2\Delta m$. (In the following, derivatives are denoted by primes) For each interval the $\tilde{I}'(m)$ curve is represented by the first three terms of a Taylor series which is expanded around the mid-point of the interval m_i.

$$\tilde{I}'(m) = \tilde{I}'(m_i) + (m-m_i)\,\tilde{I}''(m_i) + \frac{(m-m_i)^2}{2}\,\tilde{I}'''(m_i) \qquad (2.23)$$

$\tilde{I}'(m)$, $\tilde{I}''(m)$ and $\tilde{I}'''(m)$ are found by differentiation of the series 2.21. The period $2\Delta m$ is taken to be the interval between successive data points in the original data. The integral is now replaced by the summation over discrete intervals, each of which is solved analytically.

Infinite height criterion

The infinite height criterion for slit optics is met if the radiation from the two extreme ends of the primary beam are unable to enter the counter slit. From purely geometric considerations the following relationship is derived:

$$L > 2m + \sigma \qquad (2.24)$$

Where L is the height of the homogeneous part of the beam at the receiving slit, m is the angular distance measured in the plane of registration and σ is the height of the receiving slit.

2.4.3 Radius of gyration.

SAXS data from monodisperse (or near monodisperse) particles can be interpreted in terms of the radius of gyration (R_g) of the particles. There must be no inter-particle interference; this will be true if the system is sufficiently dilute. The determination does not involve any assumptions concerning the shape of the particle and hence can be used for particles of any shape- spherical, ellipsoidal, cylindrical etc. Radii of gyration may be calculated from the Guinier relation[57,59]

$$I_{(des)} = I_0 \exp(-4\pi^2 R_g^2 s^2 /3) \qquad (2.25)$$

where $I_{(des)}$ is the pinhole or slit desmeared intensity (see section 2.4.1) as a function of the angular variable s ($s = (2 \sin\theta)/\lambda$). I_0 is the intensity extrapolated to zero angle. The Guinier relation holds for dilute solutions of near spherical particles at low scattering angles. A plot of ln $I_{(des)}$ against $4\pi^2 s^2 /3$ enables the radius of gyration (R_g) to be determined from (-gradient)$^{0.5}$.

2.5 DETERMINATION OF FRINGE THICKNESS BY SAXS

2.5.1 Introduction.

An excellent review of techniques for the evaluation of fringe thicknesses by SAXS has been published by Koberstein, Morra and Stein[60].

SAXS of an ideal two phase system with sharp interfacial boundaries has been dealt with by Porod[61,62,63]. The limiting behaviour of the scattering intensity at large values of s ($s = (2 \sin\theta)/\lambda$) is known as Porod's law. Porod's law predicts a decrease in intensity proportional to the reciprocal fourth power of s.

$$\lim_{s\to\infty} [I_p(s)] = \frac{K_p}{s^4} \qquad (2.26)$$

K_p is called the Porod-law constant. Accurate determination of the value of K_p is important because it relates to certain structural parameters, eg.

$$K_p = (S/V)\, Q/8\pi^3 \phi_1\phi_2 = Q/2\pi^3 l_p \qquad (2.27)$$

where $$Q = 4\pi \int_0^\infty s^2 I(s)\, ds = V\phi_1\phi_2 (\rho_1 - \rho_2)^2$$

and (S/V) is the area of interface per unit volume, ϕ_1 and ϕ_2 are the volume fractions of the phases and ρ_1 and ρ_2 are the respective electron densities. Q is known as the Porod invariant and l_p is the Porod inhomogeneity length, a parameter that yields the average sizes of the phases. I(s), in this case, must be given on an "absolute" scale.

Polymers often show systematic deviations from Porod's law, ie $I_p(s)s^4$ does not reach a constant value. This deviation can be interpreted in terms

of the micro-structure of the polymer. A positive slope in a plot of Is^4 vs s may be interpreted in terms of thermal density fluctuations or mixing within the phases. A negative slope in a plot of Is^4 vs s may be interpreted in terms of the existence of a diffuse interfacial layer between the two phases.

2.5.2 Scattering theory.

The amplitude of scattered X-rays is proportional to the Fourier transform of the autoconvolution of the electron density profile, such that:

$$I_{obs}(s) = F\{\Delta\rho_{obs}^{*2}\} \qquad (2.28)$$

where F is a three dimensional Fourier transform, $\Delta\rho_{obs}$ is the difference between the local electron density and the average electron density, and *2 represents the self-convolution. For the situation with sharp boundaries the intensity in the Porod region is expressed by Porod's law. According to Ruland[64], for the diffuse boundary situation the electron density profile can be expressed as the product of the ideal profile, $\rho(r)$ and a smoothing function, h(r):

$$\Delta\rho_{obs}(r) = \Delta\rho(r) * h(r) \qquad (2.29)$$

where r is the distance along an arbitrary vector within the scattering volume. The Fourier transform of a convolution product in real space is equivalent to the product of the transforms in reciprocal space, and from 2.26, 2.27 and 2.28 it follows that:

$$I_{obs}(s) = F\{\Delta\rho^{*2}(r)\}\, F\{h^{*2}(r)\} \qquad (2.30)$$

and

$$\lim_{s\to\infty} [I_{obs}(s)] = I_p(s)H^2(s) \qquad (2.31)$$

where $I_p(s)$ is the Porod law intensity and $H^2(s)$ represents the negative deviations due to the diffuse interface.

Fluctuations in the electron density within a phase give rise to relatively low scattering intensity[65]. The level of this scattering is system dependent The scattering as a result of these fluctuations, ($I_B(s)$) can be added to equation 2.31.

$$\lim_{s\to\infty} [I_{obs}(s)] = I_p(s)H^2(s) + I_B(s) \qquad (2.32)$$

The limit as s tends to infinity implies that any calculations are strictly only applicable at very high angles, angles well beyond practical measurement.

2.5.3 Negative deviations.

The form of the smoothing function is dependent upon the model employed to describe the change in electron density between the particle core and the diluent. Two models have been employed to describe $\rho_{obs}(r)$; a linear model by Vonk[66] and a sigmoidal-gradient model by Ruland[64]. The two models are described pictorially in figure 2.7.

In the linear model of Vonk, the smoothing function is a box function; it's Fourier transform, H(s) is given by:

$$H(s) = (\sin \pi\delta s)/(\pi\delta s) \qquad (2.33)$$

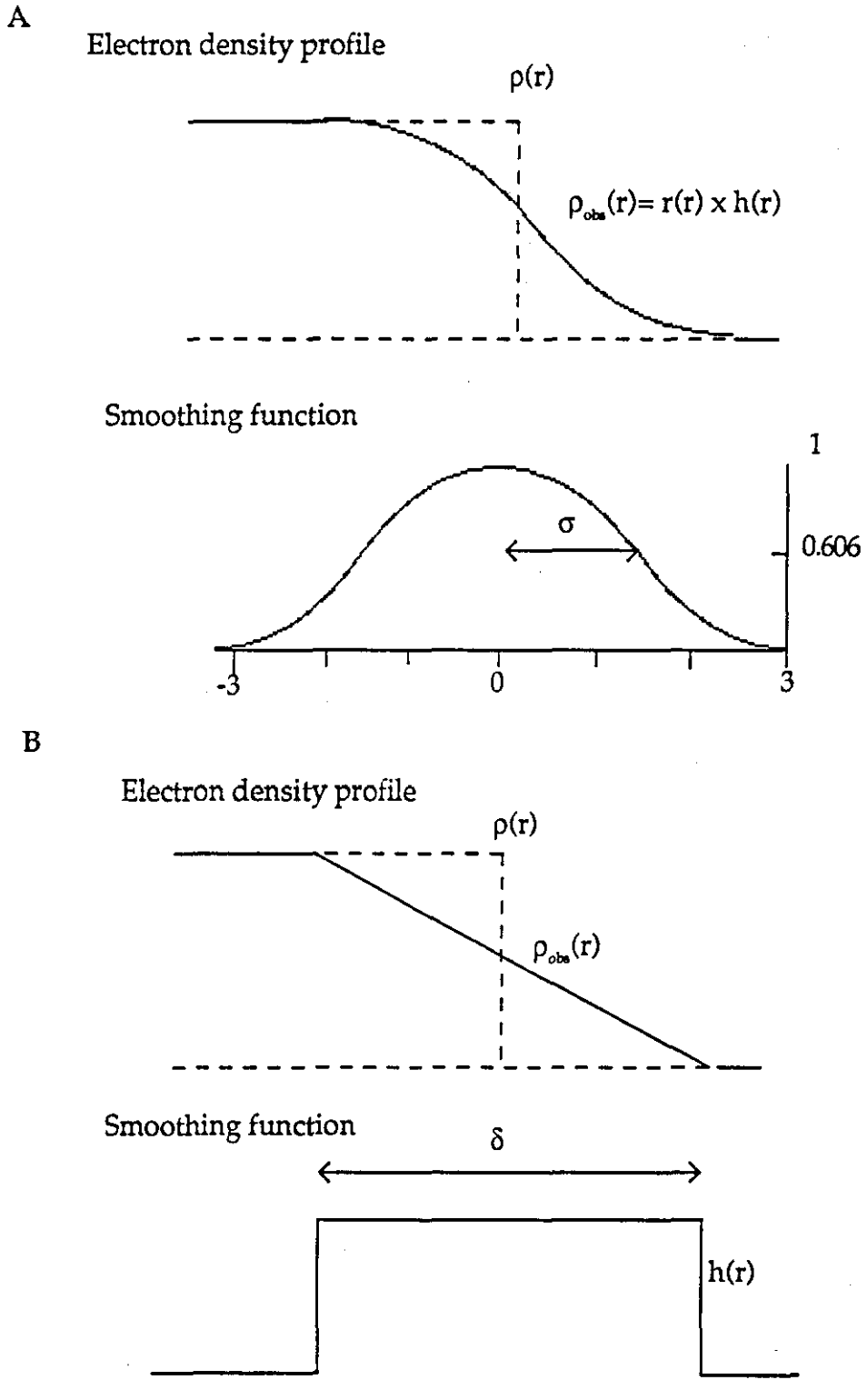

Figure 2.7: Electron density profile $\rho_{obs}(r)$ and smoothing function h(r) for A. sigmoidal model and B. linear gradient model.

where δ is the interface width. From equations 2.26, 2.31 and 2.33 for pin-hole optics the Porod intensity for this model becomes:

$$I_{obs}(s) = (K_p/s^4)\,(\sin^2 \pi\delta s)/(\pi\delta s)^2 \qquad (2.34)$$

Strictly $I_{obs}(s)$ should be at the limit as s tends to ∞ but for simplicity this has been omitted. This equation is not suited for graphical solution but if the sine function is expanded to a series and truncated after the second term a more amenable form is obtained:

$$I_{obs}(s) \approx (K_p/s^4)\,(1-\pi^2\delta^2 s^2/3) \quad \text{for} \quad \delta s \ll 1 \qquad (2.35)$$

The sigmoidal-gradient model of Ruland uses a Gaussian smoothing function where the Fourier transform of the smoothing function H(s) is given by:

$$H(s) = \exp(-2\pi^2\sigma^2 s^2) \qquad (2.36)$$

where σ is the standard deviation of the smoothing function. The corresponding Porod relationship for pin-hole optics is given by:

$$I_{obs}(s) = (K_p/s^4) \exp(-4\pi^2\sigma^2 s^2) \qquad (2.37)$$

By expanding the exponential component a form is obtained that lends itself to graphical solution.

$$I_{obs}(s) \approx (K_p/s^4)\,(1 - 4\pi^2\sigma^2 s^2) \qquad (2.38)$$

Comparison of the two parameters defining the interfacial layer thickness for the two models (Equations 2.35 and 2.38) leads to $\delta \approx 12^{0.5}\sigma$. [60]

When experimental data is obtained by a SAXS camera employing slit optics it becomes necessary to either desmear the data or smear the Porod relation applied to the data. Desmearing of the data introduces errors at the tail of the scattering curve that are difficult to estimate[67] . Therefore it is desirable to generate smeared relationships.

Guinier and Fournet[57] proposed that for negligible slit width the smeared scattering intensity may be expressed as:

$$\tilde{I}(s) = 2\int_0^{\infty} W_l(u)\, I_{obs}\, (s^2 + u^2)^{1/2}\, du \qquad (2.39)$$

where $W_l(u)$ is the slit-length weighting function and u is a constant of integration. From equation 2.32 it follows that:

$$\tilde{I}(s) = 2\int_0^{\infty} W_l(u)\, I_p\, (s^2 + u^2)^{1/2}\, H^2\, (s^2 + u^2)^{1/2}\, du \qquad (2.40)$$

For infinite slit height geometry for the one dimensional linear gradient model the slit smeared intensity is expressed by:

$$\tilde{I}(s) = 2W_l(0)\, K_p \int_0^{\infty} \frac{\sin^2 [\pi\, \delta\, (s^2 + u^2)^{1/2}]}{\pi^2\, \delta^2\, (s^2 + u^2)^3}\, du \qquad (2.41)$$

Vonk[66], utilised an expanded form of the sine function to solve the integration. The series was first truncated before integration. After integration the slit smeared intensity may be expressed by:

$$\tilde{I}(s) \approx (K'/s^3)\, (1 - 2\pi^2\, \delta^2\, s^2/3) \qquad \delta s \ll 1 \qquad (2.42)$$

where $K' = W_1(0)\, K_p\, \pi/2$. It has been noted that the expanded form of equation 2.42 is of a form where an approximation may be made to the Maclaurin power series for an exponential function. (The term contained within the brackets are the first two terms of the Maclaurin series). It is said that this exponential function takes into consideration some of the higher order terms of the expression and thus should have an improved range of applicability. The derived expression is given by:

$$\tilde{I}(s) \approx (K'/s^3) \exp(-2\pi^2 \delta^2 s^2/3) \tag{2.43}$$

There is no physical significance behind the substitution into the exponential form as such; the validity of this approximation is a little questionable.

For the situation where infinite slit height is not assumed the length weighting function may be approximated by a Gaussian distribution function.

$$W_1(u) = W_1(0) \exp(-p^2 u^2) \tag{2.44}$$

The weighting function may be determined experimentally or calculated from the slit geometry after the method of Hendricks and Schmidt[68,69]. The smeared intensity for the linear gradient model using this weighting function and equation 2.41 is given by:

$$\tilde{I}(s) = 2W_1(0)\, K_p \exp(p^2 u^2) \int_0^\infty \frac{\exp[-p^2 (s^2 + u^2)]}{(s^2 + u^2)^3} \times \frac{\sin^2 [\pi \delta (s^2 + u^2)^{1/2}]}{\pi^2 \delta^2}\, du \tag{2.45}$$

This integral may be solved by expansion of the integrand. The resultant series is truncated before integration. The smeared X-ray intensity may be expressed by:

$$\tilde{I}(s) \approx (\pi/2)\, W_l(0)\, K_p/s^3 \exp(p^2 s^2)\left(1-\frac{2}{3}\pi^2 \beta^2 s^2\right) \qquad \beta_s \ll 1 \qquad (2.46)$$

where $\beta = [\delta^2 + 3(p/\pi)^2]^{1/2}$

This equation is in the same form as the Vonk expression (equation 2.43). The essential differences are that δ is replaced by β and $\tilde{I}(s)$ is replaced by $\tilde{I}(s) \exp(-p^2 s^2)$. In the case of infinite slit height p becomes equal to 0 and the two expressions become equivalent. For all relations between smeared intensity and fringe thickness the same form is observed. For infinite slit height the equations are of the form:

$$s^3 \tilde{I}(s) = K' f(\delta s) \qquad (2.47)$$

and with the Gaussian weighting function they become:

$$s^3 \tilde{I}(s) \exp(-p^2 s^2) = K' f(\beta s) \qquad (2.48)$$

Now considering the sigmoidal gradient model, Ruland[64] proposed that for the infinite slit length situation the smeared intensity is described by:

$$\tilde{I}(s) = (K'/s^3)\,[(1-8\pi^2\sigma^2 s^2)\,\mathrm{erfc}(2\pi\sigma s) + 4\sqrt{\pi}\,\sigma s \exp(-4\pi^2\sigma^2 s^2)] \qquad (2.49)$$

The error function (erfc ($2\pi\sigma s$)) appears as a consequence of the integration limits. It is not possible to integrate between the limits of 0 to ∞. Thus the

lower limit is exchanged for the limit ($2\pi\sigma s$). This means that the integral will be missing the contribution from 0 to ($2\pi\sigma s$), the error function. As σs tends to 0 the error function tends to 1, (the error function is of an exponential form and $e^0 = 1$).

Therefore for small values of σs equation 2.49 may be approximated by:

$$\tilde{I}(s) \approx (K'/s^3)(1-8\pi^2\sigma^2 s^2) \quad \text{for } \sigma s \ll 1 \tag{2.50}$$

In a similar manner to the treatment of the linear model of Vonk an exponential approximation to equation 2.50 may be made. Again this approximation has no physical basis and thus this author has reservations over it's application. The exponential form is given as equation 2.51.

$$\tilde{I}(s) \approx (K'/s^3)\exp(-8\pi^2\sigma^2 s^2) \tag{2.51}$$

Bonart and Müller[70] have shown an alternative approximation to the slit smeared intensity. In this approximation the slit smeared intensity is given by:

$$\tilde{I}(s) \approx 2H^2(s)\int_0^\infty W_l(u)\, I_p\, (s^2+u^2)^{1/2}\, du \tag{2.52}$$

For the sigmoidal model with infinite height optics this yields:

$$\tilde{I}(s) \approx (K'/s^3)\exp(-4\pi^2\sigma^2 s^2) \tag{2.53}$$

An empirical approximation of a similar form to the approximation of Bonart and Müller has been suggested by Koberstein, Morra and Stein[60].

$$\tilde{I}(s) = (K'/s^3) \exp [-a (\sigma s)^n] \qquad (2.54)$$

Equation 2.54 above was empirically fitted to the exact solution (2.49). A plot of ln {-ln [$s^3 \tilde{I}(s)$]} vs ln [σs] has a slope n and an intercept ln(a). This plot was shown to be linear over a large range of σs and yielded the values of 1.81 and 38 for n and a respectively. Thus the empirical form becomes:

$$\tilde{I}(s) = (K'/s^3) \exp [-38 (\sigma s)^{1.81}] \qquad (2.55)$$

The relations for finite height slit optics with the sigmoidal model may be treated in the same manner as the linear model. $\tilde{I}(s)$ is replaced by $\tilde{I}(s) \exp (-p^2 s^2)$ and σ by α where $\alpha = [\sigma^2 + (p/2\pi)^2]^{1/2}$.

Range of Applicability for smeared Porod relations (with infinite slit assumption).

The applicability of each of the solutions has been determined by the plotting of the the various approximations against the exact solution. The criteria selected for the approximation to be considered applicable was an error of ±5%. The following results were obtained [60].

Approximation	Applicability	
Linear gradient model		
Vonk		
$\tilde{I}(s) \approx (K'/s^3) (1-2\pi^2 \delta^2 s^2/3)$	$\delta s < 0.10$	(2.42 b)
Exponential		
$\tilde{I}(s) \approx (K'/s^3) \exp (-2\pi^2 \delta^2 s^2/3)$	$\delta s < 0.16$ and $0.56 < \delta s < 0.84$	(2.43 b)

Approximation	Applicability	
Sigmoidal gradient model		
Ruland		
$\tilde{I}(s) = (K'/s^3)\,(1-8\,\pi^2\,\sigma^2\,s^2)$	$\sigma s < 0.014$	(2.50 b)
Exponential		
$\tilde{I}(s) \approx (K'/s^3)\,\exp\,(-8\,\pi^2\,\sigma^2\,s^2)$	$\sigma s < 0.017$	(2.51 b)
Bonart & Müller		
$\tilde{I}(s) \approx (K'/s^3)\,\exp\,(-4\pi^2\,\sigma^2\,s^2)$	$\sigma s > 0.29$	(2.54 b)
Empirical		
$\tilde{I}(s) = (K'/s^3)\,\exp\,[-38\,(\sigma s)^{1.81}]$	$0.009 < \sigma s < 0.72$	(2.55 b)

2.6 EMULSION POLYMERISATION

In 1948 Smith and Ewart published the first paper describing quantitatively emulsion polymerisation[71]. The theory they described has become known as the "Smith-Ewart theory". This paper was preceded by many more qualitative descriptions and this paper marked the first real attempt in the literature to describe emulsion polymerisation in a thorough and rigorous manner. The theory was based on the qualitative model of Harkins[7-10].

The Smith-Ewart theory is still respected today as being a good description of the kinetics of emulsion polymerisation and such will be described here. Without removing credit from the contributions of workers early in the history of emulsion polymerisation this description will begin with the model of Harkins. An excellent review of the historical aspects may be found in "Emulsion polymerisation" by Blackley[72].

2.6.1 The Harkins Theory.

Historically the most important qualitative description of emulsion polymerisation was published by Harkins over the period 1945-50[7-10]. The essential stages of the polymerisation are represented pictorially in figure 2.8.

(a) shows the situation before the addition of a free radical source. The surfactant is distributed between the aqueous phase, micelles and the surface of monomer droplets. The bulk of the monomer is found in large droplets with a small quantity to be found in solution or within micelles.

(b) shows the situation shortly after initiation. A few, but not all, of the

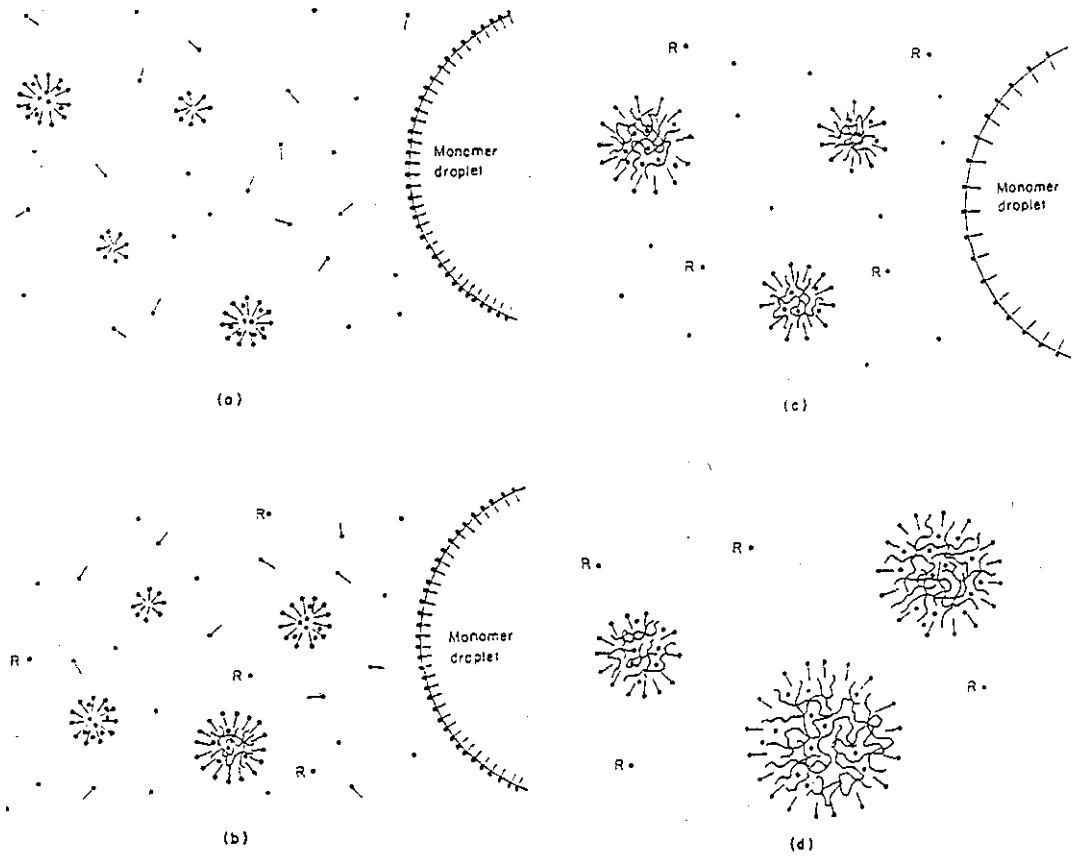

Figure 2.8: Stages of an emulsion polymerisation. Taken from Blackley[72].

micelles now contain polymer. Monomer is diffusing from the aqueous phase into these growing polymer particles and monomer is diffusing from the monomer droplets to replenish the aqueous phase. Free surfactant molecules are being taken from solution to stabilise the growing particles. Some micelles not supporting a growing polymer core begin to lose surfactant to the aqueous phase.

(c) Polymer particles continue to grow. All "free" micelles have been robbed of their surfactant molecules and there is no longer free surfactant in solution. The monomer droplets are shrinking as monomer is diffusing across to the growing particles. The surface coverage of surfactant on the monomer droplets is also being depleted. No further nucleation of polymer particles can occur.

(d) At this stage all of the monomer droplets have been used up. The concentration of monomer in the polymer particles begins to reduce as the monomer is polymerised. The rate of reaction slows down.

The essential points of the theory may be summarised as:

(1) The monomer droplets function as a reservoir of monomer from which monomer can diffuse, via the aqueous phase, to micelles and/or growing polymer particles during the progress of the polymerisation. Very little or no polymerisation occurs in these monomer droplets.

(2) The principle locus for polymerisation is within the micelle/growing polymer particle. The polymerisation rapidly depletes the micelle of monomer and the monomer is replenished by diffusion from the aqueous phase.

A small amount of polymerisation may occur in the true aqueous phase

and can lead to the formation of a particle. This is considered to have very low probability when compared to initiation within micelles.

(3) The growth of a particle results in an increase in its surface area. As a consequence it tends to adsorb surfactant from the aqueous phase. The aqueous phase in turn removes surfactant molecules from non-growing micelles.

(4) The process of continual adsorption of surfactant onto the growing polymer particles results in the eventual disappearance of micelles and eventually free surfactant molecules. At this stage of the reaction no new polymerisation loci can be formed.

(5) The continuous take up of monomer by the growing particles from the aqueous phase eventually results in the disappearance of the monomer droplets. At this stage the system only contains monomer swollen polymer particles.

(6) The primary site for the initiation of a polymerising chain is in the aqueous phase. Polymerising centres are formed in the aqueous phase and before they have propagated beyond a few monomer units they enter either growing polymer particles or micelles.

2.6.2 The Smith-Ewart theory.

The theory dealt with here has become known as the Smith-Ewart `case 2´ theory. It is this theory that has been utilised most in the literature and is considered to reflect typical emulsion polymerisation.

The model utilised by Smith and Ewart was essentially that of Harkins[7-10]. The initiating substance is found only in the aqueous phase, the monomer

is practically insoluble in water but is solublised in the surfactant micelles. Initiation occurs when a micelle captures a free radical from the aqueous phase. At this point the micelle is no longer considered as a micelle but as a polymer particle. These polymer particles form the principle loci of polymerisation and grow, adsorbing surfactant molecules from the aqueous phase. Eventually the concentration of surfactant in the aqueous phase no longer exceeds the CMC and no micelles are present in the system. From this point onwards no new polymerisation loci are formed.

The general theory (case 1) allows for a propagating radical to be lost by a polymer particle to the aqueous phase. The case 2 theory however has two simplifications: There is no mechanism by which a transfer of activity out from a polymerisation locus can occur; secondly the time elapsed between the entry of a second free radical into an active polymerisation locus to the mutual termination of both radicals is short relative to the period between the entry of successive radicals.

This second point leads directly to the conclusion that any locus of polymerisation is only active on average for approximately 50% of the time. On the entry of the first radical polymerisation commences at a constant steady rate. On the entry of a second radical for a very short period the rate doubles then drops to zero as the two radicals terminate each other. The polymer particle then remains dormant until a third radical arrives. This process is repeated throughout the polymerisation. Under these conditions the following can be assumed:

(1) On average each polymerisation locus is only active for 1/2 of the time, ie. the average number of radicals per particle (r) is 0.5.

(2) The overall rate of reaction at a given locus is 1/2 of the instantaneous rate when the locus is active.

(3) In a system with a large number of loci at any given time 1/2 of the loci will be active and 1/2 dormant.

If, in reality, the time period between the entry of a second radical and the mutual termination of the two radicals in the particle is long with respect to the period between entry of successive radicals, a polymer particle may, at a given time, contain more than 2 radicals. In this case r, the average number of radicals per polymer particle, would exceed the Smith-Ewart Case 2 value of 0.5.

Smith and Ewart state that the rate of polymerisation per unit volume of aqueous phase is given by:

$$\frac{dM}{dt} = \frac{1}{2} k_p [M] N \qquad (2.56)$$

where N is the number of loci per unit volume of aqueous phase, [M] is the molal concentration of monomer at the polymerisation locus and k_p is the rate constant for the propagation step. Blackley[72] points out that it is not clear what is meant by dM/dt. The omission of [ ] around the M appears to be intentional. Blackley's interpretation leads to dM/dt being the rate of conversion of monomer to polymer in units of number of molecules per converted to polymer per second in unit volume. These units are in fact proportional to more conventional units such as % conversion per hour.

The model employed by Smith and Ewart assumes that the rate of polymerisation occurring within a single locus is independent of the rate of entry of free radicals. Therefore the rate during stage 2 of the polymerisation should be unaffected by the concentration of initiator in the aqueous phase. Any rate dependence upon initiator concentration

must be as a direct result of the number of polymerisation loci generated during stage 1 of the polymerisation.

Smith and Ewart showed that there is a simple relationship for the time elapsed between successive entry of radicals into a locus. If ρ is the total number of radicals that enter N loci in unit time then the average time between successive entry of radicals into a given locus is N/ρ. (A factor 2 appears in the original paper of Smith and Ewart but this seems to be an error[72]).

For the purpose of calculating the number of polymerisation loci present at the stage of the reaction where there are no longer micelles present in the system the following, additional, assumptions were made.

(1) Initially all of the surfactant molecules are present in the form of micelles. The quantities in solution and at the monomer/water interfaces are considered as negligible.

(2) At all subsequent stages the surfactant is distributed between the micelles and growing particles. If S_m is the surfactant present in micelles and S_p the surfactant on the surface of the polymer particles then at all times $S = S_m + S_p$.

(3) The interfacial area ϖ occupied by unit mass surfactant is the same whether the surfactant is in a micelle or on the surface of a polymer particle as long as the system contains micelles, ie. the relationship:

$$\frac{A}{S} = \frac{A_m}{S_m} = \frac{A_p}{S_p} = \varpi \qquad (2.57)$$

where A, A_m, A_p are the respective areas holds from $S_m = S$ to the point

where $S_m = 0$.

(4) During the stage where new polymerisation loci are being formed the ratio of monomer to polymer, within the particles, remains constant.

(5) The rate of polymerisation within a given locus is constant throughout this period. This is reasonable if point 4 above is true.

Point 4 is a little difficult to justify for all systems. It is simple to accept that a crosslinked polymer particle will attain equilibrium with respect to monomer swelling but for a non-crosslinked system it would appear plausible that the polymer particle should continue to swell. Morton, Kaizerman and Altier[73] proposed that there is a restraining force that counterbalances the swelling of a polymer particle. They suggest that there is an increase in interfacial free energy as the particle swells. This is then balanced against the increase in entropy as the monomer mixes with the polymer.

Combining points 4 and 5 it follows that the increase in volume of the particle with respect to time (dv/dt) is constant and not a function of particle size. This constant is denoted by μ.

It is difficult to calculate the exact number of particles, N. Smith and Ewart approached the problem by treating two idealised situations, one which should yield a number greater than reality and the other that should yield a number smaller than reality. The assumption that, so long as there are micelles present they capture all the radicals that are available, yields too many particles as some of the radicals will be captured by existing particles. The alternative assumption is that, a given interfacial area has the same effectiveness at capturing free radicals regardless of the size / curvature of the particle upon which it is situated. This yields too few loci as, from

classical diffusion theory, the diffusion of matter across an interface is inversely proportional to the radius of curvature of the interface.

Calculation for too many loci.

From the assumption above N will be given by ρt^* where t^* is the time elapsed between the start of the reaction and the disappearance of micellar surfactant, ie. the time at which $A_p = A = \varpi S$ and $A_m = 0$. The volume $v(\tau,t)$ at time t of a particle initiated at a time τ is given by:

$$v(\tau,t) = v_o + \mu(t - \tau) \qquad (2.58)$$

where v_o is the volume of the micelle at t=0. This can be considered as negligible so $v(\tau,t) = \mu(t - \tau)$. The surface area $a(\tau,t)$ of a particle at time t can be written down from geometrical considerations:

$$a(\tau,t) = [36 \pi \mu^2 (t - \tau)^2]^{1/3} \qquad (2.59)$$

This can be written as:

$$a(\tau,t) = \theta (t - \tau)^{2/3} \qquad (2.60)$$

where $\theta = [36 \pi \mu^2]^{2/3}$ and is constant if μ is constant. Now Smith and Ewart calculated the aggregate surface area of particles generated in unit volume in the time period τ to $\tau + \delta\tau$ at a time t that is less than t^*. The total number of particles is $\rho\delta\tau$ and each has a surface area of approximately $a(\tau,t)$. Thus the aggregate interfacial area of all the particles in unit volume at time t ($A_p(t)$) is given by the integral:

$$A_p(t) = \int_0^t \rho\, a(\tau,t)\, d\tau = \int_0^t \rho\theta\, (t-\tau)^{2/3}\, d\tau \qquad (2.61)$$

Evaluation of this integral yields:

$$A_p(t) = (3/5)\rho\theta t^{5/3} \tag{2.62}$$

At time t^* at which the micellar surfactant disappears $A_p(t^*) = A = \varpi S$. Thus:

$$(3/5)\rho\theta t^{*5/3} = \varpi S \tag{2.63}$$

This rearranges to:

$$t^* = \left(\frac{5\varpi S}{3\rho\theta}\right)^{3/5} \tag{2.64}$$

and

$$N = \rho t^* = \rho^{2/5}\left(\frac{5\varpi S}{3\theta}\right)^{3/5} \tag{2.65}$$

Inserting the value for θ yields

$$N = (5/3)^{3/5}(36\pi)^{-1/5}\mu^{-2/5}\varpi^{3/5}\rho^{2/5}S^{3/5} \tag{2.66}$$

The value of $(5/3)^{3/5}(36\pi)^{-1/5}$ is normally approximated by 0.53 giving the final result:

$$N \cong 0.53\,\mu^{-2/5}\varpi^{3/5}\rho^{2/5}S^{3/5} \tag{2.67}$$

In this calculation Smith and Ewart are assuming that all particles are growing steadily throughout the time interval t-τ. No free radicals are wasted in termination steps and contrary to the earlier assumption the

average activity of each particle, r, is 1. It has been stated that the Smith-Ewart case 2 value of r = 0.5 applies for the period after the disappearance of the micellar surfactant only. If the value of i is in fact 1 for this initial stage of the polymerisation it would be reasonable to expect a maximum in the reaction rate early on in the polymerisation. This has not been reported in the literature[72].

Calculation for too few loci.

As a consequence of the assumptions relating to this case it follows that the rate of generating new loci at any given point in time is:

$$\frac{dN}{dt} = \rho \frac{A_m}{A} \qquad (2.68)$$

since only radicals captured by surfaces belonging to micelles create new loci. Application of the relationship $A_m + A_p = A = \varpi S$ yields:

$$\frac{dN}{dt} = \rho - \frac{\rho A_p}{\varpi S} \qquad (2.69)$$

The number of new loci generated in the time period τ to $\tau + \delta\tau$ is given by $(dN/d\tau)\delta\tau$, where $dN/d\tau$ is the rate at time τ. As for the case dealt with above the surface area of a particle generated at time τ at a time t is given by equation 2.60. Therefore the contribution to the aggregate surface area at time t for particles generated in the time period τ to $\tau + \delta\tau$ is given by:

$$\theta (t - \tau)^{2/3} \frac{dN}{d\tau} \delta\tau \qquad (2.70)$$

At a time t, where t is less than or equal to t^* the interfacial area of all polymer particles is given by:

$$A_p(t) = \int_0^t \theta\,(t-\tau)^{2/3}\,\frac{dN}{d\tau}\,\delta\tau \qquad (2.71)$$

Substituting this expression for Ap(t) in equation 2.69 yields:

$$\frac{dN}{dt} = \rho - \frac{\rho\theta}{\varpi S}\int_0^t \theta\,(t-\tau)^{2/3}\,\frac{dN}{d\tau}\,\delta\tau \qquad (2.72)$$

A solution of this type is known as a Volterra equation of the second kind. The method is of no interest here but the solution yields the equation:

$$\frac{dN}{dt} = \rho\sum_{s=0}^{\infty}\frac{x^s}{\Gamma(1+5s/3)} \qquad (2.73)$$

where $\Gamma(s)$ is a gamma function of s and $x = -\Gamma(5/3)\,\rho\,(36\,\pi\,\mu^2)^{1/3}\,t^{5/3}\,/\varpi S$. Smith and Ewart then assumed that at time t*, the time at which there is no longer micellar surfactant present in the system, $dN/dt = 0$. They say that by a method of successive approximations they arrived at $x = -2.13$ at the point when $dN/dt = 0$. Fitting this into the definition of x yields:

$$t^* = (2.13)^{3/5}\,\{\Gamma(5/3)\}^{-1/5}\,(36\,\pi)^{-1/5}\,\mu^{-2/5}\,\varpi^{3/5}\,\rho^{-3/5}\,S^{3/5} \qquad (2.74)$$

The value for N is derived from:

$$N = \int_0^t \frac{dN}{dt}\,dt \qquad (2.75)$$

The value for dN/dt is obtained from equation 2.73. The integration yields a series of terms of the form $f(s)t^{5s/3}$. Smith and Ewart found that only the first few terms were required to determine the magnitude of the result.

They reported the final result as:

$$N = 0.370\,\mu^{-2/5}\,\varpi^{3/5}\,\rho^{2/5}\,S^{3/5} \qquad (2.76)$$

Direct comparison of equation 2.67, the equation related to too many loci to equation 2.76 above, the equation for too few loci, shows that they are of the same form. It is therefore concluded that for the real situation the equation is of the form:

$$N = \chi\,\mu^{-2/5}\,\varpi^{3/5}\,\rho^{2/5}\,S^{3/5} \qquad (2.77)$$

where χ is a constant and $0.37 < \chi < 0.53$.

The final equation describing the rate of polymerisation in units of molecules of monomer converted to polymer per unit time in unit volume of aqueous phase during the stage where no micellar surfactant remains, but a separate monomer droplet still exists follows from equation 2.56.

$$\frac{dM}{dt} = \frac{\chi}{2}\,k_p[M]\,\mu^{-2/5}\,\varpi^{3/5}\,\rho^{2/5}\,S^{3/5} \qquad (2.78)$$

2.6.3 Non-ionic surfactants

Non-ionic micelle generating substances (or surfactants) have been applied to emulsion polymerisation where the latex produced is required to be relatively pH insensitive. A large family of surface active non-ionic materials exist based on PEO. The range of materials is almost limitless as there are a large number of potential hydrophobic head groups and the possibility of variation in molecular weight of the PEO chain length. There

has been shown a rather "loose" correlation between the hydrophilic / lipophilic balance (HLB) and the behaviour of a non-ionic surfactant as a stabiliser.

Of more interest to this thesis are the polymeric or oligomeric non-ionic surfactants. There are a range of commercially available copolymers sold under the name Pluronic™. These are block copolymers / oligomers of PEO and poly (propylene oxide) (PPO). The group of Vincent[74,75,76] in Bristol, England have worked with block copolymers of polystyrene (PS) and PEO to stabilise PS emulsions.

Considering the kinetics of emulsion polymerisations Blackley[72] points out that the conversion rates of emulsions stabilised with non-ionic surfactants are lower than for similar formulations with ionic surfactants, eg. sodium salts of fatty acids. It is also pointed out that maximum rates are achieved with surfactants with an HLB value close to the upper limit to confer stability.

2.6.4 Emulsion polymerisation with MMA.

The kinetics of the polymerisation of MMA with an anionic surfactant and initiated by potassium persulphate at 60°C were compared to the equivalent system with styrene by Zimmt[77]. His main conclusion was that the two systems differed in the timing of the autoacceleration effect or `gel´ effect after Norrish[78], Schultz[79] and Trommsdorff[80]. With styrene the `gel´effect appears when the polymer concentration reaches 70%. This is not achieved in the emulsion particle until the monomer droplets have been used up. With MMA the `gel´effect is observed at conversions much lower, ie before the end of the Smith-Ewart stage 2. Zimmt points out that at a conversion of 30% the rate constant for the termination step is 2 orders of magnitude lower than at the beginning of the polymerisation.

This can be expected to effect the average number of free radicals in an emulsion particle, ie. make this number larger than the 0.5 assumed by Smith and Ewart[71].

Gershberg[81] studied the effects of the solubility of the monomer in water. He found that for monomers with solubilities greater than 0.04- 0.07% deviations from the Smith-Ewart theory occur. Smith-Ewart theory predicts that the rate of polymerisation is proportional to the soap concentration to the power 0.6. Gershberg suggests that for MMA as a monomer this proportionality is to the power 0.3 to 0.4. Lee and Longbottom[82] have reconsidered this finding and come to the conclusion that this proportionality is interrelated with initiator type. They have obtained proportionality to soap concentration in the range 0.18 to 0.55 depending on the initiator used.

Emelie, Pichot and Guillot[83] have considered the copolymerisation of MMA with n-butyl acrylate with a non-ionic surfactant PEO-dodecyl ether. They have made comparisons to sodium dodecyl ether (SDS) as an ionic surfactant. They report higher rates of polymerisation for the non-ionic surfactant. They conclude that this polymerisation system has a micellar mechanism for particle nucleation contrary to SDS where homogeneous nucleation also occurs. They report that the system is complicated by the partitioning of surfactant between monomer droplets and the aqueous region and predict that the non-ionic surfactant is buried inside the emulsion particle as it grows, ie. the low HLB material is significantly soluble in the polymer.

3. EXPERIMENTAL

3.1 SYNTHESIS OF BLOCK COPOLYMERS

A series of five AB block copolymers of poly(methyl methacrylate) (PMMA) and poly(ethylene oxide) (PEO) was synthesised by the condensation of carboxyl terminated PMMA with hydroxyl-terminated PEO.

The PMMA component for the five copolymers used in the solution characterisation experiments was generated in a single polymerisation. Therefore, the PMMA components of these copolymers were identical in molecular weight distribution. The PEO components were of five different molecular weights,with nominal molecular weights in the range 550 to 4000 g mol^{-1}. The PEO polymers were products provided by ICI Paints division. The PEO 550 and 750 samples were Union Carbide products and the PEO 1000, 2000 and 4000 were experimental samples made at ICI Petrochemicals, Billingham. The ICI samples were made by the ethoxylation of methoxy ethanol.

At a later stage in this project a second batch of PMMA homopolymer was synthesised. This was undertaken to facilitate the expansion of the investigation into the application of the copolymer in the emulsion polymerisation experiments. The procedure used for the production of the PMMA was a repeat of the original synthesis. This second batch of PMMA was then coupled to the PEO of nominal molecular weight 2000. Characterisation data for this copolymer are provided with the data for the original five copolymers.

A full description of the synthesis of the copolymers is given below.

3.1.1 Purification of Reagents

Methyl methacrylate - Aldrich Chemical Co. Ltd.
Stabiliser was removed by washing with sodium hydroxide solution (0.1 mol/dm^3), followed by washing with distilled water three times. The monomer was then dried over anhydrous calcium sulphate. Finally, immediately prior to use, the monomer was distilled under vacuum.

2-Ethoxyethanol - Fisons SLR grade.
Used as supplied.

4,4′-Azobis(4-cyano-pentanoic acid) - kindly supplied by ICI Paints, Slough.
Recrystallised from warm methanol, dried, then stored under vacuum until used.

Thioglycollic acid - Sigma Chemical Co. Ltd.
Stored at ca. 255K - used as supplied.

Oxalyl chloride - Koch Light Laboratories - kindly supplied by ICI Paints, Slough.
Used as supplied.

Toluene - Aldrich Chemical Co. Ltd.
SLR grade. Used as supplied.

Methanol - Aldrich Chemical Co. Ltd.
SLR grade. Used as supplied.

Petroleum Ether (40-60) - Aldrich Chemical Co. Ltd.
SLR grade. Used as supplied

3.1.2 Preparation of Carboxyl Terminated PMMA

The PMMA sample was prepared by the matched chain transfer method [84,85,86]. The polymerisation was performed in solution with a carboxyl-functionalised azo initiator. Chain transfer was to a carboxyl-functionalised mercaptan.

A flask with reflux condenser and nitrogen purge was charged with 2-ethoxyethanol (160g). The flask was heated to 393K and maintained at this temperature ±5°. To this a pre-mix of monomer, initiator and chain transfer agent (Table 3.1) was added at a constant rate over a period of 1.5 hours.

Table 3.1: Pre-mix of reagents for PMMA synthesis.

Reagent	Weight
2-Ethoxyethanol	80g
Methyl methacrylate	160g
Thioglycollic acid	14.4g
4,4´-Azobis(4-cyano-pentanoic acid)	14.4g

The reaction mixture was maintained at 393K for a further hour before cooling to room temperature. The polymer formed was recovered by precipitation into a solution of sodium chloride in cold distilled water (5%, g/100cm^3). Satisfactory separation could not be obtained with the use of water alone. Isolated polymer was then dissolved in hot methanol and reprecipitated into cold distilled water - this cycle was repeated a further 3 times. The purified polymer was then dissolved in toluene and residual water removed by distillation: Finally the polymer was isolated as a dry white powder by precipitation into petroleum ether (40-60), filtering, and drying under vacuum.

3.1.3 Conversion to Acid Chloride

PMMA (105g) synthesised above was placed in a flask with dry toluene ($300cm^3$). The flask was equipped with a magnetic stirrer, a dropping funnel, a nitrogen purge and a condenser with a drying tube packed with soda lime and silica gel. The polymer solution was cooled to 273K and oxalyl chloride (15g) was added dropwise. The mixture was stirred overnight with the temperature being permitted to rise slowly to 293K.

Oxalyl chloride was selected here in preference to thionyl chloride because of the absence of non-volatile by-products from its reactions. It is conventional to distil off the product after chlorination by thionyl chloride. This is not possible with a polymeric product. Excess oxalyl chloride was removed by vacuum distillation at ca. 10 mm Hg, 293K.

3.1.4 Esterification to form Diblock Copolymer

The PEO samples used were terminated at one end by a methoxy group and at the other end by a hydroxyl group. In the esterification reaction only the hydroxyl group can take part, eliminating the production of ABA copolymers. The PEO samples used had nominal molecular weights of 550, 750, 1000, 2000 and 4000 g mol^{-1}.

Weighed samples of the five PEO homopolymers were dissolved in toluene and dried over molecular sieve 4Å. Concentrations of PEO solutions were determined by solids evaluation after the drying process. PEO is hygroscopic and tends to collect water from the air. Thus, weighing of the solid polymers to establish concentrations would include unnecessary errors.

Portions of the five toluene solutions, each containing approximately 0.02 moles of the appropriate polymer were placed in flasks protected by drying tubes. Table 3.2 contains the weights used.

Table 3.2: Weights of PEO used in the syntheses.

Polymer	Weight
Methoxy - PEO 550	11g
Methoxy - PEO 750	15g
Methoxy - PEO 1000	20g
Methoxy - PEO 2000	40g
Methoxy - PEO 4000	80g

The acid chloride terminated PMMA solution produced in section 3.1.3 was divided into five equal portions and added to the five PEO samples. At all times solutions were kept under a dry nitrogen atmosphere and protected by drying tubes containing anhydrous silica-gel. Each of these mixtures was heated to 383K and maintained at this temperature with a rapid flow of nitrogen through the solution for approximately 24 hours.

3.1.5 Isolation of Block Copolymers

Each solution of copolymer was decanted into cold petroleum ether (40-60), filtered, and the white precipitate or, in low molecular weight cases, clear yellow liquid retained and dried under vacuum. Copolymers were then reintroduced to water and passed through an ion-exchange resin IRA-400 (Fisons). This resin removes anions from solution, i.e. any unreacted acid terminated PMMA.

In each case the copolymer was removed from the water by heating the solution to a temperature above the cloud point of the copolymer but

below that of the PEO, permitting the copolymer to settle, then decanting off the aqueous phase. Any unreacted PEO should preferentially remain in the aqueous phase. The polymer was redissolved and this procedure repeated three times.

Purified copolymers were finally dissolved in toluene. Water was removed by distillation and copolymer then precipitated into petroleum ether (40-60). Dried samples were bottled and labelled as:-

Table 3.3: Labelling of copolymers.

Nominal PEO Molecular weight	Label
550 g mol^{-1}	Copolymer 550
750 g mol^{-1}	Copolymer 750
1000 g mol^{-1}	Copolymer 1000
2000 g mol^{-1}	Copolymer 2000
4000 g mol^{-1}	Copolymer 4000
Sample from repeat synthesis	
2000 g mol^{-1}	Copolymer 2000b

3.2 POLYMER CHARACTERISATION

3.2.1 Titrimetric End Group Analysis

The number average molecular weight ($\overline{M}_n$) of the PMMA was determined by end group analysis. Each chain was expected to contain one carboxylic acid group.

Three parallel determinations were performed. In each polymer (1g) was accurately weighed and then dissolved in ethanol. The resultant solutions were titrated with standardised ethanolic sodium hydroxide using phenolphthalein as an indicator. $\overline{M}_n$ was then calculated assuming one acid group per chain.

3.2.2 Infra-red Spectroscopy (IR)

Infra-red spectra were recorded using a Perkin Elmer 257 infra-red spectrophotometer for solutions of PEO and PMMA at concentrations of 0.5 mg cm^{-3} to 3.0 mg cm^{-3}. Plots were made of absorbance at 1110 cm^{-1} and 1730 cm^{-1} vs. concentration. Spectra were recorded for all copolymer samples at concentrations of 2.5 mg cm^{-3}. From the measured absorbances at 1110 cm^{-1} and 1730 cm^{-1} the composition of copolymers was calculated.

3.2.3 Gel Permeation Chromatography

Preliminary GPC work was carried out at Loughborough but it was found that the column set available was not suited to polymers of such a low molecular weight.

Subsequent characterisation work was carried out with the aid of GPC

instrumentation at the PSCC, RAPRA, Shawbury, Shrewsbury, Shropshire. All samples were run with tetrahydrofuran (THF) as solvent, and with ultraviolet (UV), infra-red (IR), and refractive index (RI) detectors in operation. The column set was the RAPRA set `A´. This set comprises two PLgel columns (2x60cm) having 500Å and 100Å nominal exclusion limits (Polymer Laboratories Limited). This set has an exclusion limit at a molecular weight of approximately 5000 g mol^{-1}. The detectors were arranged in the order UV, IR, RI. The UV detector was set at 246nm. This value is as close to the maximum absorbance for PMMA as could be attained in THF. THF itself absorbs below 240nm. The IR detector was used at a wavelength of 5.80μm (wavenumber 1724 cm^{-1}) to respond to the carbonyl function on the PMMA. The RI detector responds to the presence of both PEO and PMMA polymers.

Samples of all homopolymers, copolymers and mixtures of homopolymers corresponding to the expected composition of the copolymers were studied.

3.2.4 Characterisation of PEO by ^1H Nuclear Magnetic Resonance Spectroscopy (^1H nmr)

An adaptation of the work of Goldwasser and Adolf[87] was employed to quantify the hydroxyl content of the five PEO samples used in the synthesis of the copolymers.

The ^1H nmr of PEO is dominated by the methylene ($-CH_2-$) protons centred at δ = 3.8ppm. The methoxy protons (CH_3-O-) are at δ = 3.65ppm and on a 60MHz ^1H nmr are not totally separable from the methylene protons. The integrated spectra can give estimates of molecular weight but with a large degree of uncertainty.

The method of Goldwasser and Adolph involves reacting the hydroxyl groups with trifluoroacetic anhydride to give quantitatively the trifluoro-acetate.

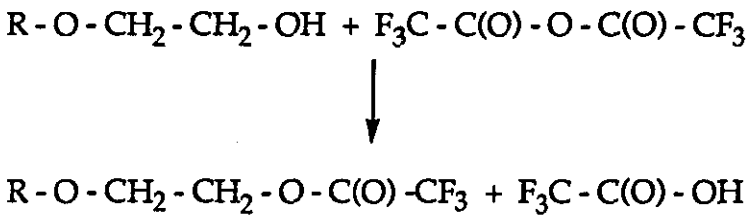

This derivative shows, in the ^1H nmr spectrum, complete resolution of the terminal methylene peak. The terminal methylene peak is shifted to about δ =4.48 ppm. The penultimate methylene peak is also shifted downfield but only enough to be partially resolved.

Each polymer (50mg) was weighed into a nmr sample tube. Deuterated trichloromethane (approximately 0.5cm^3) was added and the polymers given time to swell and dissolve. An excess of trifluoroacetic anhydride (50µl) was added to each and the tube agitated to ensure good mixing. TMS was added and then spectra recorded on a `Varian XL-300´ 300MHz nmr spectrometer.

3.2.5 Characterisation of Copolymers by ^1H Nuclear Magnetic Resonance Spectroscopy.

A Varian EM-360 60 MHz nmr spectrometer was used to obtain spectra for all homopolymer and copolymer samples. Spectra were obtained from polymer solutions in deuterated trichloromethane. The integrated spectra were used to estimate relative proportions of PMMA and PEO in the copolymer.

3.3 CHARACTERISATION OF COPOLYMER IN SOLUTION

3.3.1 Cloud Point Determination

Each copolymer was dissolved in the minimum quantity of spectroscopic grade methanol. Water was slowly added with the solution being rapidly stirred. The solution was then distilled at reduced pressure (<0.1 Torr) and ambient temperature to approximately 60% its original volume. The polymer concentration of each solution was determined by solids determination and water was added to each to reduce the concentration to 1%.

Visual determination

Each solution was slowly heated until the first sign of haze was observed. The solution was permitted to cool by a few degrees and given time to re-equilibrate. The solution was then very slowly heated (ca. 1° every 2 mins). The temperature corresponding to the first sign of a haze was noted as the visual cloud point.

Automated determination

The cell depicted in figure 3.1 was designed to fit within the sample chamber of a Unicam SP 600 UV spectrophotometer. It comprises a water jacket connected to an external thermostatically controlled water bath. The cell itself is constructed of glass with two of its sides being planar and serving as windows for the spectrometer beam. The cell is provided with a glass stirrer and a copper / constantan thermocouple. The water temperature supplied to the outer jacket was slowly raised and the absorbance of light monitored as a function of the temperature.

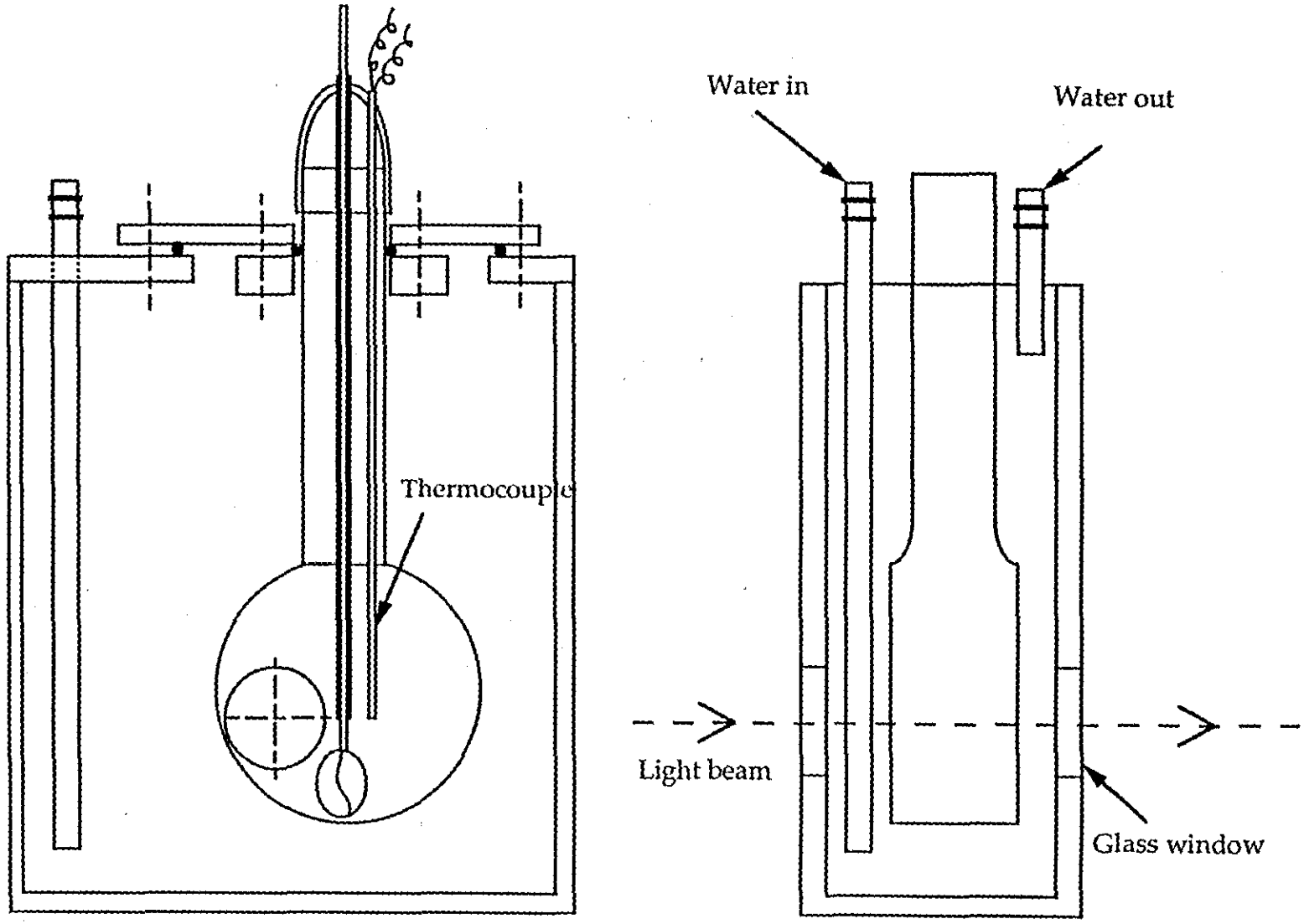

Figure 3.1: Cell for cloud point analysis of copolymers in solution

3.3.2 UV/Vis spectroscopy

Samples of copolymers 1000 and 2000 were dissolved in the minimum quantity of spectroscopic grade methanol. Water was slowly added to each solution. The solutions were then distilled at reduced pressure (<0.1 Torr) and ambient temperature to approximately 60% their original volumes. The copolymer concentration of each solution was established by solids determination and water was added to each to reduce the concentration to 5%. From these stock solutions ranges of copolymer solutions (1% solids) were prepared with methanol contents of 0% to 80% at intervals of 10% for each copolymer. In every case the water dilution took place before the introduction of methanol. Ultra-Violet/Visible spectra were recorded on a Shimadzu UV/Vis spectrophotometer UV-160.

3.3.3 Small Angle X-ray Scattering (SAXS)

Small Angle X-ray Scattering (SAXS) was used to study the micellar nature of the five copolymers both in aqueous solution and, for two of the copolymers, in water/methanol mixtures. If a core-shell structure of spherical micelles is assumed SAXS data can be used to calculate both core dimensions and shell thicknesses.

a) The camera, detector and data logging

A Rigaku Denki (catalogue No. 2202) camera with slit collimation and counter detector was employed for all SAXS work in this project. The X-ray source was a fine focus copper target tube coupled to a Hiltonbrooks 3kW generator operating at 40kV and 24mA. Before collimation CuK_β X-rays were selectively removed with the aid of a nickel filter. Thus the X-rays used for the scattering experiment were CuK_α with a wavelength of λ

= 1.542 Å.

Collimation was achieved with the aid of 3 slits before the sample, and two immediately before the detector. The camera is displayed schematically in figure 3.2 with the inter-slit distances tabulated in table 3.4. The slit positions and dimensions were identical to those reported by Warner[88]. Slits 1, 2, 4 and 5 were of fixed dimensions. Slit 3 consisted of two blocks which could be moved independently. The slit dimensions are recorded in table 3.5. The slit width of slit 3 varied slightly each time it was realigned but 0.12 mm was the approximate dimension.

Table 3.4: Inter Slit Dimensions for the Rigaku Denki Camera.

From	To	Dimension
Cu Target	Slit 1	80 mm
Cu Target	Slit 2	430 mm
Cu Target	Slit 3	510 mm
Cu Target	Sample	520 mm
Sample	Slit 4	330 mm
Sample	Slit 5	370 mm

Table 3.5: Slit Dimensions for the Rigaku Denki Camera.

Slit	Height	Width
1	10 mm	0.2 mm
2	10 mm	0.1 mm
3	20 mm	~0.12 mm
4	8 mm	0.3 mm
5	15 mm	0.1 mm

Scattered X-rays were measured by a Nuclear Enterprise DMI-2 beryllium windowed scintillation detector.(sodium iodide activated with thallium)

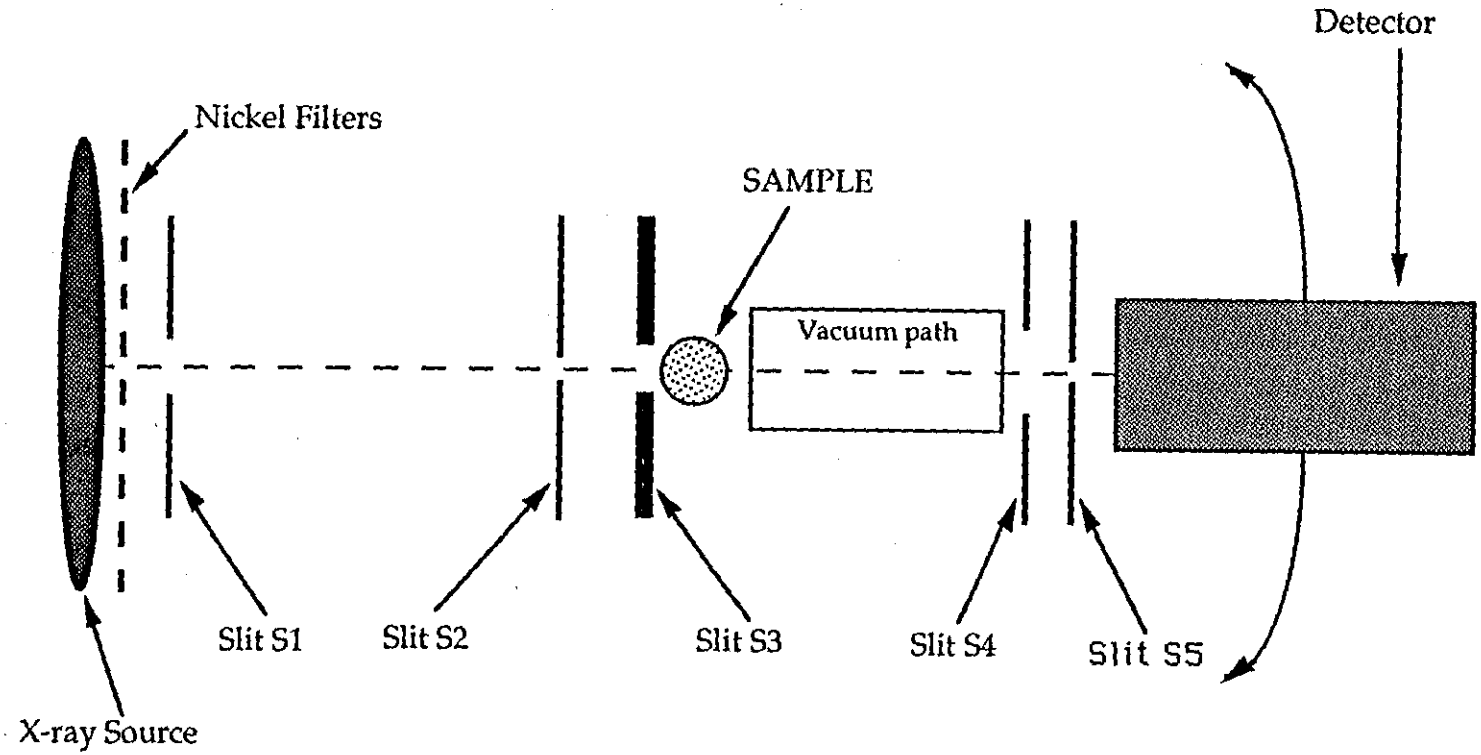

Figure 3.2 Rigaku Denki SAXS Camera

Pulse height discrimination was used to obtain monochromatic measurements. In early experiments data were collected and stored on a Laben 100 spectroscope. This spectroscope was restricted to collecting 100 data points. Later in the project, the equipment was upgraded with a stepping motor being fitted and data collection control transferred to an Apple microcomputer. The computer, in addition to data collection, was used for all timings and operation of the stepping motor.

b) Camera Alignment

The camera was aligned at the commencement of this study, and after replacement of the copper target tube, in accordance with the procedure described in the Rigaku Denki manual. Slit 3 was periodically realigned in accordance with the procedure described by Warner [88].

Slit 3 was opened to approximately 0.3mm. The detector was set at an angle of 0.07° to the right hand side of the beam. Whilst monitoring the intensities of the beam on the spectroscope, the left hand block of slit 3 was slowly moved into the beam. At the point where the beam begins to reflect from the edge of the slit the detected intensity increased dramatically. From this position the block was moved back 0.03 mm. The detector was then moved to the left side of the beam and the procedure repeated with the right hand block. Symmetry was checked by locating a Lupolen polyethylene standard sample (Kindly supplied by Professor Kratky, University of Graz) in the camera and counting at the two positions plus and minus 0.05°. This simple test was performed before each use of the camera. Realignment was deemed to be necessary when the symmetry in this test was lost.

c) Infinite Height Criteria

As described in the theory section of this thesis (section 2.4.1), the

desmearing techniques employed in the interpretation of SAXS data assume infinite height slit optics. To meet this requirement, the relation L $\geq 2m + \sigma$ as in equation 2.24 must be satisfied, where L is the height of the homogeneous part of the beam, σ is the height of the detector slit and m is the angular distance measured in the plane of the measurement. For the given optics (tables 3.4 and 3.5) L = 34 mm, σ = 8 mm, thus in the limit of L = $2m + \sigma$, σ = 13 mm. Therefore, the angle over which the infinite optics assumption is valid is given by:

$$2\theta = 2 \sin^{-1} (\sigma / 2 / \text{Distance from sample to S4})$$

$$2\theta = 2.26°$$

d) Controlled Temperature Sample Cell

The thin glass capillary sample tubes were mounted in a brass sample holder. An electrical heating coil and thermistor was mounted within the walls of the holder. Proportional control enabled the block temperature to be thermostatically controlled to better than ± 0.5°. A copper/constantan thermocouple was positioned close to the sample to monitor the actual sample temperature. In order to restrict cooling by air flow, two X-ray transparent windows, (Mylar films), were located one each side of the sample holder. Figure 3.3 shows the construction of this cell.

Figure 3.3. Cell for Temperature Control of SAXS Samples

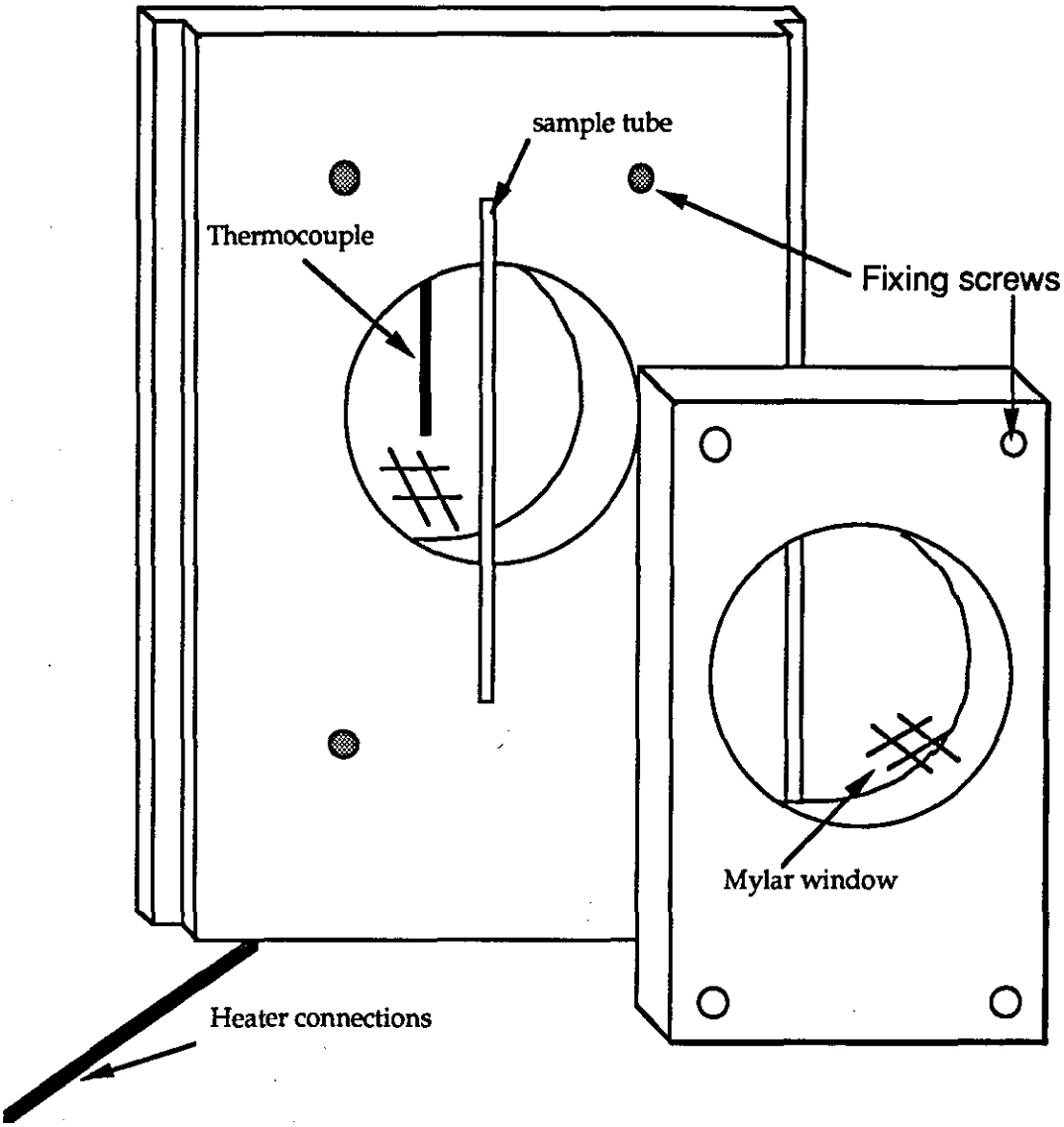

e) Sample preparation

Samples of copolymers were dissolved in the minimum quantity of spectroscopic grade methanol. Water was slowly added to each solution. The solutions were then distilled at reduced pressure (<0.1 Torr) and ambient temperature to approximately 60% their original volumes. Care was taken not to exceed the cloud point temperature of the given copolymer. The copolymer concentration of each solution was established

by solids determination, and water was added to each to reduce the concentration to that required for the particular experiment. SAXS investigations were carried out on copolymers 750, 1000, 2000 and 4000 in aqueous solutions at concentrations from ca. 1 to 10 wt.%

Investigations were also carried out on copolymer solutions in methanol / water mixed solvent systems. In these cases solutions of the copolymer in water were made as above and subsequently diluted with water and methanol to give a concentration of 1% polymer. In every case the water dilution took place before the introduction of methanol.

Solutions were filtered in order to remove dust then introduced into Lindemann glass capillary tubes. The tube tops were sealed in a propane gas flame. Care was taken to minimise the heating of the sample during the sealing operation. Sealing was required to prevent evaporation of solvent during an experiment.

f) Data acquisition

Samples were placed in the camera in either the thermostatically controlled sample holder or in an ambient temperature sample holder. All samples were scanned over an angular range of 0.06° to 1.05° in increments of 0.01°. Counts were made over 100, 200 or 500 seconds at each position. The selection of the time period was dependent upon the concentration of the sample and the scattering intensity from the sample.

After each sample had been scanned the sample tube was replaced by a tube containing distilled water. This `Blank´ sample was then scanned over the complete angular range. This background count was subtracted from the sample count before further processing.

g) Determination of Attenuation Factor

In order to obtain a measure of the attenuation factor, a strongly scattering sample was placed in the scattering position. The scattering intensity was measured at an appropriate angle for 500 seconds. The sample was then located in an absorbing position, behind slit 5, and the intensity measured again. The attenuation factor was taken to be the ratio of the intensity recorded with the sample in the absorbing position to that recorded with no sample.

h) Absolute Intensities

The Rigaku Denki camera was calibrated to give absolute intensities with the aid of the Lupolen standard supplied by Professor Kratky. The standard was placed in the scattering position and the intensity measured by counting over 1000 seconds at an angle of 0.589°. The measurement with the standard in the scattering position multiplied by the attenuation factor gave the standard intensity `I_S´.

i) Processing of `Raw Data´

The scattering data with the background data subtracted were plotted against 2θ over the angular range 0.06° to 1.05°. In order to carry out the desmearing of the data the curve was fitted to a Fourier series. To assist this process the data for the region 0° to 0.06° were estimated. It was not possible to obtain experimental information in this region because of the proximity to the high intensity of the main beam. It is difficult to model a curve with a Fourier series if it has a large gradient at its extremities. This was considered in the extrapolation of the curve over these additional 5 data points, the curve was smoothed over to give a gradient close to zero at the point $2\theta = 0°$. As a result of the nature of the experiment there is a

large statistical spread in the results. To prevent the computer program from attempting to model every statistical fluctuation a slight smoothing of the curve was performed before the data were entered into the desmearing program. The desmearing program was a Fortran program kindly supplied to the University by Professor Vonk[89]. Approximately 25 to 30 terms of the fourier series were required to model the scattering curves.

Further calculations on the scattering data will be handled in the results section of this thesis.

3.4 POLYMERISATION OF METHYL METHACRYLATE USING COPOLYMER STABILISERS

3.4.1 Purification of Reagents

Water

Doubly distilled water was used for all experiments.

Methyl methacrylate monomer - Aldrich Chemical Company.

Stabiliser was removed by washing with dilute sodium hydroxide followed by three washes with distilled water. The monomer was dried over anhydrous calcium sulphate, then decanted into a vacuum vessel and degassed. The monomer was vacuum distilled at room temperature immediately prior to use.

Methanol - Aldrich Chemical Co. Ltd.

Spectroscopic grade, used as supplied.

Ammonium Persulphate - B.D.H.Chemicals Ltd.

Used as supplied

Sodium Metabisulphite - Fisons

Used as supplied

L-Ascorbic Acid - Fisons

Used as supplied

Potassium Permanganate - B.D.H. Chemicals Ltd

Used as supplied

4,4′-Azobis(4-cyano-pentanoic acid) - kindly supplied by I.C.I. Paints Slough

4,4′-Azobis(4-cyano-pentanoic acid) was recrystallised from warm methanol, dried, then stored under vacuum.

2,2′-Azobisisobutyronitrile

2,2′-Azobisisobutyronitrile was recrystallised from warm methanol, dried, then stored under vacuum.

3.4.2 Procedures for Emulsion Polymerisations

The emulsion polymerisation experiments were very sensitive to variations in the form of the copolymer on addition to the reaction vessel. There were three basic methods employed differing in the method of copolymer addition.

1) Copolymer dissolved directly in water.
2) Copolymer dissolved in monomer.
3) Copolymer dissolved in methanol before introducing it to water.

Methods for Polymerisation.

The aqueous phase was introduced into a reaction vessel provided with a water cooled condenser, a nitrogen bleed, magnetic stirrer and a side arm with a rubber seal. The side arm was used for the addition of reagents and for the removal of samples. The reaction vessel was immersed in a constant temperature water bath (controlled to ± 0.1°). During the period of thermal equilibration a strong flow of nitrogen was used to purge the system of oxygen. The nitrogen flow was reduced to a slow 'trickle' and the monomer added. A small quantity of sodium metabisulphite was added to remove any remaining oxygen. After a period of three minutes

the appropriate initiator was added in a small quantity of water.

The three methods of polymerisation differ in the addition of the copolymer to the system.

Method 1.

The copolymer was added to the reaction vessel before the water, and time allowed for the copolymer to fully dissolve before the monomer was added. Heat was used to assist the dissolving of the copolymer but this temperature did not exceed the polymerisation temperature.

Method 2.

The copolymer was added to the monomer and time allowed for the copolymer to dissolve; slight warming was generally employed to speed up this process.

Method 3.

The copolymer was first dissolved in the minimum quantity of spectroscopic grade methanol and then water was added slowly with rapid stirring. The methanol was then removed from the system by vacuum distillation. Care was taken not to exceed the cloud point of the copolymer during this stage. Finally the solids content of the solution was determined and the appropriate dilution performed. Batches of about 200cm^3 of 5% copolymer solution were prepared at a time and were stored under nitrogen in the absence of light until used.

3.4.3 Initiator Systems

Two redox initiator systems were employed: Ammonium persulphate/ sodium metabisulphite and ascorbic acid/potassium permanganate.

Two azo type initiators were employed: 4,4′-Azobis(4-cyano-pentanoic acid) from the aqueous phase and 2,2′-Azobisisobutyronitrile from the organic (monomer) phase.

3.4.4 Thermocouple method for Monitoring Polymerisations

It was found that for the ammonium persulphate/ sodium metabisulphite redox initiator system that the rate of reaction was very high. In order to follow the progress of this rapid reaction a copper/constantan thermocouple sheathed in a thin glass tube was introduced into the centre of the reaction mixture (after the methods of Bengough and Melville[90,91]). During the reaction the rise in potential created by the reaction exotherm was plotted against time. The loss of energy from the system was assumed to be proportional to the temperature difference between the reactor and the surrounding water. Hence the energy liberated by the polymerisation reaction can be considered to be proportional to the rise in temperature. This method is similar to the technique of Differential Thermal Analysis (DTA) where ΔT is recorded as a function of time.

3.4.5 Differential Scanning Calorimetry for Monitoring Polymerisations

A Perkin-Elmer® DSC 4 was used in an isothermal mode to follow reaction kinetics quantitatively. Perkin-Elmer high pressure steel capsules (part no. B011-7623) with aluminum inserts designed by the author and manufactured at Loughborough University were used to contain the samples.

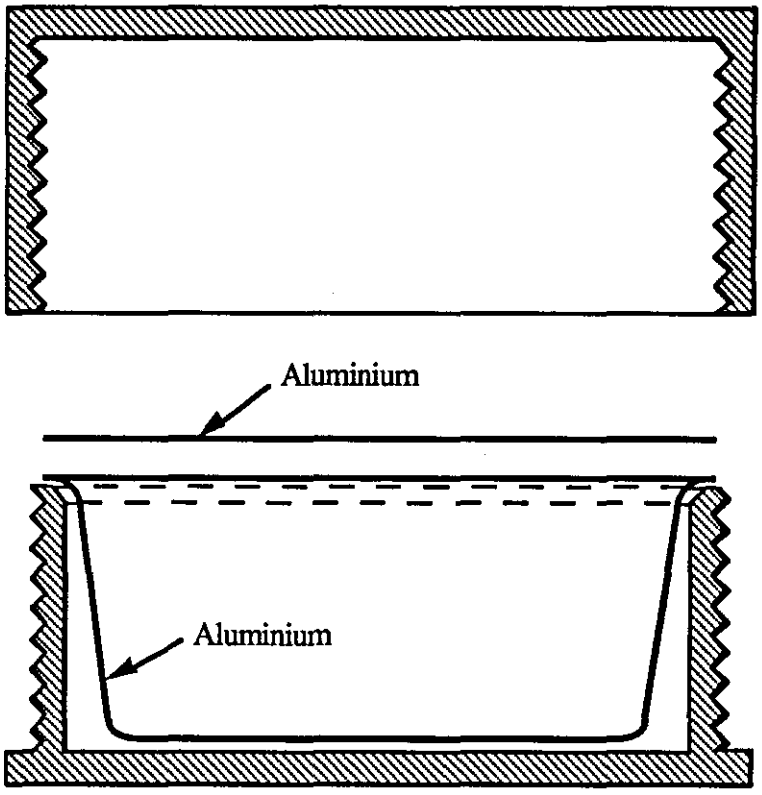

Figure 3.4 DSC Sample Encapsulation For Emulsion Polymerisation.

The procedure for a large scale polymerisation was followed but the reagents were mixed at 278K and not the reaction temperature. From this mixture a sample of approximately 10 mg was loaded into the capsule. The capsule was then introduced into the DSC 4, with the instrument at 278K. The DSC was then programmed to heat to the reaction temperature at the fastest possible rate. This is nominally 200° min^{-1} but as a consequence of the large mass of the sample pan (ca. 0.5g) the real heating rate is estimated to be approximately 100° min^{-1}. The reaction temperature was maintained until the reaction exotherm had ceased and the DSC trace returned to a level baseline.

3.4.6 Solids Content Determination for Monitoring Polymerisations

Small scale polymerisations were performed with a total volume of about 14.5 cm^3. At intervals, typically every 15 minutes, during the reaction samples of approximately 0.2 g of reaction mixture were removed and placed in pre-weighed sample tubes. Immediately after extraction the samples were quenched in liquid nitrogen. After re-weighing sufficient acetone was added to flocculate the polymer. The samples were dried, under vacuum at room temperature, to constant weight. From the solids contents of the samples plots of conversion vs. time were constructed.

3.5 CHARACTERISATION OF EMULSION POLYMERS

3.5.1 Transmission Electron Microscopy (TEM)

Two transmission electron microscopes were used during this project, a Joel TEM 100CX and an AEI EM6G. Samples were prepared by diluting with distilled water, (1 drop in 5 cm^3). A carbon film on a copper grid was prepared for each sample and used with the film still moist. A dry carbon film tended to be lifted from the grid by the surface tension of these dilute emulsions. One drop of emulsion was placed on the grid and the excess water drawn away by the use of a filter paper. Final drying occurred during the evacuation of the microscope.

A minimum of three photographs was taken of particles from each sample, each photograph displaying typically 20 particles. The diameter of each particle was measured manually. Calibration of the microscope was carried out each time the microscope was used. Calibration was achieved by photographing a standard grid at each magnification used.

3.5.2 Gel Permeation Chromatography (GPC)

Selected emulsion polymers were characterised by GPC at RAPRA, Shawbury, Shrewsbury, Shropshire. The column set used comprised $1x10^6$Å, $1x10^5$Å, $1x10^4$Å and $1x10^3$Å PLgel® columns. THF was used as the solvent and refractive index and UV detectors used to monitor the eluting polymer. Calibration was performed with polystyrene standards and correction performed via a universal calibration curve. The values for the constants used in the modified Mark Houwink equation [$\eta=KM^{\alpha}$] were:

PS	$K=1.21x10^{-4}$	$\alpha= 0.71$
PMMA	$K=1.28x10^{-4}$	$\alpha=0.69$

3.5.3 Electrophoresis

The electrophoretic mobilities of selected emulsions were measured using a Rank Brothers electrophoresis instrument fitted with a Helium/Neon laser and rotating prism.

Averaging over a large number of particles was achieved by the use of the rotating prism. For each sample the prism rotational speed and the applied potential were adjusted until as many particles as possible appeared stationary on the monitor. In order to avoid errors in the measurement of the applied potential, secondary electrodes were used to measure the real potential across the sample.

A cylindrical cell was used and measurements were made at the calculated stationary levels at a distance `s´ from the cell wall where :

$$s = d \times 0.146$$

and d was the diameter of the cell

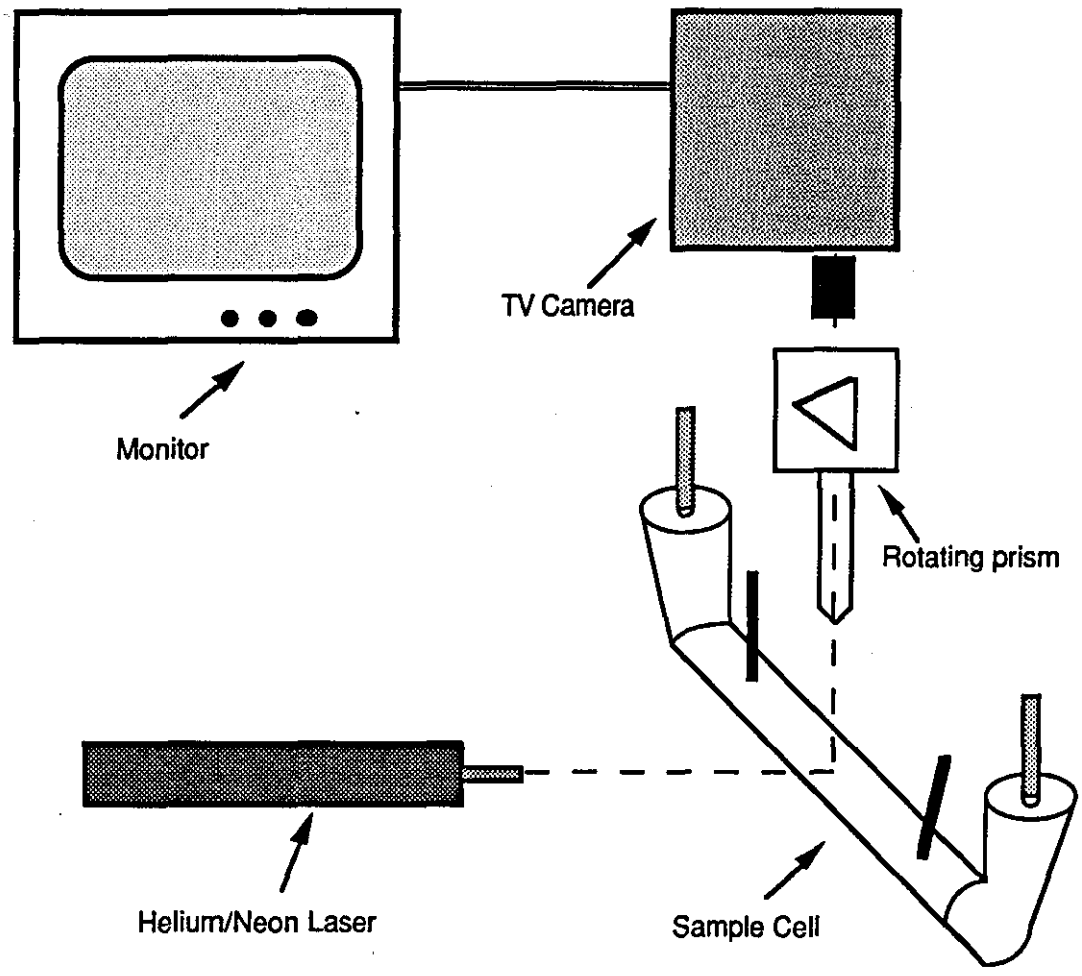

Figure 3.4 Electrophoresis instrumentation.

3.6 SUBSIDIARY EXPERIMENTS

3.6.1 Determination of monomer solubility in water

The solubility of methyl methacrylate monomer (MMA) in water was determined over the temperature range 283K to 353K by Gas Liquid Chromatography (GLC). The instrumentation used was a Perkin-Elmer 3920.

Samples for analysis were prepared by placing 100 cm^3 of distilled water along with 10 cm^3 in a stoppered flask. The flask was maintained at the desired temperature for 15 minutes with vigorous shaking approximately every 2 minutes. The two phases, still at the test temperature, were then permitted to separate (ca. 15 minutes) and a 1 cm^3 sample of the aqueous phase extracted. This sample was then mixed with 1 cm^3 of water containing 1wt.% of acetone. Three 100 μm^3 samples of the mixture were injected onto the GLC column and the ratio of the areas of the peaks corresponding to MMA and the acetone were recorded. At each temperature three such samples were extracted and the MMA content determined.

Calibration of the GLC was achieved by injecting five samples of water containing 1.0 wt.% MMA and 1.0 wt.% acetone. The arithmetic mean of these results was used as the calibration constant.

4.RESULTS

4.1 RESULTS OF BLOCK COPOLYMER SYNTHESIS

Samples of six diblock copolymers were successfully synthesised and recovered. With the exception of copolymer 2000b (Nomenclature from table 3.3), the samples originated from a single polymerisation of methyl methacrylate. Copolymer 2000b originated from a duplication of the polymerisation and is characterised separately. The physical appearance of the samples is described in table 4.1 below.

Table 4.1: Physical description of copolymers.

Copolymer	Description
550	Clear/yellow viscous liquid
750	Clear/yellow viscous liquid
1000	White waxy solid melts just above room temperature.
2000	White powder
4000	White powder
2000b	Slightly yellow solid

Copolymer 2000b was not isolated as a powder but as a granular solid. The molten polymer was poured as a thin stream into liquid nitrogen. The resulting fibres were broken into small lengths (~2-5mm).

4.2 CHARACTERISATION OF HOMO- AND CO-POLYMERS

4.2.1 End group analysis of PMMA.

Each of the two batches of homopolymer was analysed in triplicate. The mean of these results was taken to be the number average molecular weight ($\overline{M}_n$) in each case.

PMMA first batch $\overline{M}_n = 908$ gmol^{-1}, second batch $\overline{M}_n = 920$ gmol^{-1}

4.2.2 Infra-red Spectroscopy.

Calibration plots for concentration of PEO vs. absorbance at 1110 cm^{-1} and for concentration of PMMA vs. absorbance at 1730 cm^{-1} are displayed as figures 4.1 and 4.2 respectively.

Results from the I-R spectra recorded on samples of each of the six copolymers are presented in table 4.2 below. The calculated compositions are given as the weight fraction PEO assuming the weighed polymer sample to be 100% polymer with no residual solvent or absorbed water.

Table 4.2: Summary of I-R analysis of copolymer composition.

Copolymer	Absorbance at 1110 cm^{-1}	Absorbance at 1730 cm^{-1}	% PEO from 1110 cm^{-1}	% PEO from 1730 cm^{-1}
550	0,160	0.382	32	32
750	0.180	0.387	36	32
1000	0.253	0.340	52	40
2000	0.352	0.205	68	64
4000	0.335	0.200	64	64
2000b	0.343	0.206	66	65

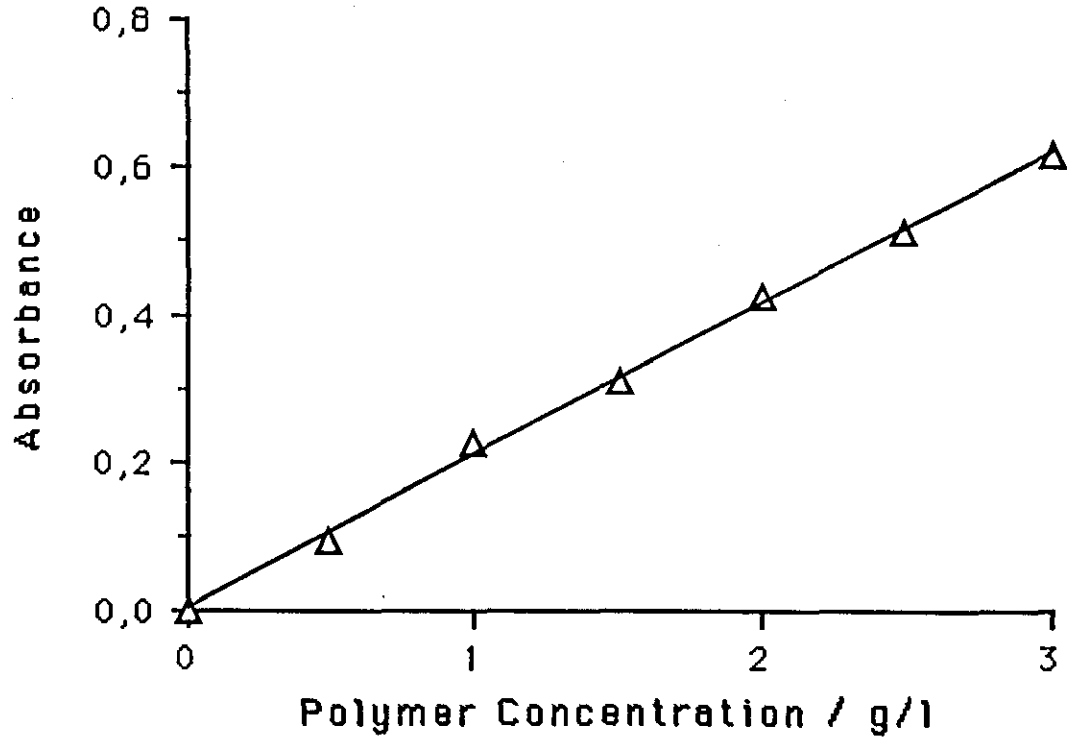

Figure 4.1: Plot of absorbance at 1110 cm^{-1} as a function of PEO concentration.

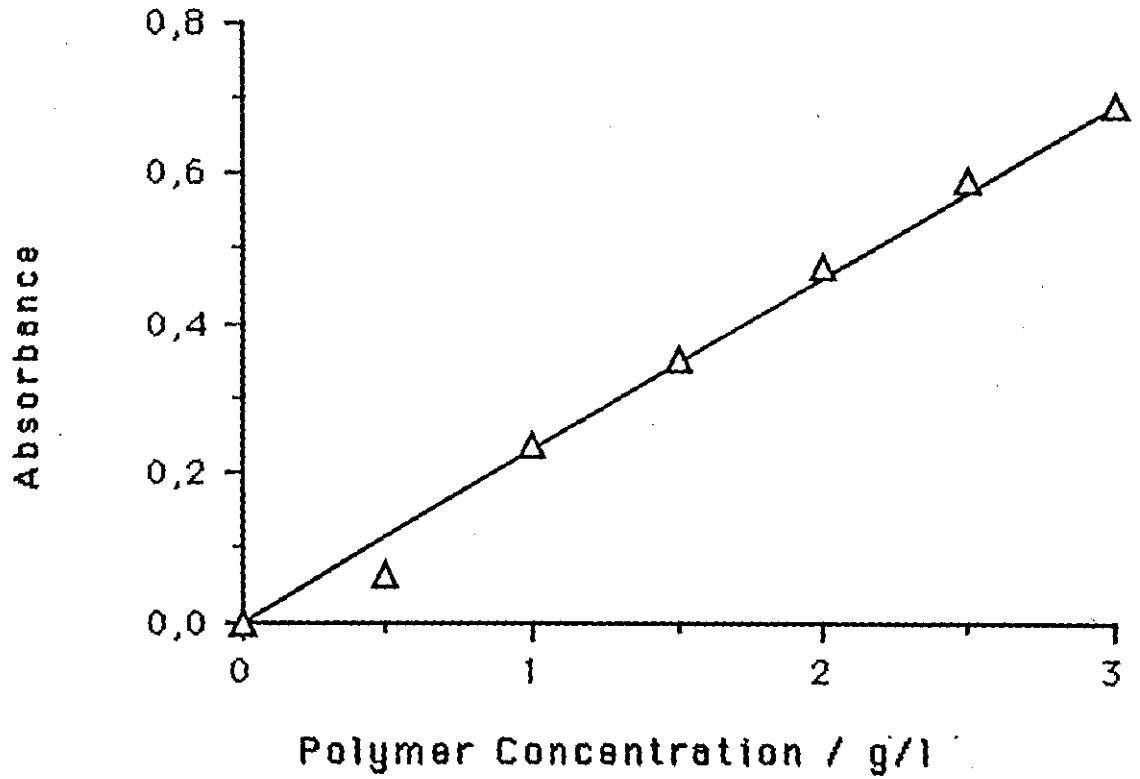

Figure 4.2: Plot of absorbance at 1730 cm^{-1} as a function of PMMA concentration.

These results are subject to a large degree of uncertainty as; firstly, no account was made for the contribution of the second polymer to the absorbance at each wavelength; and secondly, for practical reasons, peak heights rather than peak areas were used in the determinations.

4.2.3 Gel Permeation Chromatography.

Chromatograms obtained with the refractive index (RI) detector are presented for each of the original five copolymers with chromatograms of the corresponding homopolymers displayed alongside. These chromatograms are labelled as figures 4.3, 4.4, 4.5, 4.6, and 4.7 which correspond to copolymers 550, 750, 1000, 2000, and 4000 respectively.

The data computed from the above chromatograms are summarised in table 4.3 below. All molecular weights are quoted as polystyrene equivalents.

Table 4.3: GPC data calculated from RI detector chromatograms.

SAMPLE	M_p	$\overline{M}_n$	$\overline{M}_w$	$\overline{M}_w/\overline{M}_n$
PMMA	1405	1237	1605	1.30
PEO 550	845	760	810	1.07
Copolymer 550	1720	1600	2110	1.32
PEO 750	1060	862	1130	1.32
Copolymer 750	2020	2010	2700	1.34
PEO 1000	1310	1320	1420	1.07
Copolymer 1000	2230	2410	3160	1.31
PEO 2000	2630	2610	2740	1.05
Copolymer 2000	3570	2700	3860	1.43
PEO 4000	4760	4240	5290	1.25
Copolymer 4000	5470	2690	5480	2.03

All values polystyrene equivalents

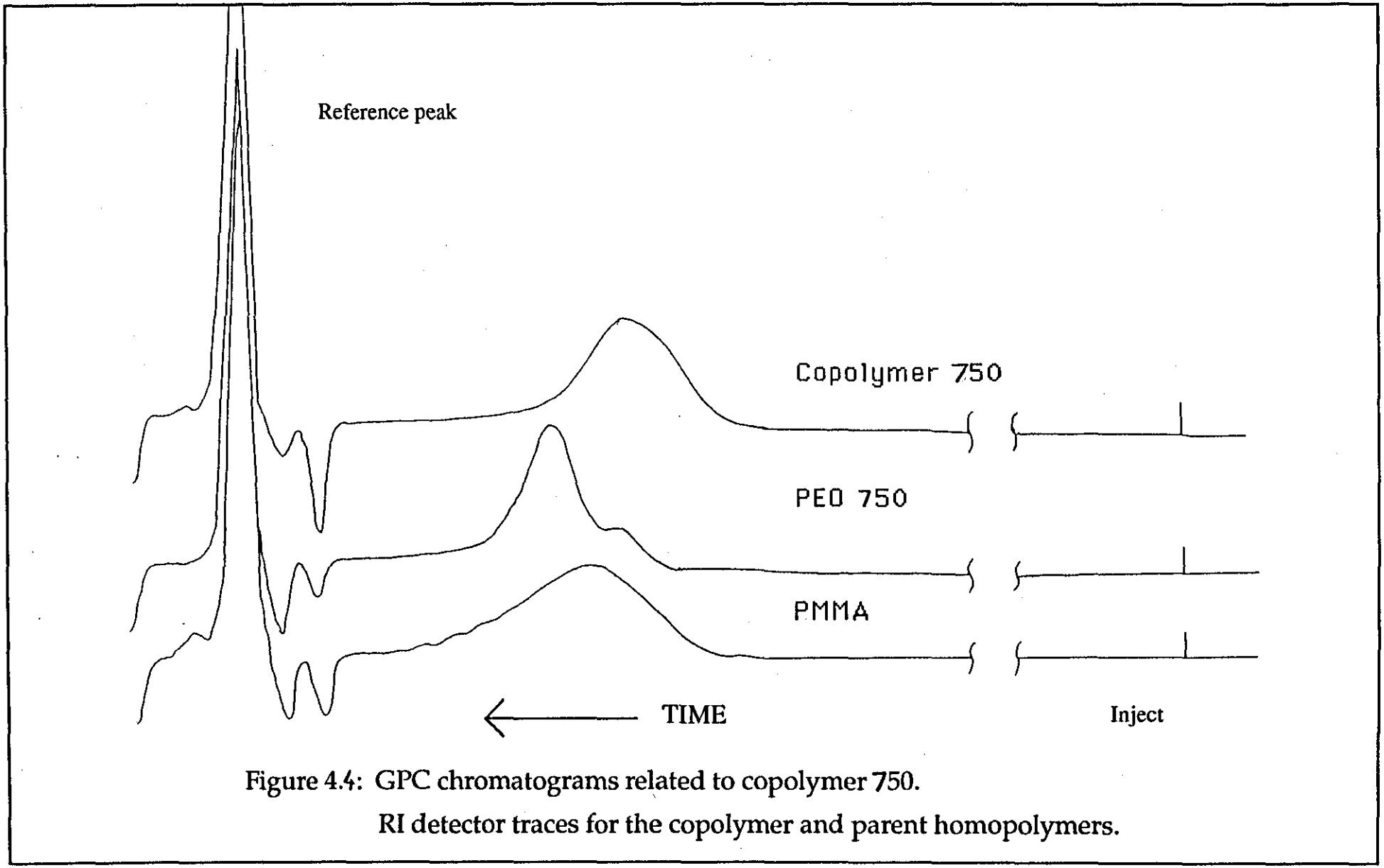

Figure 4.4: GPC chromatograms related to copolymer 750.
RI detector traces for the copolymer and parent homopolymers.

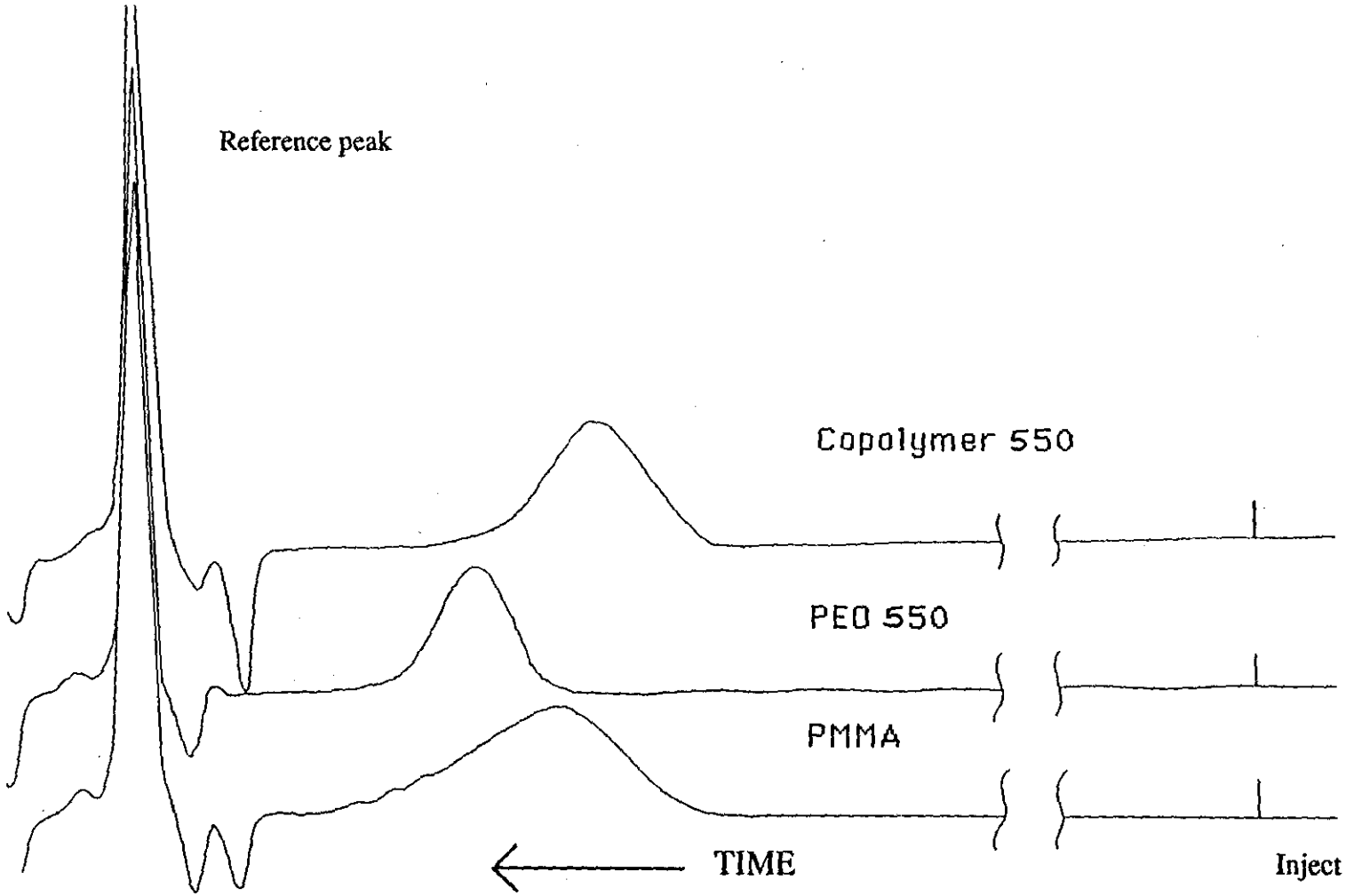

Figure 4.3: GPC chromatograms related to copolymer 550.
RI detector traces for the copolymer and parent homopolymers.

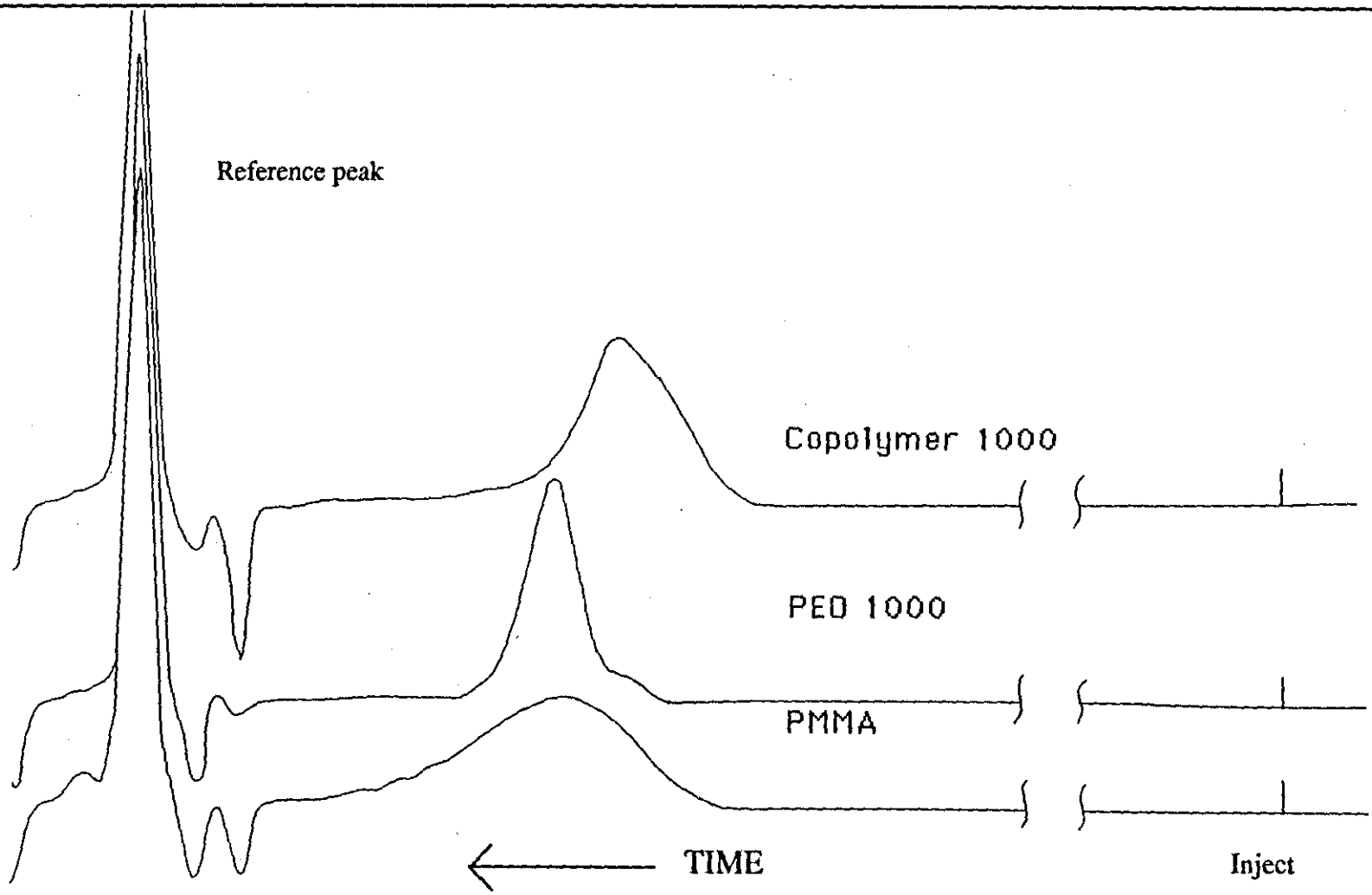

Figure 4.5: GPC chromatograms related to copolymer 1000.
RI detector traces for the copolymer and parent homopolymers.

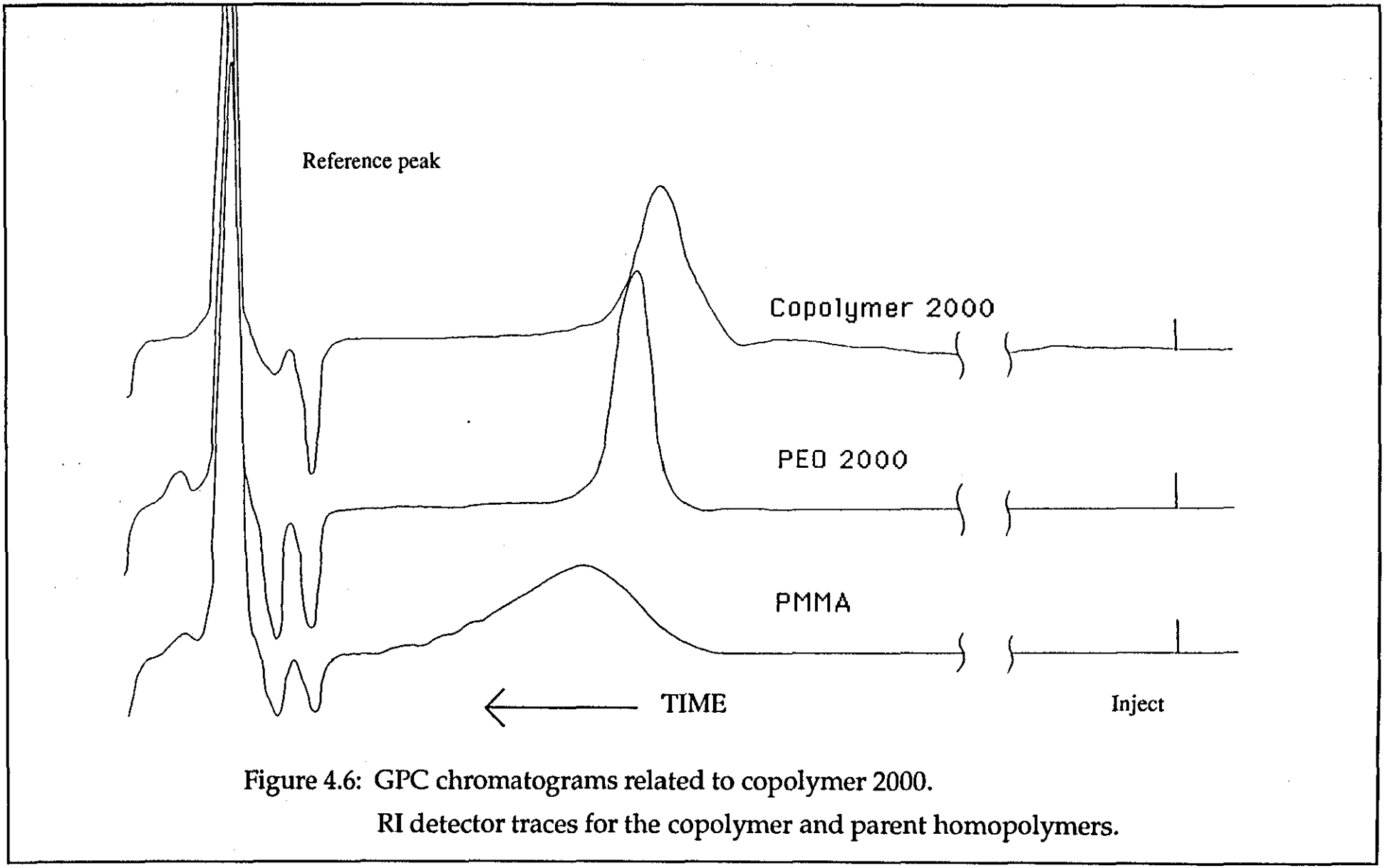

Figure 4.6: GPC chromatograms related to copolymer 2000.
RI detector traces for the copolymer and parent homopolymers.

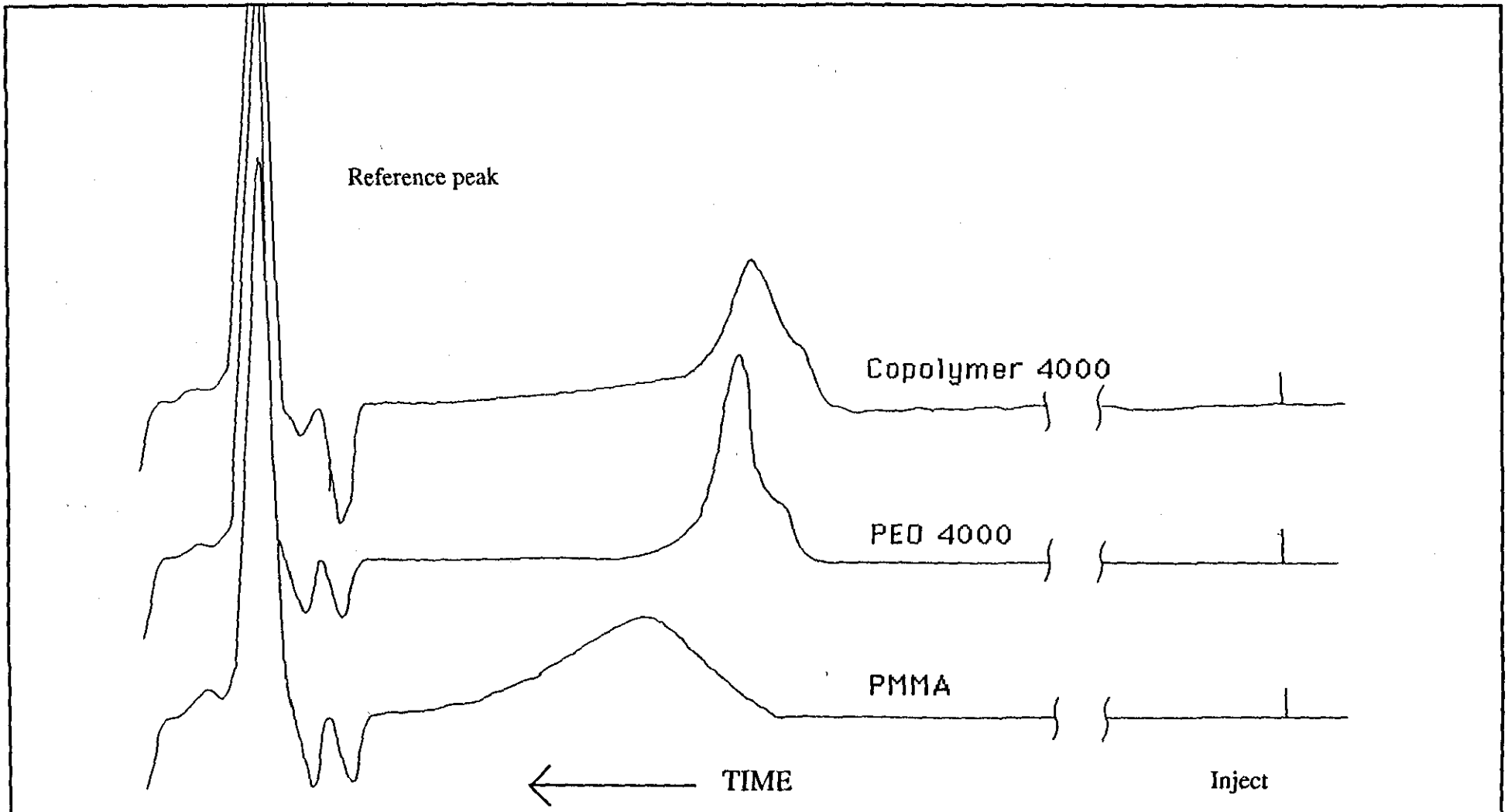

Figure 4.7: GPC chromatograms related to copolymer 4000.
RI detector traces for the copolymer and parent homopolymers.

Chromatograms obtained with the aid of the UV detector were produced to show the molecular weight distribution of the molecules containing PMMA. A bimodal distribution would indicate the presence of free/ unreacted PMMA as a contaminant of the copolymer. With the copolymers based on PEO 550, 750 and 1000 there was no evidence of a bimodal peak. Figures 4.8 and 4.9 show, for copolymers based on PEO 2000 and 4000, the UV chromatograms of the PMMA homopolymer and the copolymer alongside the RI chromatogram of the copolymer. With the copolymer 4000 and, to a much lesser extent, copolymer 2000 a small, broad peak to the low molecular weight side of the main peak could be seen. This observation explains the high polydispersity of copolymer 4000 reported in table 4.3 ($\overline{M}_w/\overline{M}_n = 2.03$) and the apparently low PEO content as calculated from the I-R determination in table 4.2 (section 4.2.1).

As a consequence of a very poor signal to noise ratio no useful results were obtained from the IR detector.

End group effect on exclusion time for oligomeric PEO

A sample of α-hydroxy-ω-methoxy PEO (PEO 550) and an α,ω- dihydroxyl terminated PEO standard sample with an M_p of 150 $gmol^{-1}$ were both run on a GPC equipped with two 60cm PLgel columns, both with nominal exclusion limits of 100Å. Chromatograms are shown as figures 4.10 and 4.11. Resolution of both chromatograms was good enough to assign retention times for individual oligomers up to n=12, where `n´ is defined from:

α,ω- dihydroxyl PEO $\quad HO - (CH_2 - CH_2 - O)_n - H$

α-hydroxy-ω-methoxy PEO $\quad HO - (CH_2 - CH_2 - O)_n - CH_3$

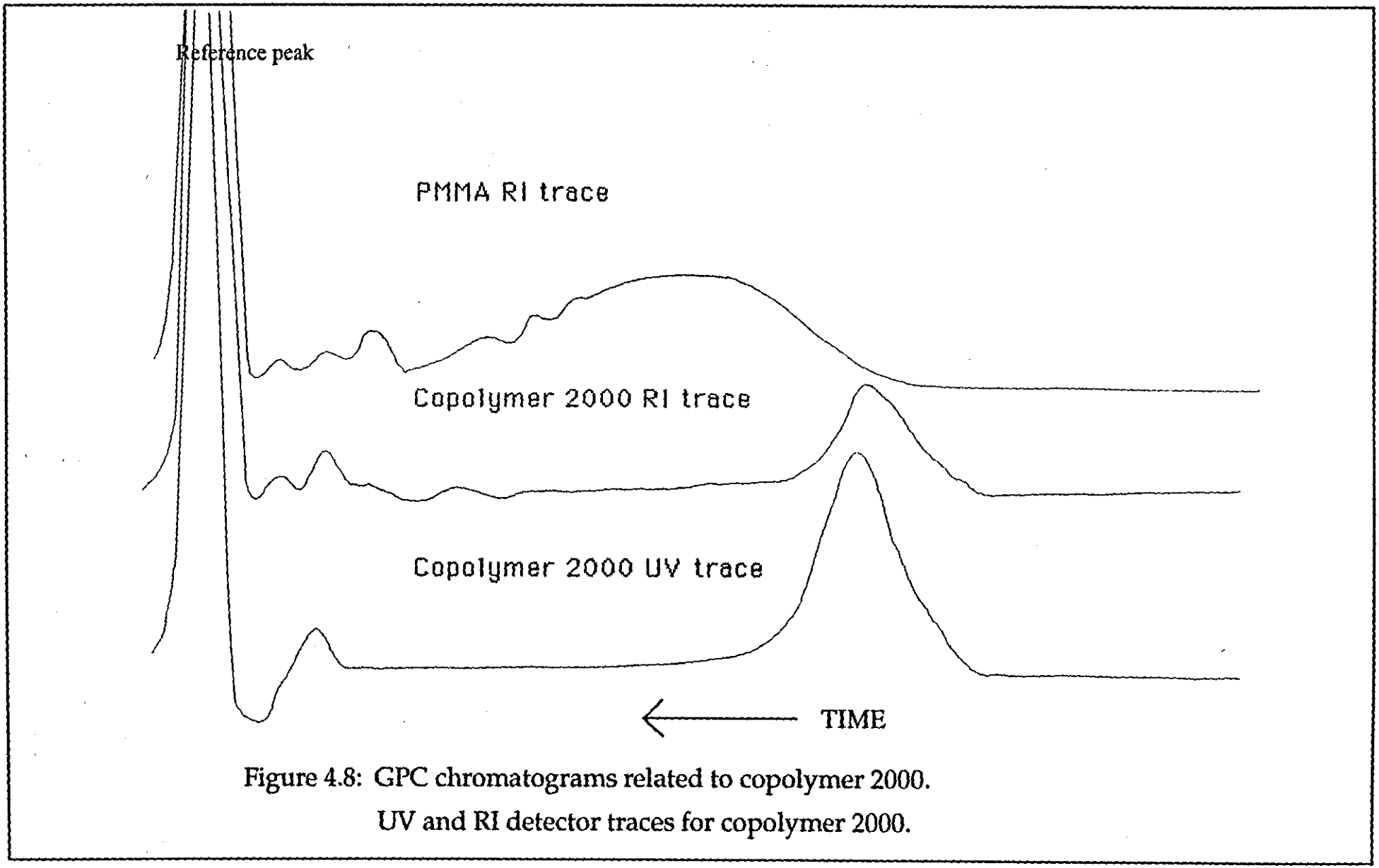

Figure 4.8: GPC chromatograms related to copolymer 2000.
UV and RI detector traces for copolymer 2000.

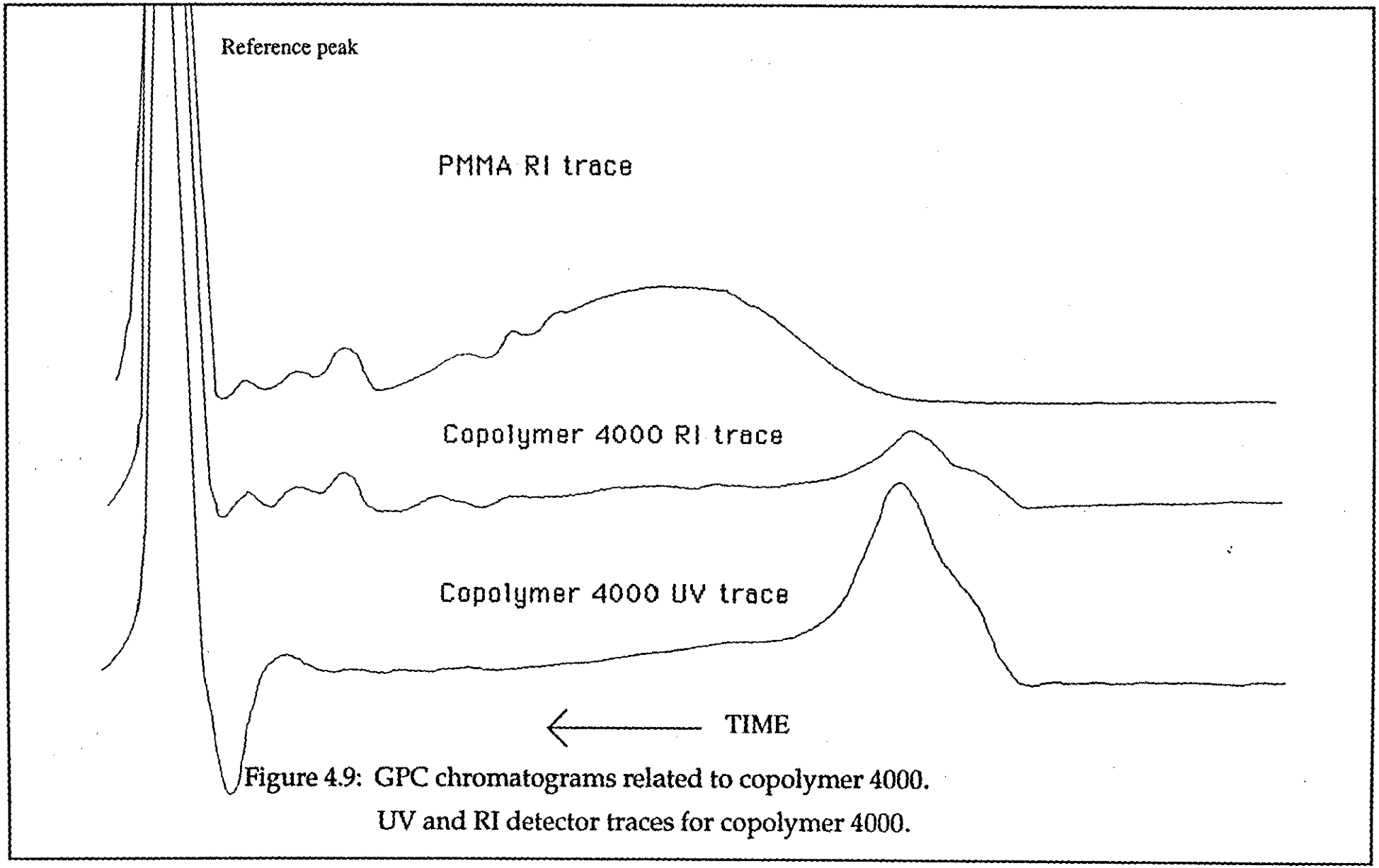

Figure 4.9: GPC chromatograms related to copolymer 4000.
UV and RI detector traces for copolymer 4000.

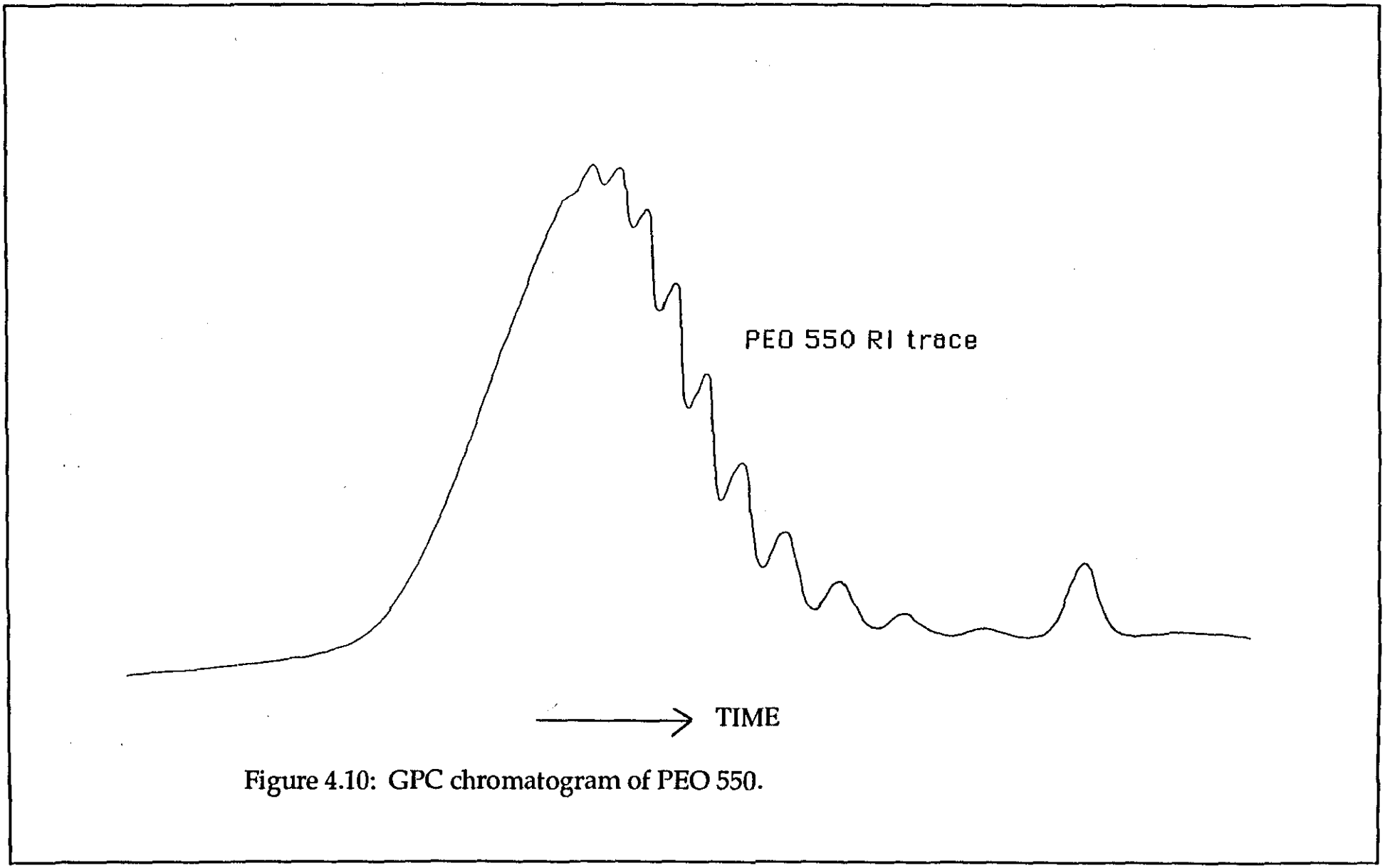

Figure 4.10: GPC chromatogram of PEO 550.

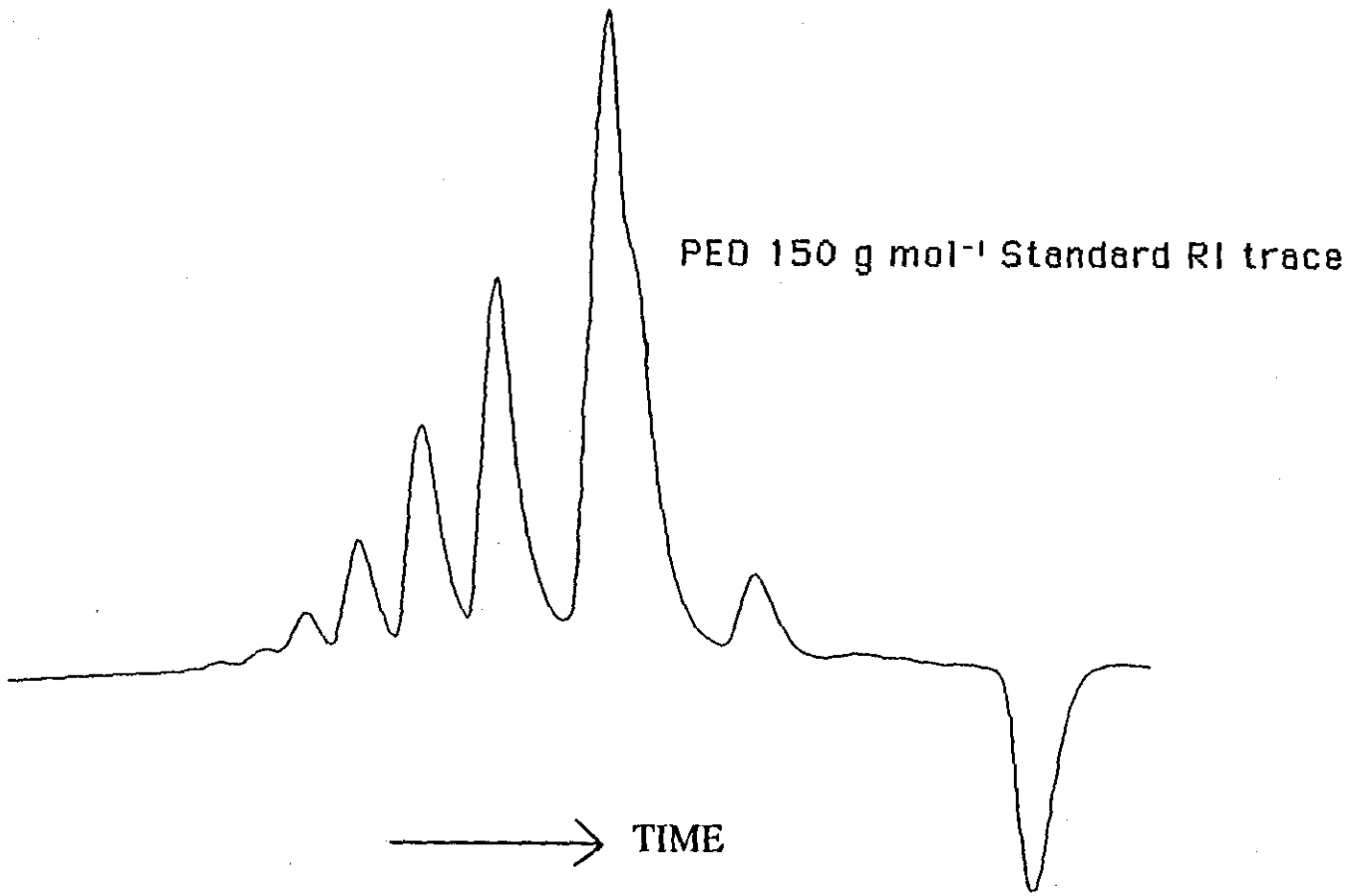

Figure 4.11: GPC chromatogram of PEO 150 g mol^{-1} standard.

A plot of molecular weight vs. retention time is presented as figure 4.12. It can be seen that the exchange of a methyl group for a hydroxyl group has a significant effect on polymer retention time up to a molecular weight of about 500. The retention time is decreased for the methoxy terminated molecule indicating that the effect could be caused by an increase in solvated volume for the molecule or as a result of interactions between the hydroxyl group and the column.

4.2.4 Characterisation of PEO by ^1H Nuclear Magnetic Resonance.

Spectra were recorded for the five trifluroacetic anhydride derivatives of the PEO homopolymers. Two example spectra, those of the derivatives of PEO 750 and PEO 4000, are displayed as figure 4.13 and 4.14 respectively. The separation of the terminal methylene peak at $\delta = 4.48$ was clear for all polymers. The ratio of the integrated peak areas corresponding to the terminal methylene protons and the protons from the rest of the molecule were calculated and from these values, assuming one OH group per molecule, number average molecular weights were calculated.

$$CH_2 \; : \; CH_3 - O - (CH_2 - CH_2 - O)_{n-1} - CH_2 \_\_ O - (CO) - CF_3$$
$$= 2 : 4 \times (n-1) + 5$$

$$\overline{M}_n = n \times 44 + 15 + 16 + 1$$

$(CH_2 - CH_2 - O)$ CH_3 O H

The largest error in these calculations was in the integration of the methylene nmr peak. With PEO 4000 an integration value of 1.2 was obtained. This integration value is only given to one decimal place. Assuming an uncertainty of ±0.1 the final molecular weight is subject to an uncertainty of about ±8%.

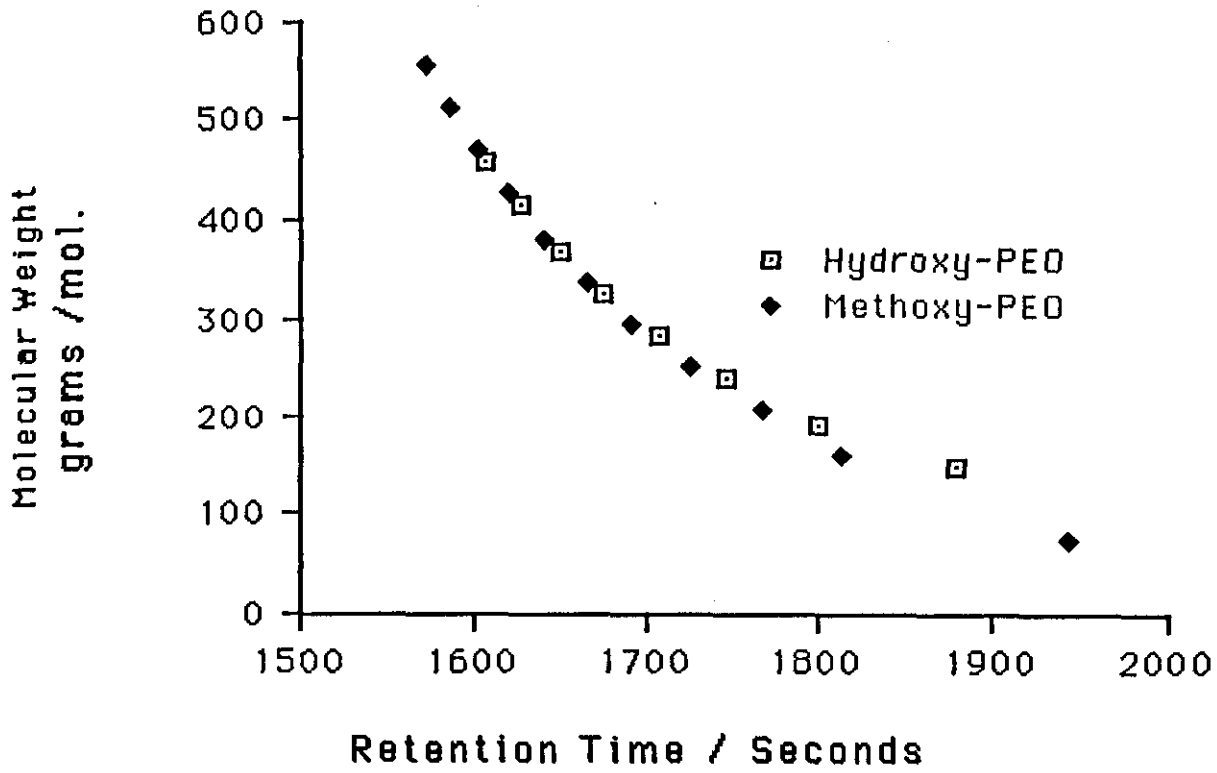

Figure 4.12: Plot of oligomer molecular weight as a function of GPC retention time

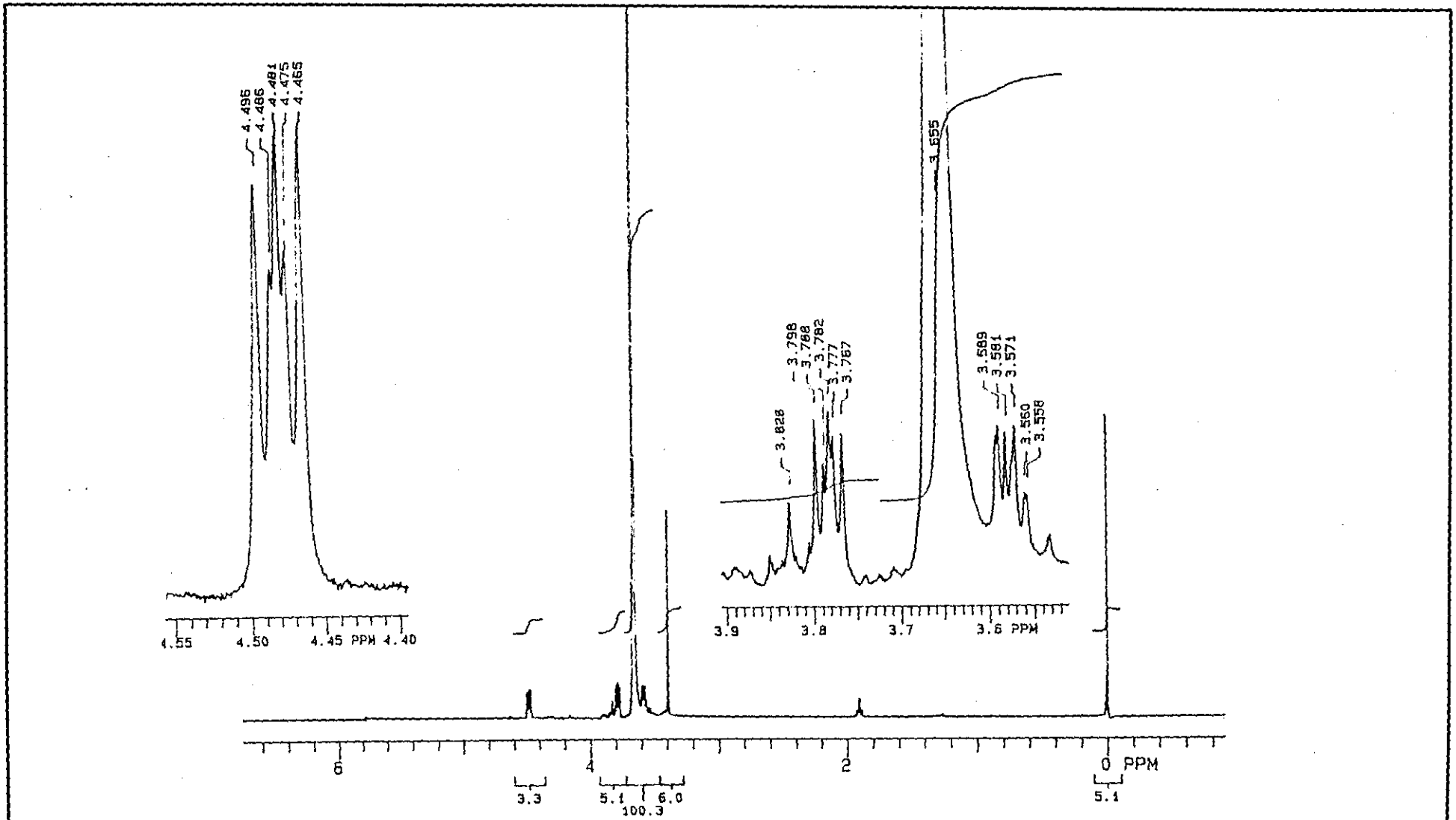

Figure 4.13: ^{1}H nmr of the trifluroacetic anhydride derivative of PEO 750.

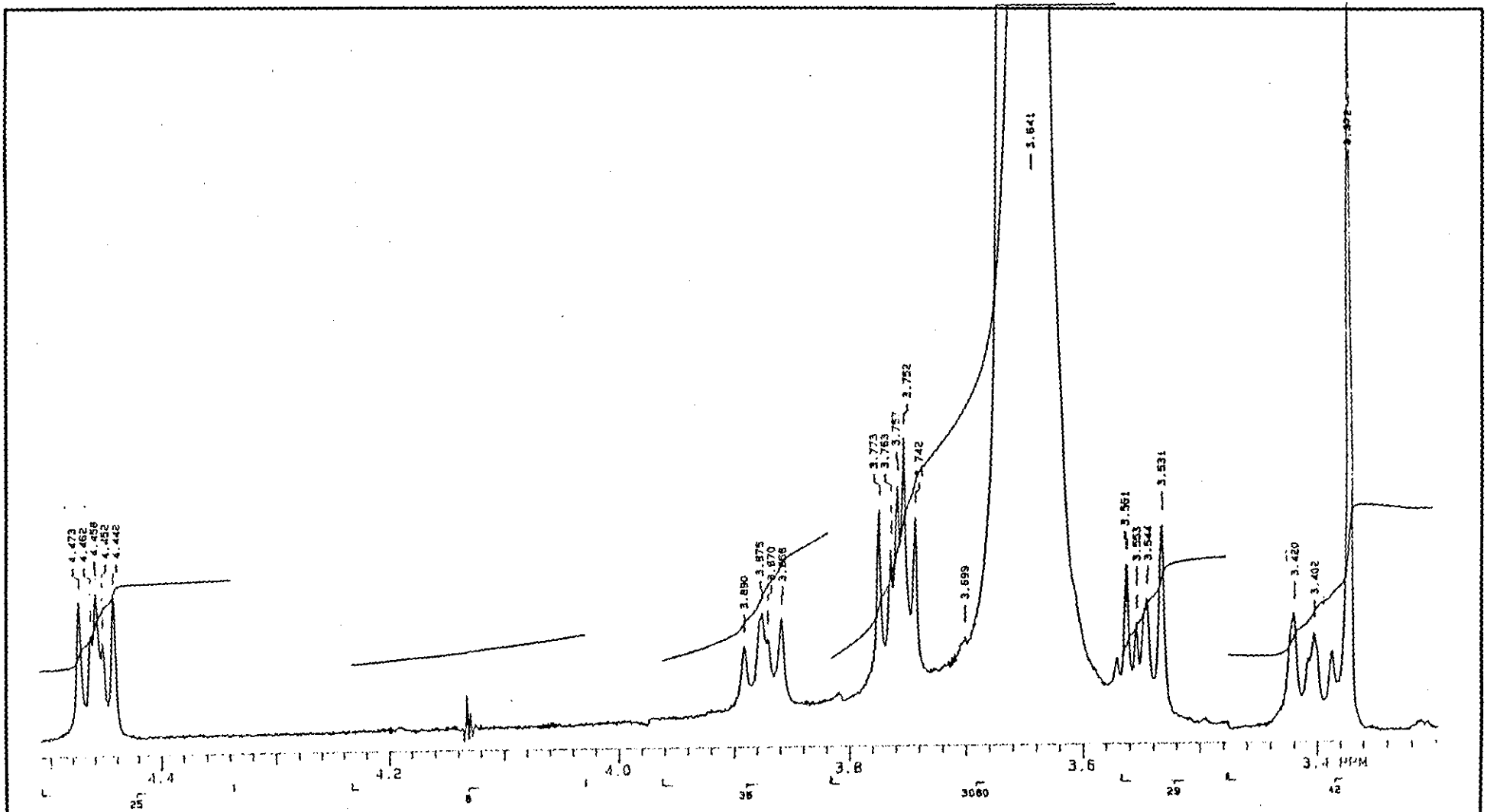

Figure 4.14: ^{1}H nmr of the trifluroacetic anhydride derivative of PEO 4000.

Table 4.4: Summary of ^1H Nuclear Magnetic Resonance results.

SAMPLE	INTEGRATION		n-1	$\bar{M}_n$
	CH_2	Remainder		
PEO 550	6.0	157.0	11.8	596
PEO 750	3.3	100.3	13.95	689
PEO 1000	2.3	100.1	20.5	979
PEO 2000	1.1	100.1	40.25	2023
PEO 4000	1.2	158.0	64.5	2884

These values agree very well to the titration values supplied by Doroszkowski[92], ICI Paints, Slough with the exception of PEO 4000.

4.2.5 Characterisation of Copolymers by ^1H Nuclear Magnetic Resonance.

On a 60 MHz ^1H nmr spectra of these copolymers it is not possible to separate the resonance from the O-Me of the PMMA and that from the CH_2 of the PEO. This makes the determination of the composition from the integrated spectra a little more complex than expected. The O-Me from PMMA and the CH_2 from PEO show a resonance at $\delta = 3.55$. The CH_2 and CH_3 from the PMMA show resonances at $\delta = 1.85$ and $\delta = 1.05$ respectively. From the ratio of the integrated spectra over the region around $\delta = 3.55$ to the area covering $\delta = 1.85$ and $\delta = 1.05$ it is possible to estimate the compositions.

If X = the integration around $\delta = 3.55$ and Y = the integration around $\delta = 1.85$ and $\delta = 1.05$

Then the ratio of

$$X / Y = (3 \times C_{PMMA} + 4 \times C_{PEO}) / 5 \times C_{PMMA}$$

where the ratio of weights of the two polymers

$$PEO / PMMA = C_{PEO} \times 44 / C_{PMMA} \times 100$$

In table 4.5 the results calculated from the above method are given. The values are expressed as the PEO weight fraction of the polymer

Table 4.5: Summary of copolymer composition determined from ^1H nmr.

COPOLYMER	Weight % PEO
550	41.8
750	44.3
1000	63.0
2000	74.1
4000	76.7

4.3 CHARACTERISATION OF COPOLYMERS IN SOLUTION

4.3.1 Visual Cloud Point Determination

The automated method for the determination of cloud point onset illustrated well the need for very slow heating rates. The faster the rate of heating the higher the measured onset of the cloud point. In the table of results below the temperature cited for the `UV/Vis´ cloud point is the lowest value obtained from a number of measurements. Heating rates were of the order 1° every three minutes. An example trace from the cloud point apparatus is presented as figure 4.15

Visual determination of cloud point proved to be more practical at the higher temperatures required for copolymers 2000 and 4000. Comparing the values obtained for copolymers 750 and 1000 the eye is less sensitive to the onset of the cloud point resulting in a slightly higher recorded temperature for the visual determination.

Table 4.6: Cloud point determination of copolymers in aqueous solution.

Copolymer	UV/Vis cloud point	Visual cloud point
550	-	<275K
750	306K	308K
1000	331.5K	333K
2000	-	366K
4000	-	368K

4.3.2 UV/Vis Spectroscopy in mixed solvents

From UV/Vis spectra for copolymers 1000 and 2000 at solvent

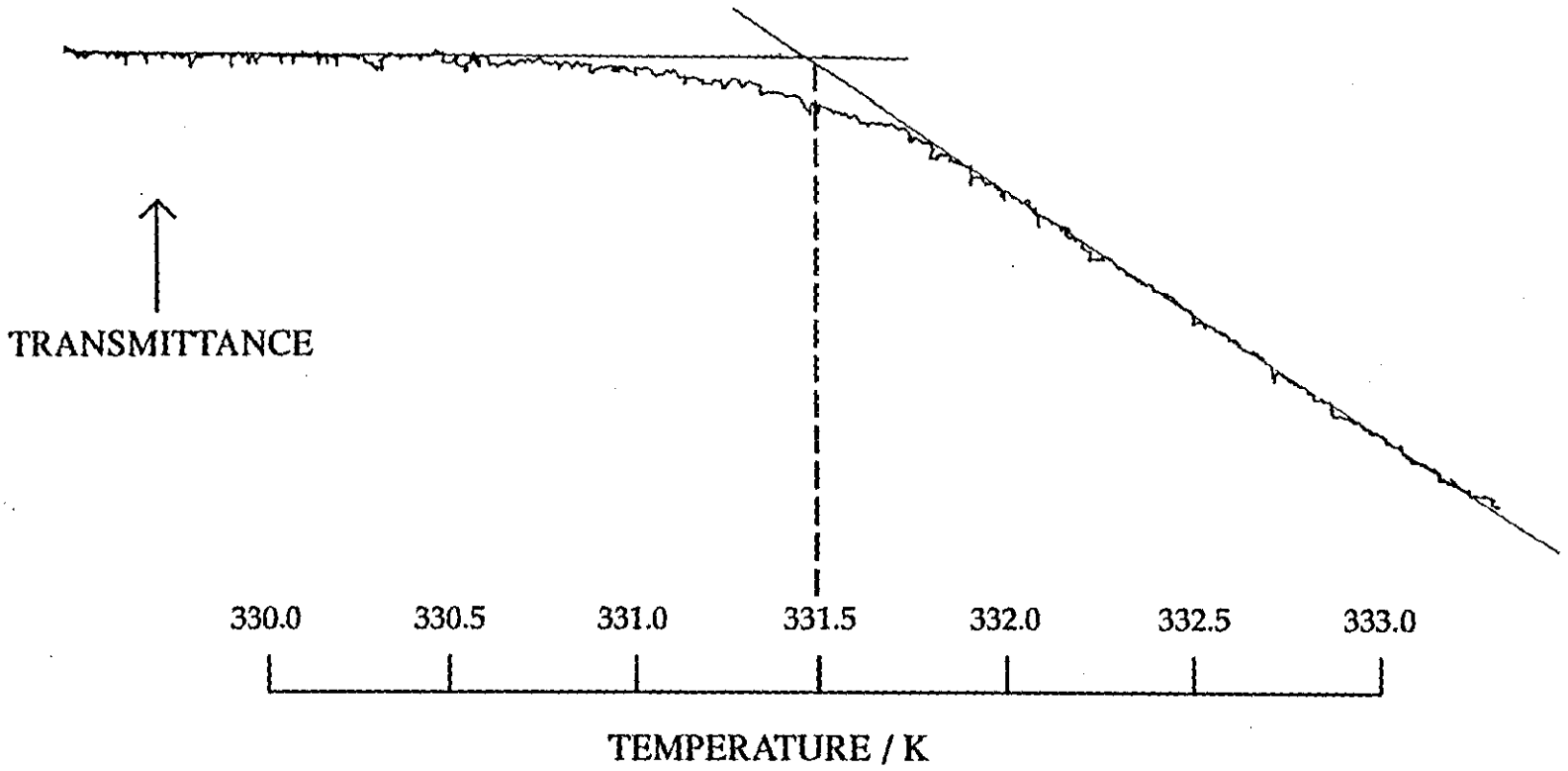

Figure 4.15: Cloud point behaviour of copolymer 1000

compositions from 20% methanol/ 80% water to 100% water at intervals of 10% absorbance data at three wavelengths, 350, 500 and 800nm, have been extracted and plotted against solvent composition. These plots for copolymers 1000 and 2000 are presented as figures 4.16 and 4.17 respectively.

Copolymer 1000 shows a marked maximum in absorbance at a solvent composition of 60% methanol/ 40% water. Copolymer 2000 shows a similar maximum absorbance but at a slightly higher methanol concentration (somewhere between 60 and 65% methanol) and over a wider range of compositions. There is in addition a second maximum in absorbance at a composition of approximately 40% methanol/ 60% water for copolymer 2000. The maximum absorbance measured for copolymer 2000 is notably larger than that for copolymer 1000.

4.3.3 Small Angle X-ray Scattering

4.3.3 a) Data handling

From each SAXS experiment performed, two sets of data were obtained; background scattering and sample scattering. Firstly, the background data was subtracted from the sample scattering data. The derived data set was then plotted as a graph of Smeared Intensity ($\tilde{I}$) against 2 Theta. Figure 4.18 shows such a plot for copolymer 2000 in water. To remove the statistical scatter from the data a smooth curve was drawn through the data points (this line is also shown on figure 4.18). This smoothed curve was used for all subsequent calculations.

Desmearing of the slit smeared data was performed with the Fortran program developed by Dijkstra, Kortleve and Vonk[58]. In most cases 30

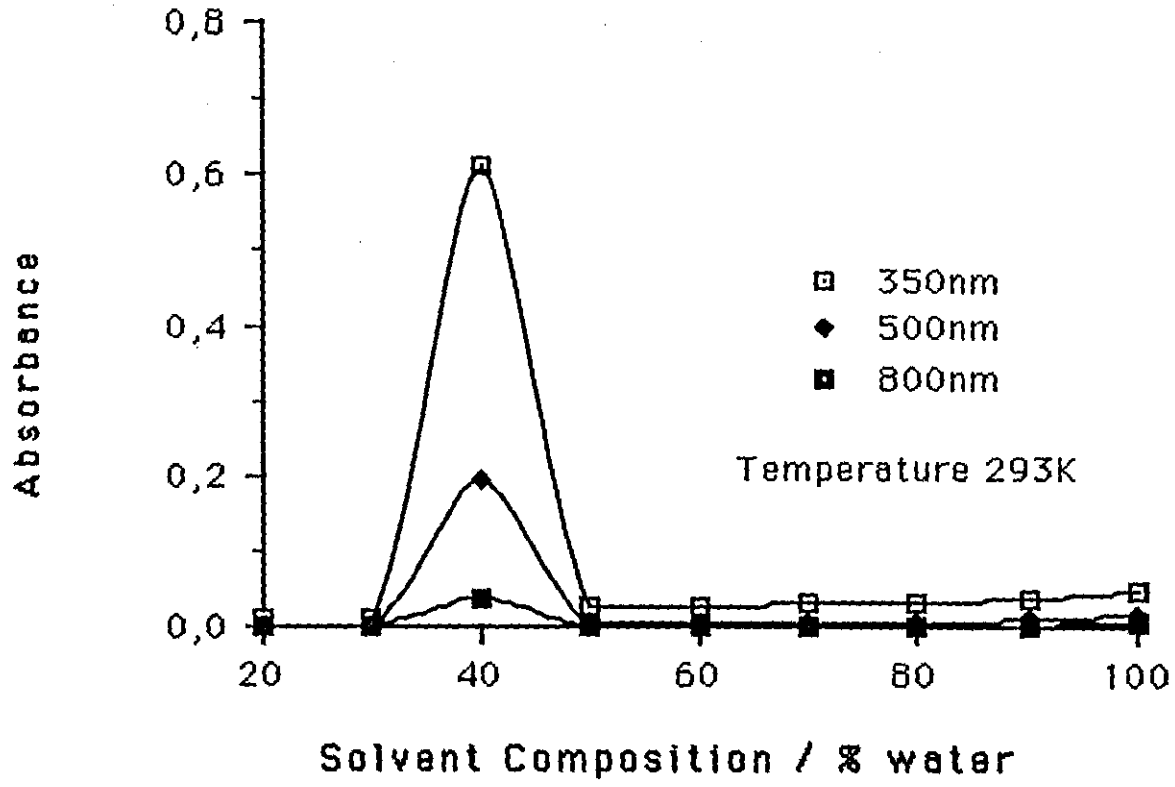

Figure 4.16: Plot of absorbance at various wavelengths as a function of solvent composition for a 1% copolymer 1000 solution in water / methanol mixtures

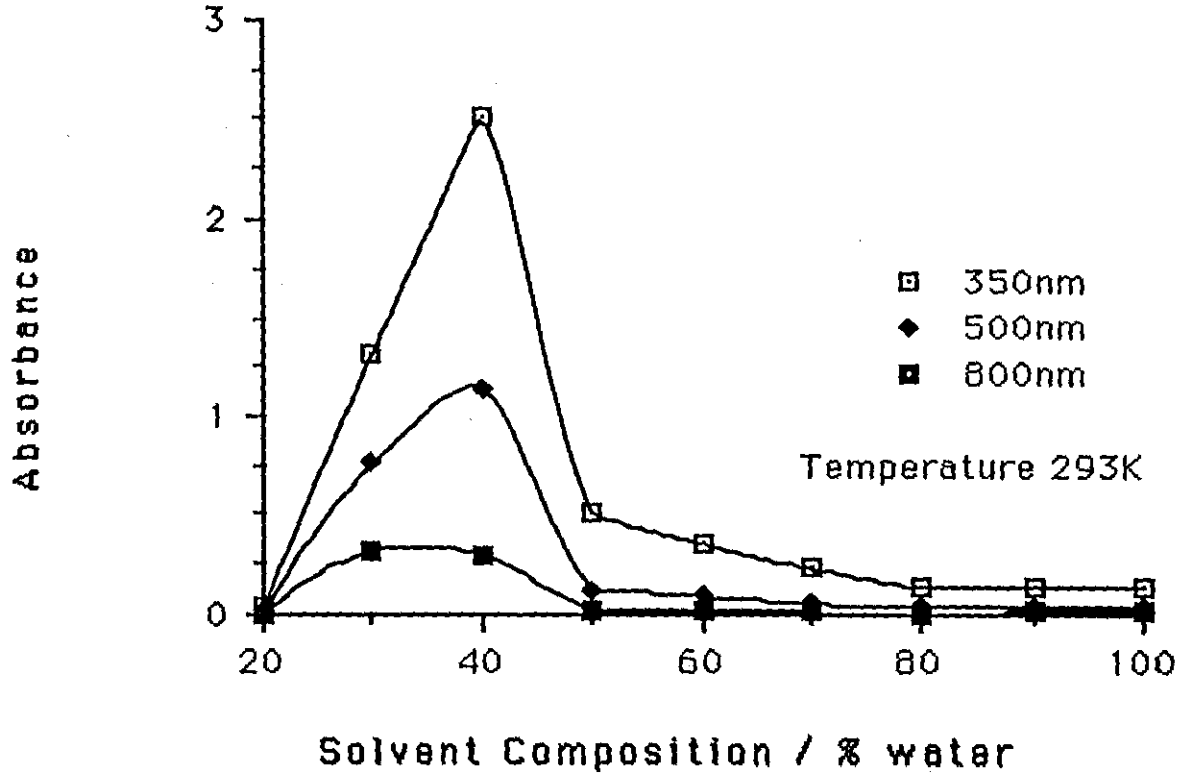

Figure 4.17: Plot of absorbance at various wavelengths as a function of solvent composition for a 1% copolymer 2000 solution in water / methanol mixtures

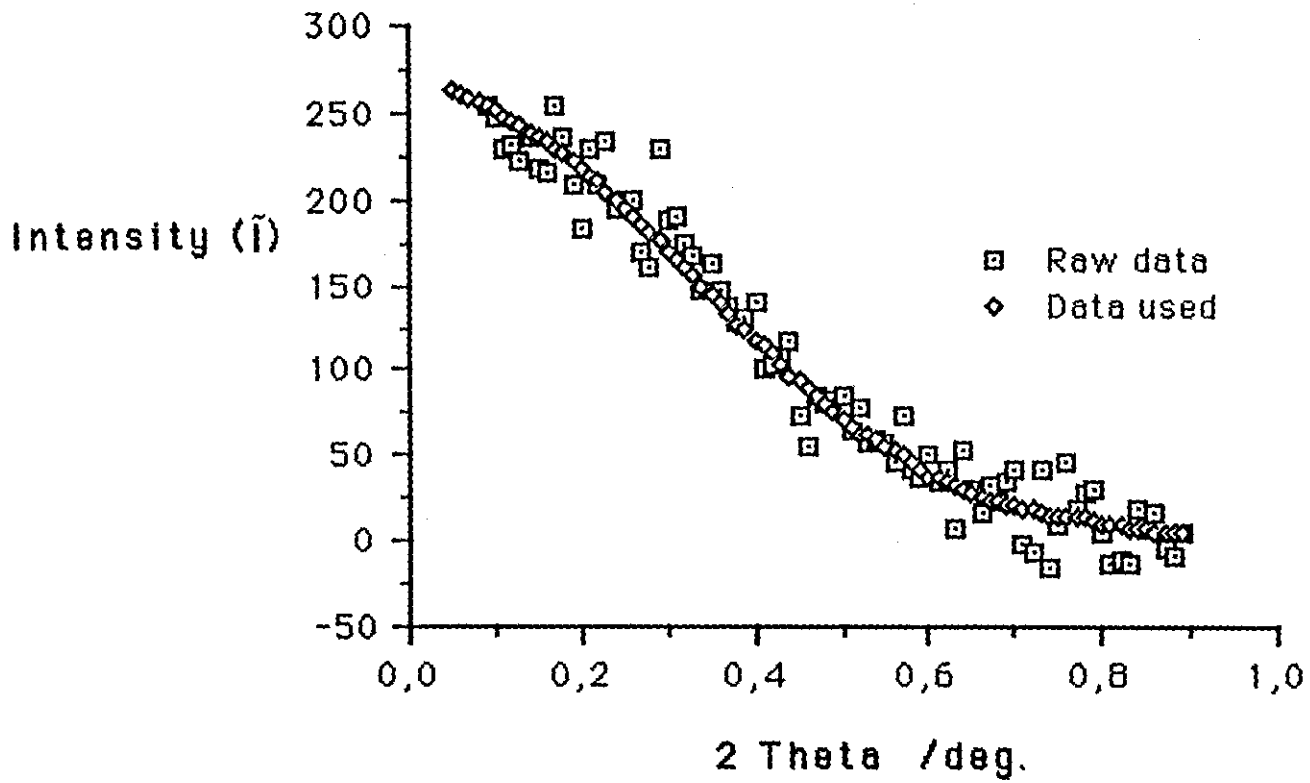

Figure 4.18: SAXS analysis of copolymer 2000 in water:
Plot of Scattering intensity against 2 Theta.

terms of the Fourier series were required to model the curve. The desmeared scattering intensity for the copolymer 2000 data referred to above is presented as a plot of Desmeared Intensity against 2 Theta in figure 4.19.

b) Core size determination

Determination of the micellar core radius of gyration (R_g) by the method proposed by Guinier[57,59] was carried out by producing a plot of ln(Desmeared Intensity) against $4\pi^2 s^2$ /3. This plot, for the data shown in figure 4.19, is presented as figure 4.20.

In accordance with equation 2.25 the value of R_g is given by (-Gradient)$^{0.5}$. The gradient was, in each case, measured at the lowest angle at which the plot could be considered as linear.

Where results are reported for R_g, a value for the spherical micellar radius (R_{sp}) is also given. R_g is a shape independent measure of the core size, ie. no assumption of micellar shape has been made in its determination. R_{sp} has been calculated from R_g assuming the micelle cores to be spherical. The values for R_{sp} are calculated using the relationship:

$$R_{sp} = (5/3)^{0.5} R_g \qquad (4.1)$$

c) Fringe thickness

Six methods for the determination of fringe thickness were considered. As described in section 2.4.2, all six methods are suited to graphical determination.

The first stage with all six methods was to construct a plot of $s^3\tilde{I}$ against s.

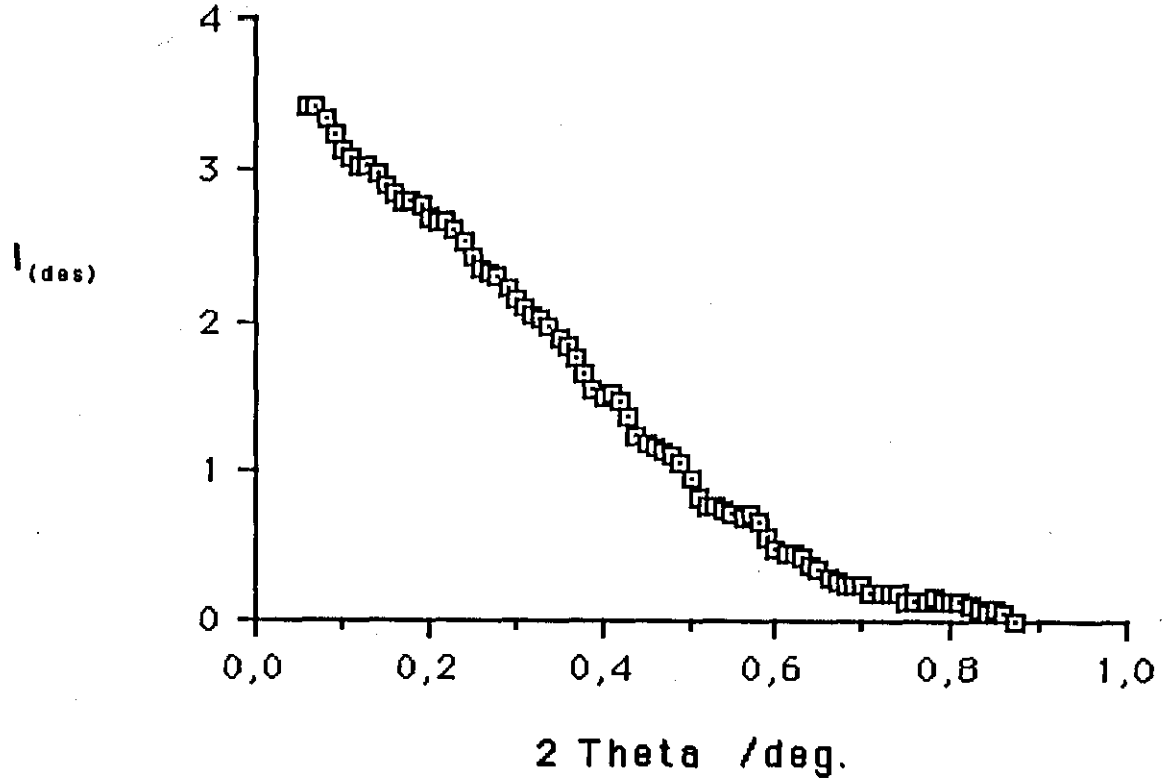

Figure 4.19: SAXS analysis of copolymer 2000 in water
Plot of Desmeared Intensity against 2 Theta.

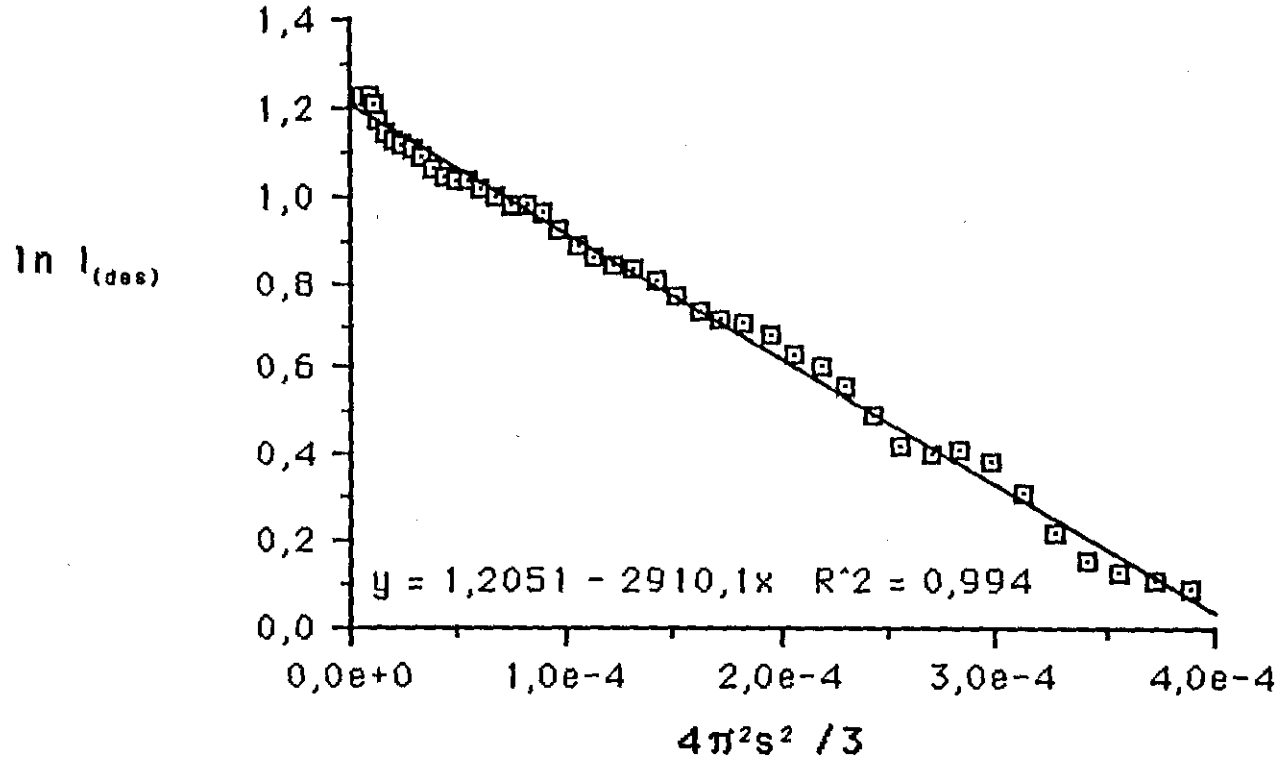

Figure 4.20: SAXS analysis of copolymer 2000 in water:
Plot of ln Desmeared Intensity ($\tilde{I}$) against $4\pi^2s^2/3$.

This plot is referred to as the Porod plot. If, from this plot, a negative deviation from Porod's law was observed (see section 2.4.1), determination of fringe thickness could proceed. Observance of positive deviations from Porod's law excluded the determination of fringe thickness. An example of a Porod plot demonstrating a negative deviation from Porod's law is presented as figure 4.21.

Considering the linear gradient model for the interfacial fringe layer, two approximations to Porod's law were considered; the Vonk[66] approximation and the Exponential.

The Vonk approximation

The Vonk approximation for infinite slit optics is given by equation 2.42b. If a plot of $s^3\tilde{I}$ vs s^2 is constructed the interfacial fringe thickness δ is given by:

$$\delta = \left(\frac{-3 \text{ x Grad.}}{2\,\pi^2 \text{ x Int.}} \right)^{1/2} \qquad (4.2)$$

where "Grad." is the gradient of the plot and "Int." is the intercept of the plot.

Figure 4.22 shows a plot of the $s^3\tilde{I}$ vs s^2 for the data presented earlier. Only the highest angular region is plotted where the relationship is linear. Linear regressional analysis gives the "best fit" line which is drawn on the plot and given in equation form in the lower left hand corner.

The Exponential approximation

The Exponential approximation is given by equation 2.43 b. Thus from a

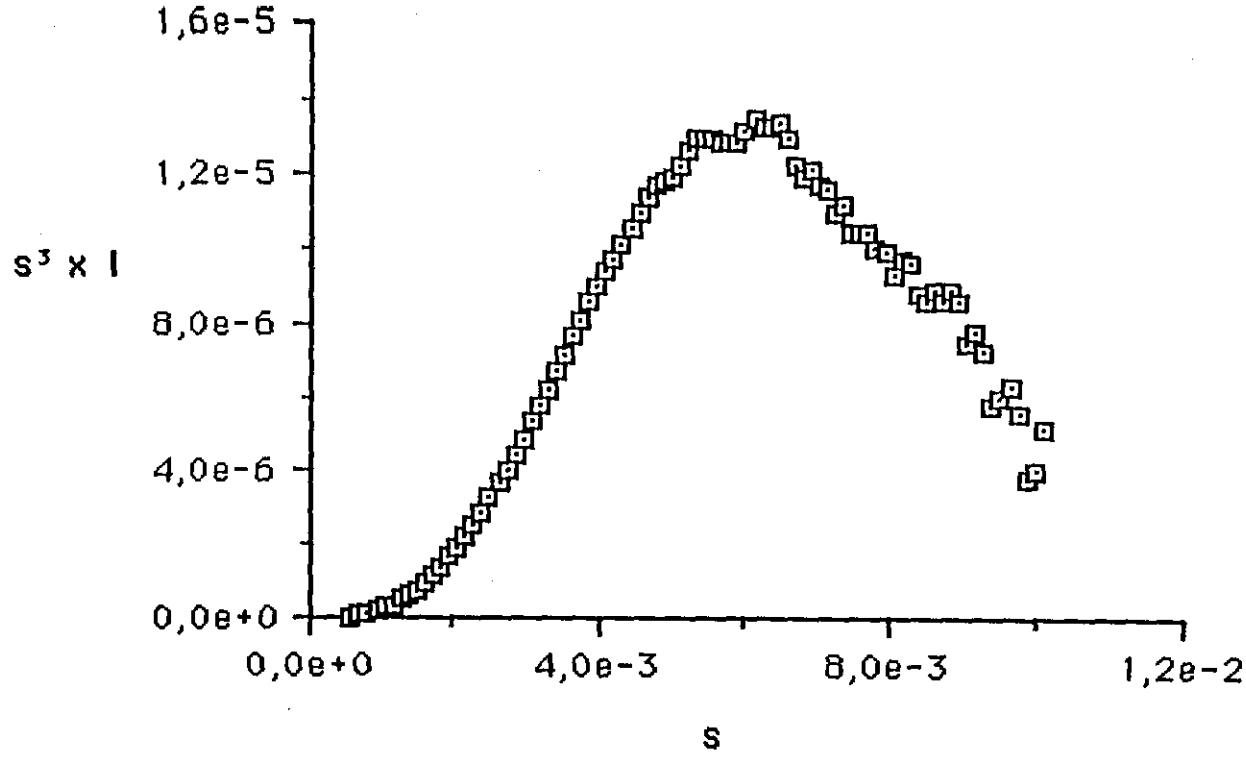

Figure 4.21: SAXS analysis of copolymer 2000 in water:
Plot of $s^3 \times I$ against s

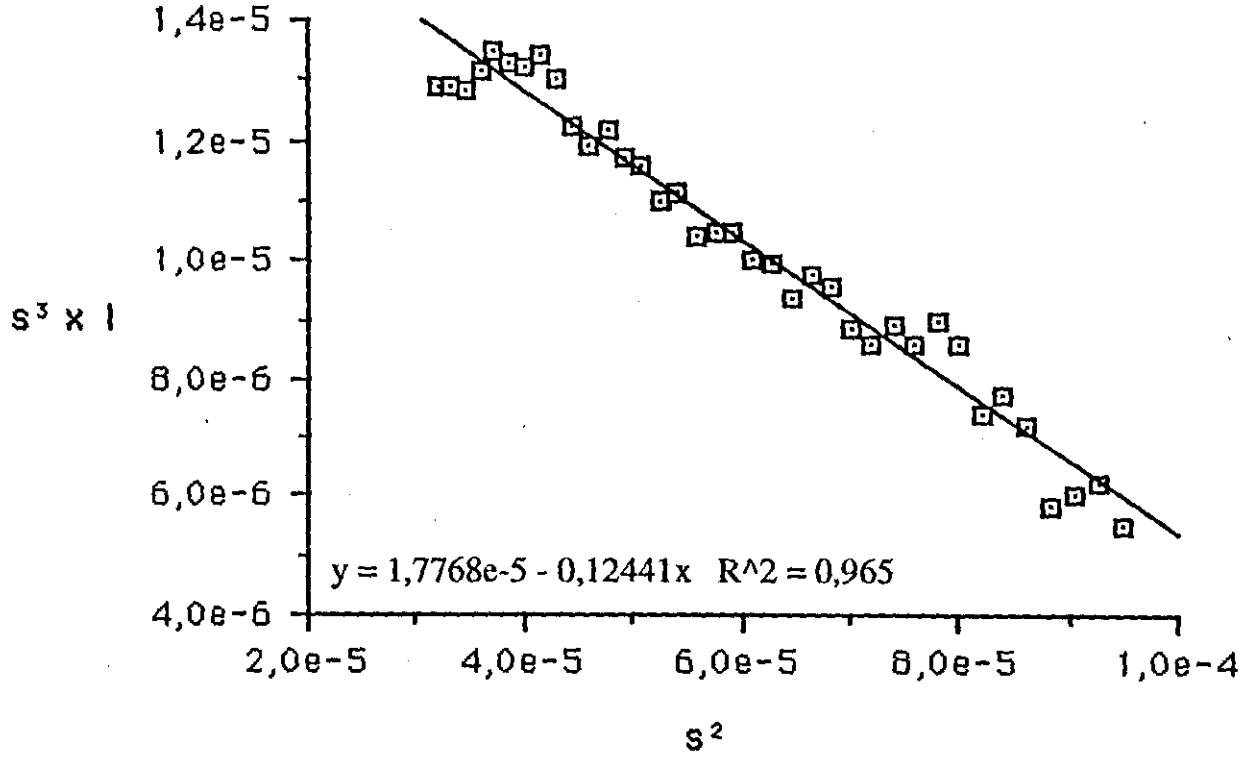

Figure 4.22: SAXS analysis of copolymer 2000 in water:
Plot of $s^3 \times I$ against s^2.

plot of $\ln(s^3\tilde{I})$ vs. s^2 the interfacial fringe thickness δ is given by:

$$\delta = \left(\frac{-3 \times \text{Grad.}}{2\pi^2} \right)^{1/2} \qquad (4.3)$$

Figure 4.23 shows a plot of $\ln(s^3\tilde{I})$ vs. s^2 for the data referred to above. The plot covers the highest angular region of the data available. Linear regressional analysis was used to construct the "best fit" line which is superimposed on the data and also presented numerically in the bottom left hand corner of the plot.

Considering the sigmoidal-gradient model there were four approximations to Porod's law considered: Ruland and Müller, Exponential, Bonart and Empirical approximations.

The Ruland approximation

The Ruland approximation is given by equation 2.50 b. Thus if a plot of $s^3\tilde{I}$ vs. s^2 is constructed the standard deviation of the Gaussian function (σ) is given by:

$$\sigma = \left(\frac{-\text{Grad.}}{8\,\pi^2 \times \text{Int.}} \right)^{1/2} \qquad (4.4)$$

A plot of $s^3\tilde{I}$ vs. s^2 was shown earlier as figure 4.22.

The Exponential approximation

The Exponential approximation is given by equation 2.51 b. If a plot of

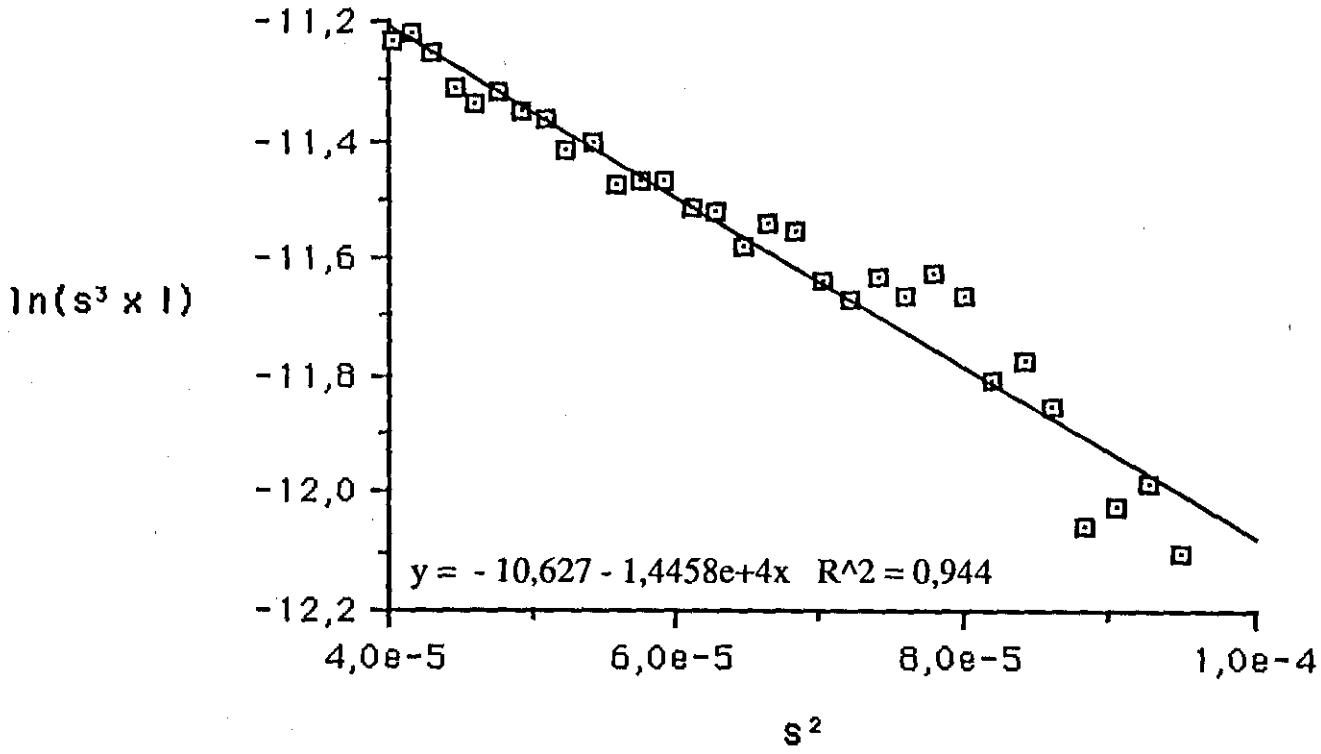

Figure 4.23: SAXS analysis of copolymer 2000 in water:
Plot of $\ln(s^3 \times I)$ against s^2

$\ln(s^3\tilde{I})$ vs. s^2 is constructed (see figure 4.23) then the standard deviation of the Gaussian function (σ) is given by:

$$\sigma = \left(\frac{-\text{Grad.}}{8\,\pi^2} \right)^{1/2} \qquad (4.5)$$

The Bonart approximation

The Bonart approximation is given by equation 2.54 b. If a plot of $\ln(s^3\tilde{I})$ vs. s^2 is constructed (see figure 4.23) then the standard deviation of the Gaussian function (σ) is given by:

$$\sigma = \left(\frac{-\text{Grad.}}{4\,\pi^2} \right)^{1/2} \qquad (4.6)$$

The Empirical approximation

The Empirical approximation is given by equation 2.55 b. To produce a graphical solution for the Empirical approximation a plot of $\ln(s^3\tilde{I})$ vs. $s^{1.81}$ is required. This plot for the data shown in figure 4.21 is displayed as figure 4.24. Linear regressional analysis was used to construct the "best fit" line which is superimposed on the data and also presented numerically in the bottom left hand corner of the plot. From this plot the standard deviation of the Gaussian function (σ) is given by:

$$\sigma = \left(\frac{-\text{Grad.}}{38} \right)^{1/1.81} \qquad (4.7)$$

In an attempt to establish the relative suitability of the six approximations

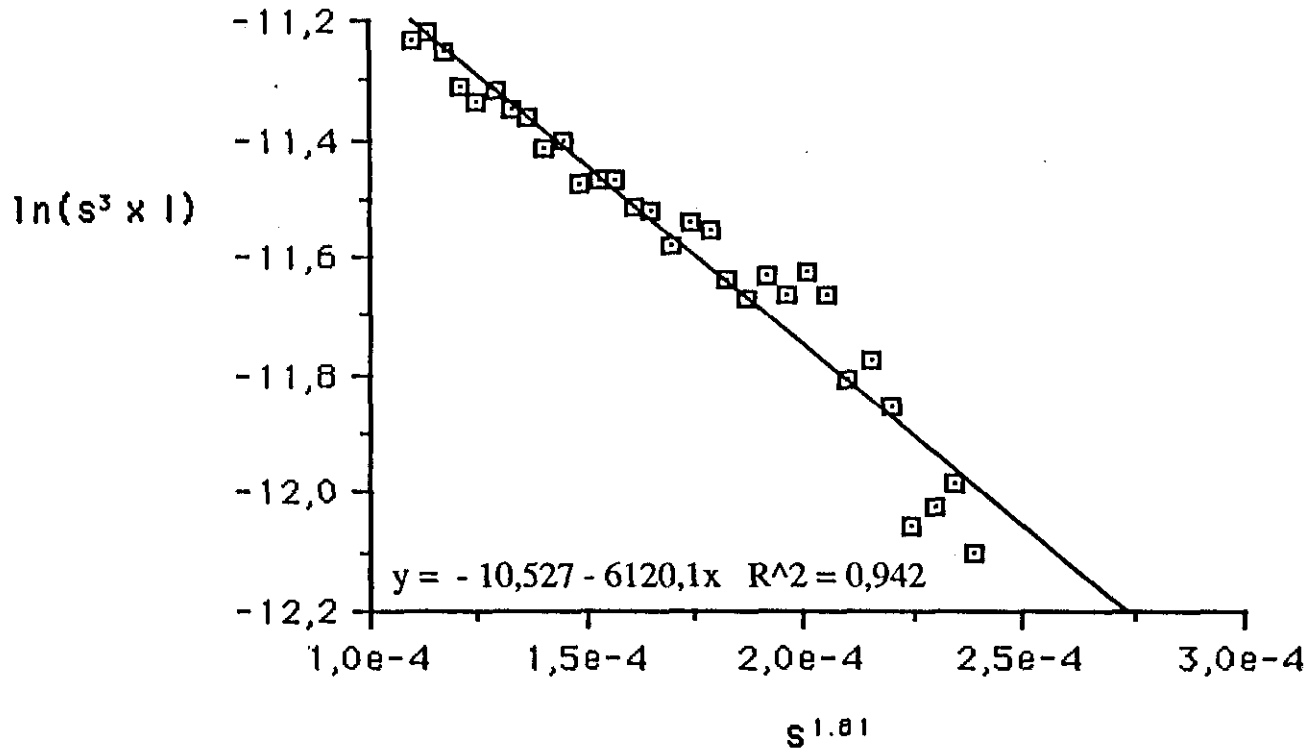

Figure 4.24: SAXS analysis of copolymer 2000 in water:

Plot of $\ln(s^3 \times I)$ against $s^{1.81}$

above, SAXS data from four 5% copolymer solutions have been treated by all six methods. Table 4.7 shows the gradient and intercept data obtained from the three different plots described above. Table 4.8 gives the calculated interfacial fringe dimensions as described by equations 4.2, 4.3, 4.4, 4.5, 4.6, and 4.7 for the four polymer solutions. Core size data are also given.

Table 4.7: Summary of gradient and intercept data derived from plots made in accordance with equations 2.25, 2.42b, 2.43b, 2.50b, 2.51b 2.54b and 2.55b for SAXS data from 5% aqueous solutions of copolymers 750, 1000, 2000 and 4000.

COPOLYMER		PLOT			
		Guinier	$s^3\tilde{I}$ vs. s^2	$\ln(s^3\tilde{I})$ vs. s^2	$\ln(s^3\tilde{I})$ vs. $s^{1.81}$
750	Int.	-	4.76×10^{-5}	-9.93	-9.91
	Grad.	-2733	-7.85×10^{-2}	-2.03×10^{3}	-8.94×10^{2}
1000	Int.	-	4.42×10^{-5}	-9.99	-9.97
	Grad.	-3812	-1.17×10^{-1}	-3.44×10^{3}	-1.48×10^{3}
2000	Int.	-	4.23×10^{-5}	-9.45	-9.45
	Grad.	-3222	-2.14×10^{-1}	-1.19×10^{4}	-5.30×10^{3}
4000	Int.	-	2.70×10^{-5}	-10.21	-10.16
	Grad.	-5464*	-1.42×10^{-1}	-1.79×10^{4}	-6.94×10^{3}

* large degree of uncertainty

(Note: $s = 2\sin\theta / \lambda$)

Table 4.8: Core size and interfacial fringe dimensions as calculated from equations 2.25,4.2, 4.3, 4.4, 4.5, 4.6, and 4.7 for 5% aqueous solutions of copolymers 750, 1000, 2000 and 4000.

			COPOLYMER	
Method	750	1000	2000	4000
Core size				
R_g	52.3Å	61.7Å	56.7Å	73.9Å
R_{sp}	67.5Å	79.7Å	73.2Å	95.5Å
Linear gradient		δ =		
Vonk	15.8Å	20.1Å	27.7Å	43.4Å
Exponential	17.6Å	22.8Å	42.6Å	52.2Å
Sigmoidal gradient		σ =		
Ruland	4.6Å (15.9Å)	5.8Å(20.1Å)	8.0Å(27.7Å)	12.4Å(43Å)
Exponential	5.1Å(17.7Å)	6.6Å(22.9Å)	12.3Å(42.6Å)	15.0Å(52Å)
Bonart	7.7Å(26.7Å)	9.3Å(32.2Å)	17.3Å(59.9Å)	21.3Å(73.8Å)
Empirical	5.7Å(19.7Å)	7.6Å(26.3Å)	15.3Å(53Å)	17.8Å(61.7Å)

The numbers in parenthesis are δ values calculated after ref. 60

After consideration of these results in relation to the mathematical ranges of applicability of the various approximations (see section 2.4.2) only the Vonk approximation for the linear-gradient model and the Empirical approximation for the sigmoidal-gradient model will be considered for the remaining results. See section 5.2.3 for a full discussion of the suitability of the various models.

Table 4.9: Copolymer 1000 at various temperatures.- Summary of gradient and intercept data from SAXS analysis.

Temperature		PLOT			
		Guinier	$s^3\tilde{I}$ vs. s^2	$\ln(s^3\tilde{I})$ vs. s^2	$\ln(s^3\tilde{I})$ vs. $s^{1.81}$
20°C	Int.	-	4.42x10-5	-9.99	-9.97
	Grad.	-3812	-1.17x10-1	$-3.44x10^3$	$-1.48x10^3$
50°C	Int.	-	4.18x10-5	-10.07	-10.05
	Grad.	-3635	-1.18x10-1	$-3.28x10^3$	$-1.35x10^3$
55°C	Int.	-	3.98x10-5	-10.11	-10.08
	Grad.	-3728	-1.04x10-1	$-3.28x10^3$	$-1.41x10^3$
60°C	Int.	-	3.84x10-5*	-10.08*	-10.02*
	Grad.	-4658	-2.05x10-1*	$-8.08x10^{3}$*	$-3.41x10^{3}$*
65°C	Int.	-	+ve deviation from		
	Grad.	-4655	Porod's law		
70°C	Int.	Guinier plot	+ve deviation from		
	Grad.	curved	Porod's law		

* Plot curved thus values in doubt.

Table 4.10: Copolymer 1000 at various temperatures.- Calculated micellar dimensions.

SAMPLE	R_g	R_{sp}	δ (Vonk)	σ (Empirical)
20°C	61.7Å	79.7Å	20.1Å	7.6Å(26.3Å)
50°C	60.3Å	77.8Å	20.7Å	7.2Å(24.9Å)
55°C	60.1Å	78.7Å	19.9Å	7.4Å(25.6Å)
60°C	68.2Å	88.0Å	28.5Å	12.0Å(41.6Å)
65°C	68.2Å	88.0Å	-	-
70°C	-	-	-	-

The numbers in parenthesis are δ values calculated after ref. 60

Table 4.11: Copolymer 2000 at various concentrations.- Summary of gradient and intercept data from SAXS analysis.

Concentration		PLOT			
		Guinier	$s^3\tilde{I}$ vs. s^2	$\ln(s^3\tilde{I})$ vs. s^2	$\ln(s^3\tilde{I})$ vs. $s^{1.81}$
0.9 wt%	Int.	-	4.46x10-5	-9.52	-9.37
	Grad.	-2718	-3.55x10-1	-1.97×10^{4}	-8.41×10^{3}
2.0 wt%	Int.	-	1.78×10^{-5}	-10.63	-10.53
	Grad.	-2910	-1.24×10^{-1}	-1.45×10^{4}	-5.12×10^{3}
4.9 wt%	Int.	-	4.23×10^{-5}	-9.45	-9.45
	Grad.	-3222	-2.14×10^{-1}	-1.19×10^{4}	-5.30×10^{3}
9.8 wt%	Int.	-	4.50×10^{-5}	-9.66	-9.56
	Grad.	-3257	-3.20×10^{-1}	-1.50×10^{4}	-6.40×10^{3}

Table 4.12: Copolymer 2000 at various concentrations.- Calculated micellar dimensions.

SAMPLE	R_g	R_{sp}	δ (Vonk)	σ (Empirical)
0.9%	52.1Å	67.3Å	34.8Å	19.7Å(68.2Å)
2%	53.9Å	69.6Å	32.6Å	15.0Å(52Å)
4.9%	56.7Å	73.2Å	27.7Å	15.3Å(53Å)
9.8%	57.0Å	73.7Å	32.9Å	17.0Å(58.9Å)

The numbers in parenthesis are δ values calculated after ref. 60

Table 4.13: Copolymer 2000 at various temperatures.- Summary of gradient and intercept data from SAXS analysis.

Temperature		PLOT			
		Guinier	$s^3\tilde{I}$ vs. s^2	$\ln(s^3\tilde{I})$ vs. s^2	$\ln(s^3\tilde{I})$ vs. $s^{1.81}$
20°C	Int.	-	4.23×10^{-5}	-9.60	-9.45
	Grad.	-3222	-2.14×10^{-1}	-1.19×10^{4}	-5.30×10^{3}
30°C	Int.	-	6.33×10^{-5}	-9.23	-9.10
	Grad.	-2907	-4.70×10^{-1}	-1.78×10^{4}*	-7.62×10^{3}*
40°C	Int.	-	4.83×10^{-5}	-9.59	-9.47
	Grad.	-3582	-3.10×10^{-1}	-1.42×10^{4}	-6.14×10^{3}
50°C	Int.	-	6.89×10^{-5}	-8.92	-8.74
	Grad.	-3439	-6.06×10^{-1}	-2.49×10^{4}*	-1.06×10^{4}*
60°C	Int.	-	5.99×10^{-5}	-9.25	-9.11
	Grad.	-3251	-4.02×10^{-1}	-1.67×10^{4}	-7.19×10^{3}
70°C	Int.	-	7.08×10^{-5}	-8.94	-8.77
	Grad.	-3429	-6.06×10^{-1}	-2.22×10^{4}	-9.45×10^{3}

* Plot curved thus values in doubt.

Table 4.14: Copolymer 2000 at various temperatures.- Calculated micellar dimensions.

SAMPLE	R_g	R_{sp}	δ (Vonk)	σ (Empirical)
20°C	56.7Å	73.2Å	27.7Å	15.3Å(53Å)
30°C	53.9Å	69.6Å	33.6Å	18.7Å(64.8Å)
40°C	59.9Å	77.3Å	31.2Å	16.6Å(57.5Å)
50°C	58.6Å	75.6Å	36.6Å	22.4Å(77.6Å)
60°C	57.0Å	73.6Å	31.9Å	18.1Å(62.7Å)
70°C	58.6Å	75.7Å	36.0Å	21.0Å(72.7Å)
MEAN VALUES	57.5Å		33.0Å	18.2Å(63Å)

The numbers in parenthesis are δ values calculated after ref. 60

Table 4.15: Copolymer 2000 in water saturated with Methyl methacrylate monomer.- Summary of gradient and intercept data from SAXS analysis.

SAMPLE		PLOT			
TEMPERATURE		Guinier	$s^3\tilde{I}$ vs. s^2	$\ln(s^3\tilde{I})$ vs. s^2	$\ln(s^3\tilde{I})$ vs. $s^{1.81}$
21°C	Int.	-	1.08×10^{-5}	-10.94	-10.81
	Grad.	-4480	-1.07×10^{-1}	-2.44×10^{4}	-1.01×10^{4}
29°C	Int.	-	$2{,}00\times10^{-5}$	-10.48	-10.37
	Grad.	-4056	-1.67×10^{-1}	-1.79×10^{4}	-7.51×10^{3}
35°C	Int.	-	1.51×10^{-5}	-10.88	-10.79
	Grad.	-3958	-1.00×10^{-1}	-1.24×10^{4}	-5.27×10^{3}
40°C	Int.	-	2.30×10^{-5}*	-10.34*	-10.22*
	Grad.	-3331	-2.39×10^{-1}*	-2.21×10^{4}*	-9.14×10^{3}*
50°C	Int.	-	4.40×10^{-5}	-9.92	-9.86
	Grad.	-3218	-2.05×10^{-1}	-8.96×10^{3}	-378×10^{3}
60°C	Int.	-	5.92×10^{-5}	-9.50	-9.41
	Grad.	-3165	-3.23×10^{-1}	-1.02×10^{4}	-4.45×10^{3}

* Plot very curved thus result very uncertain.

Table 4.16: Copolymer 2000 in water saturated with Methyl methacrylate monomer.-Calculated micellar dimensions.

TEMPERATURE	R_g	R_{sp}	δ (Vonk)	σ (Empirical)
21°C	66.9Å	86.3Å	38.8Å	21.9Å(75.9Å)
29°C	63.7Å	82.2Å	35.6Å	18.6Å(64.4Å)
35°C	62.9Å	81.2Å	31.8Å	15.3Å(53Å)
40°C	57.7Å	74.5Å	*	*
50°C	56.7Å	73.1Å	29.3Å	12.7Å(44Å)
60°C	56.3Å	72.7Å	28.8Å	13.9Å(48.2Å)

* Plots curved thus no value determined

The numbers in parenthesis are δ values calculated after ref. 60

Table 4.17: 5% Copolymer 2000 dissolved directly in water with and without added MMA monomer.- Summary of gradient and intercept data from SAXS analysis.

Sample		PLOT			
		Guinier	$s^3\tilde{I}$ vs. s^2	$\ln(s^3\tilde{I})$ vs. s^2	$\ln(s^3\tilde{I})$ vs. $s^{1.81}$
Direct	Int.	-	3.07×10^{-5}	-10.39	-10.39
	Grad.	-3660	-3.98×10^{-2}	-1.44×10^{3}	-1.44×10^{3}
Direct + MMA	Int.	-	1.90×10^{-5}	-10.34	-10.18
	Grad.	-5193	-2.38×10^{-1}	-3.13×10^{4}	-1.28×10^{4}

Table 4.18: 5% Copolymer 2000 dissolved directly in water with and without added MMA monomer.- Calculated micellar dimensions.

Sample	R_g	R_{sp}	δ (Vonk)	σ (Empirical)
Direct	60.5Å	78.1Å	14.0Å	7.4Å(25.6Å)
Direct +MMA	76.9Å	99.3Å	43.6Å	24.9Å(86.3Å)

The numbers in parenthesis are δ values calculated after ref. 60

4.4POLYMERISATION OF METHYL METHACRYLATE USING COPOLYMER STABILISERS

4.4.1 Mode of addition of copolymer.

Dissolution of copolymer 2000 directly in water prior to the addition of water and the ammonium persulphate/sodium metabisulphite initiator yielded no emulsion polymer after 24 hours at 60°C. The content of the reactor at the end of 24 hours had a slightly grey appearance and no polymer precipitated on the addition of acetone.

Dissolution of the copolymer in the monomer prior to addition to the water and addition of the initiator produced milk white emulsions after a few minutes at 60°C. After 24 hours at 60°C addition of acetone to the cooled reaction mixture caused the emulsion to flocculate and form a single "lump" of polymer on the bottom of the vessel.

Dissolving the copolymer in methanol, mixing the solution slowly into water, then removal of the methanol by vacuum distillation before addition of monomer and initiator produced milk white emulsions after a few minutes at 60°C. Addition of acetone to the cooled reaction mixture caused the emulsion to flocculate and form a single "lump" on the bottom of the vessel.

The behavior of the polymerisation reactions with the copolymer addition via the monomer and via methanol were indistinguishable in terms of reaction rates and particle sizes of the emulsions produced. The results quoted below relate to the method of addition of copolymer via the monomer.

4.4.2 ΔT method of following the polymerisation.

Polymerisations initiated by the ammonium persulphate / sodium metabisulphite redox were observed to be very rapid. Conversions of approximately 90% of added monomer to polymer in 10 to 20 minutes were observed. For this system it was found that the best way to follow the progress of the polymerisation was to monitor the reaction exotherm. During the polymerisation the temperature difference between the thermostatically controlled water bath and the reaction mixture was recorded as a function of time. At the point at which the temperature difference returned to 0° a sample was extracted for solids analysis and the remaining reaction mixture cooled. A typical plot for ΔT vs. Time is shown in figure 4.25.

Assuming the flux of energy from the reaction vessel to the surrounding water is proportional to the temperature difference the integral of ΔT with respect to time can be directly equated to the progress of the reaction. Information relating to the degree of conversion of monomer to polymer is readily available at two points: At the begining where it is zero and at the end where a simple solids determination yields the quantity of polymer formed. Thus a solids analysis of the sample at the end of the experiment was used as a reference point from which the data were normalised. The resultant plot of "calculated" conversion vs. Time is also shown in figure 4.25.

The assumption that the heat flux from the reaction vessel is proportional to ΔT and that the rate of reaction is proportional to ΔT is reasonable if ΔT remains small. There are two major mechanisms by which energy can be removed from the reaction vessel: conduction through the glass walls to the surrounding water; or evaporation of liquid followed by transfer of energy to the cooling water of the condenser. Both of these can be considered to be proportional to ΔT over a small range of temperature.

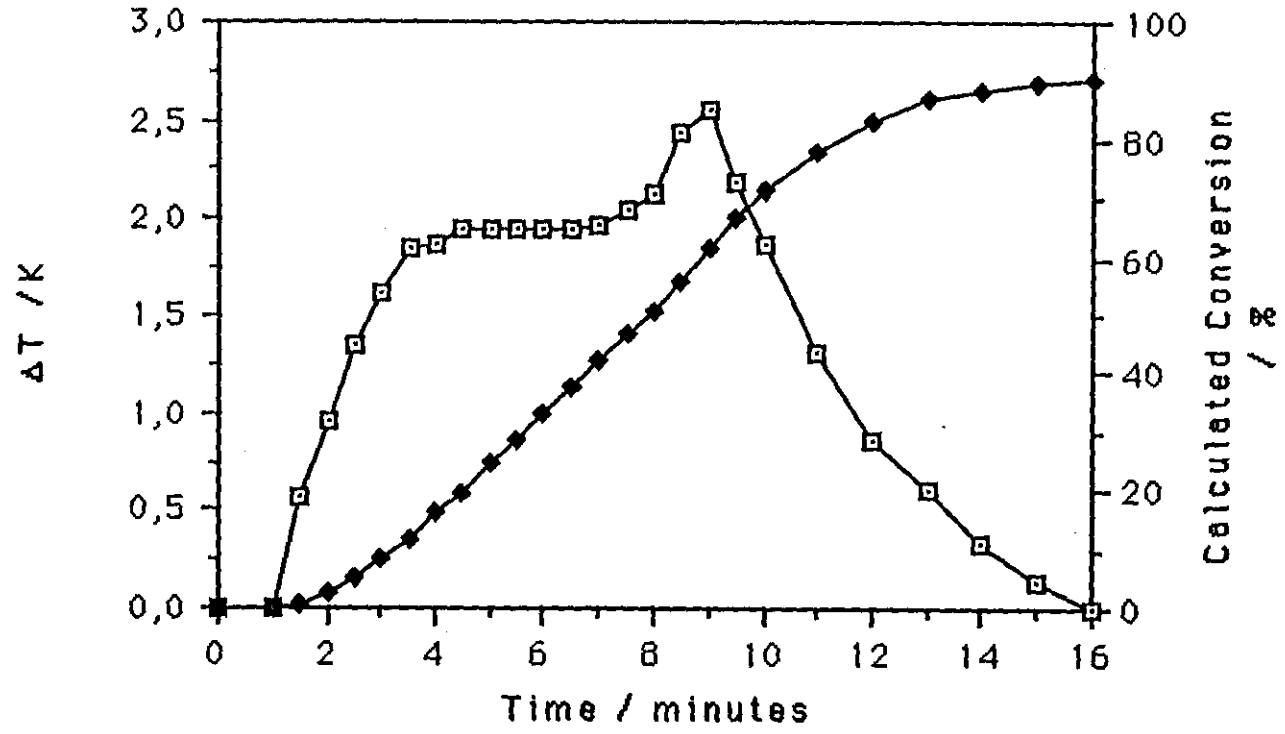

Figure 4.25: Plot of ΔT as a function of time and the integral of this curve normalised against a solids determination Polymerisation initiated by ammonium persulphate / sodium metabisulphite redox.

Proportionality of reaction rate to ΔT will only occur when the first derivative of the reaction rate is zero. When this occurs ΔT will be constant. During the period where ΔT is increasing the rate of energy liberated exceeds that transferred out of the reactor. As ΔT decreases the rate of energy transferred exceeds that liberated. As a consequence the conversion vs. time plot generated will under-estimate the conversion rate early in the reaction and over estimate the conversion rate towards the end. The region of steady reaction will be closest to correct. It is this region that has been utilised to calculate relative rates of reaction.

Table 4.19 gives details of the formulations of polymerisations performed with the ammonium persulphate / sodium metabisulphite redox initiator system and with the copolymer added via the monomer. The monomer in all cases was methyl methacrylate.

Figure 4.26 shows plots of calculated conversion as a function of time for various concentrations of ammonium persulphate. The polymerisations were performed with a fixed concentration of sodium metabisulphite and at a temperature of 323K. Figure 4.27 shows a plot of ln conversion rate as a function of ln $[S_2O_8^{2-}]^{1/2}[S_2O_5^{2-}]^{1/2}$ concentration. The equation given on the figure is a least squares fit for the data.

Figure 4.28 shows plots of calculated conversion as a function of time for various concentrations of copolymer 2000. The polymerisations were performed at 323K. Figure 4.29 shows a plot of ln conversion rate as a function of ln copolymer 2000 concentration. The equation given on the figure is a least squares fit for the data.

Table 4.19: Formulations for the emulsion polymerisation of methyl methacrylate initiated by persulphate/metabisulphite redox.

Nr.	Copolymer		Ammonium Persulphate	Sodium Metabisulphite	Total Water	Monomer	Temperature
1	2000	1.00g	5x10-4g	0.04g	22ml	5ml	50°C
2	2000	1.00g	1x10-3g	0.04g	22ml	5ml	50°C
3	2000	1.00g	2x10-3g	0.04g	22ml	5ml	50°C
4	2000	1.00g	4x10-3g	0.04g	22ml	5ml	50°C
5	2000	1.00g	8x10-3g	0.04g	22ml	5ml	50°C
6	2000	0.75g	2x10-3g	0.04g	22ml	5ml	50°C
7	2000	1.25g	2x10-3g	0.04g	22ml	5ml	50°C
8	2000	1.50g	2x10-3g	0.04g	22ml	5ml	50°C
9	2000	1.75g	2x10-3g	0.04g	22ml	5ml	50°C
10	2000	1.00g	2x10-3g	0.04g	22ml	3ml	60°C
11	2000	1.00g	2x10-3g	0.04g	22ml	5ml	60°C
12	2000	1.00g	2x10-3g	0.04g	22ml	6ml	60°C
13	2000	1.00g	2x10-3g	0.04g	22ml	7.5ml	60°C
14	2000	1.00g	2x10-3g	0.04g	22ml	8ml	60°C
15	2000	1.00g	2x10-3g	0.04g	22ml	5ml	40°C
16	2000	1.00g	2x10-3g	0.04g	22ml	5ml	65°C
17	2000	1.00g	2x10-3g	0.04g	22ml	5ml	70°C
18	750	1.00g	2x10-3g	0.04g	22ml	5ml	65°C
19	1000	1.00g	2x10-3g	0.04g	22ml	5ml	65°C
20	4000	1.00g	2x10-3g	0.04g	22ml	5ml	65°C

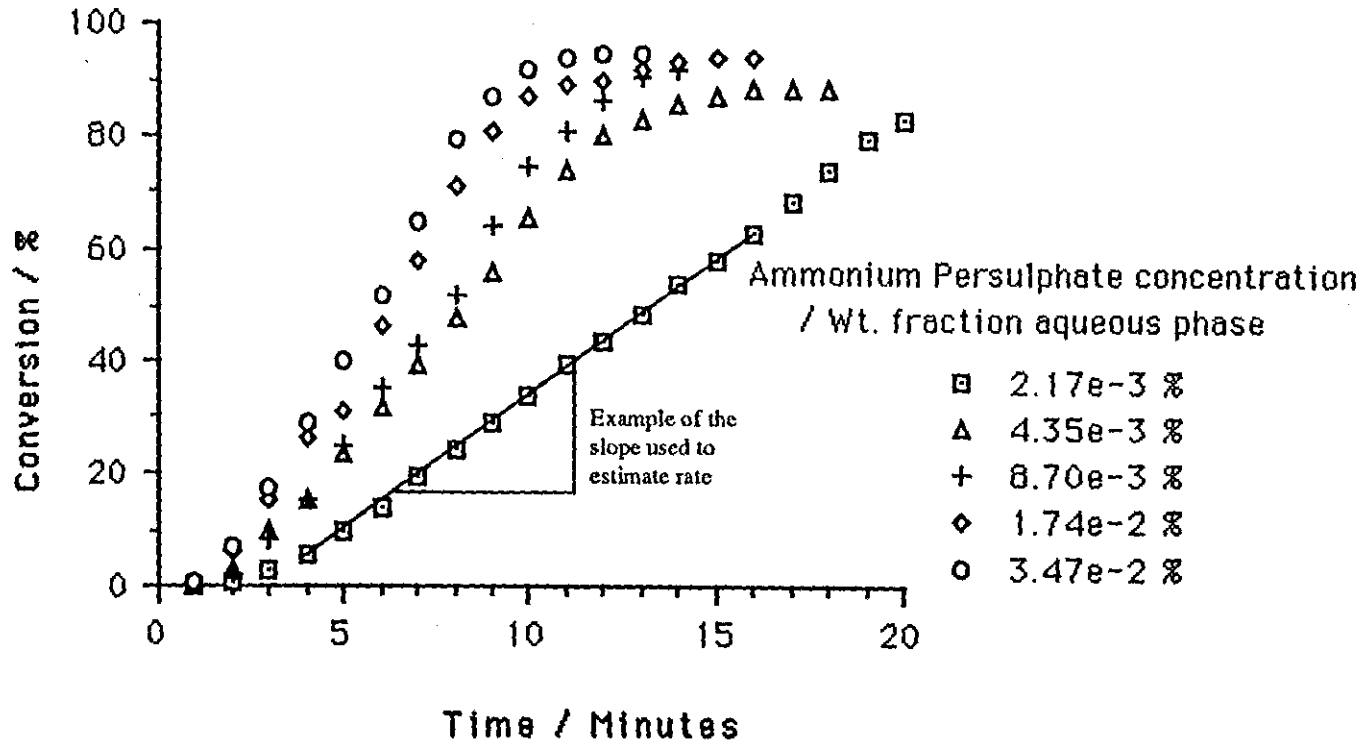

Figure 4.26: Plots of conversion vs time for various initiator concentrations.
Polymerisation stabilised by copolymer 2000, initiated by persulphate / metabisulphite

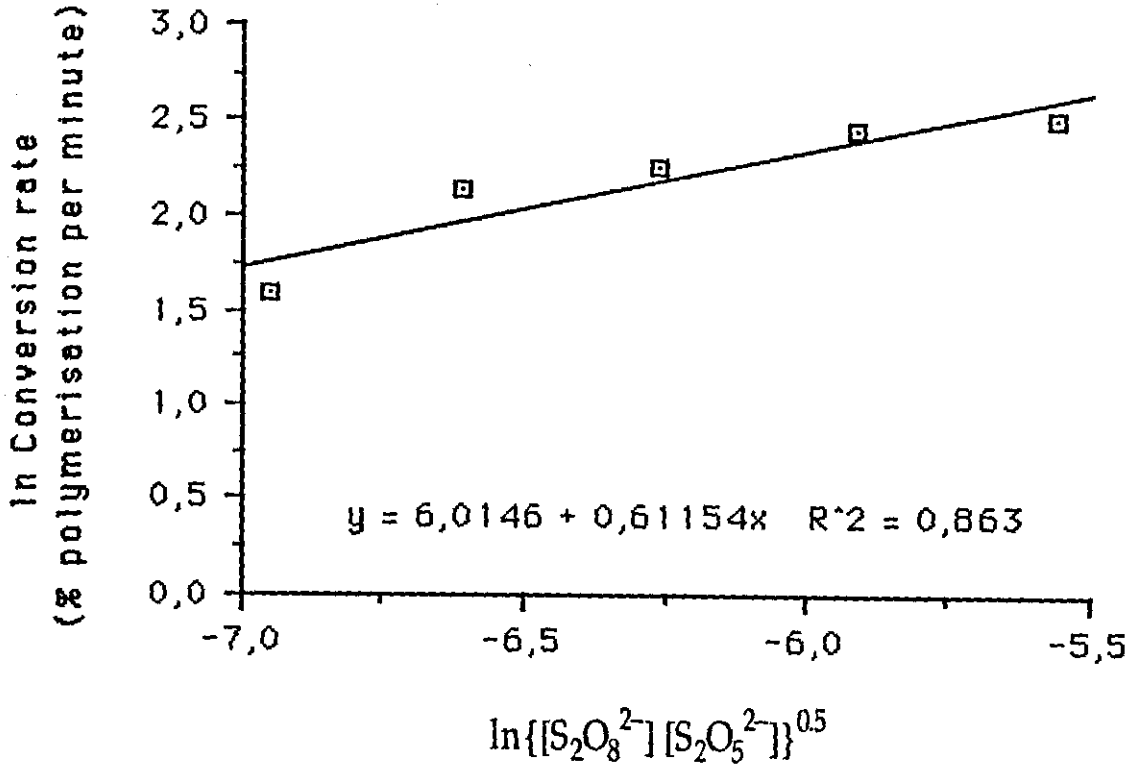

Figure 4.27: Plot of ln (conversion rate) as a function of $\ln\{[S_2O_8^{2-}]\,[S_2O_5^{2-}]\}^{0.5}$
Initiation by persulphate / metabisulphite redox, stabilised by copolymer 2000.

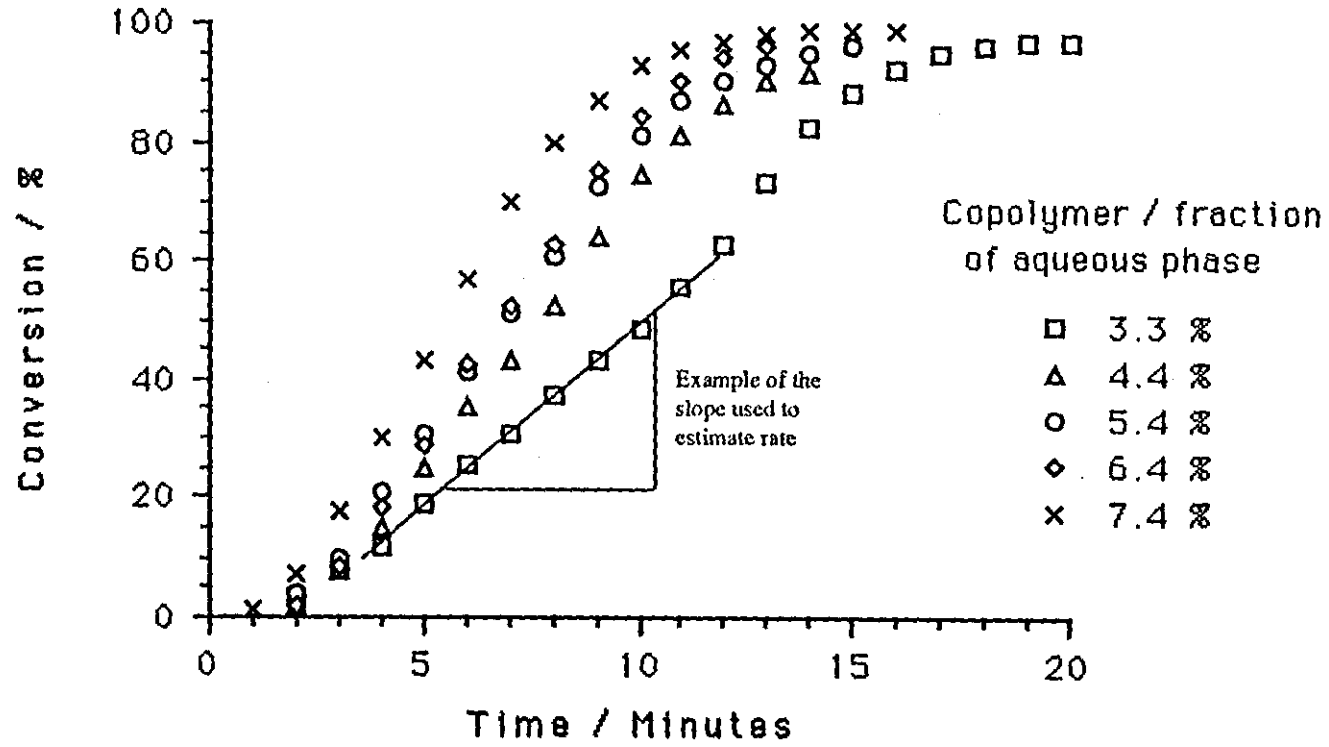

Figure 4.28: Plots of conversion vs time for various copolymer concentrations.
Polymerisation stabilised by copolymer 2000, initiated by persulphate / metabisulphite

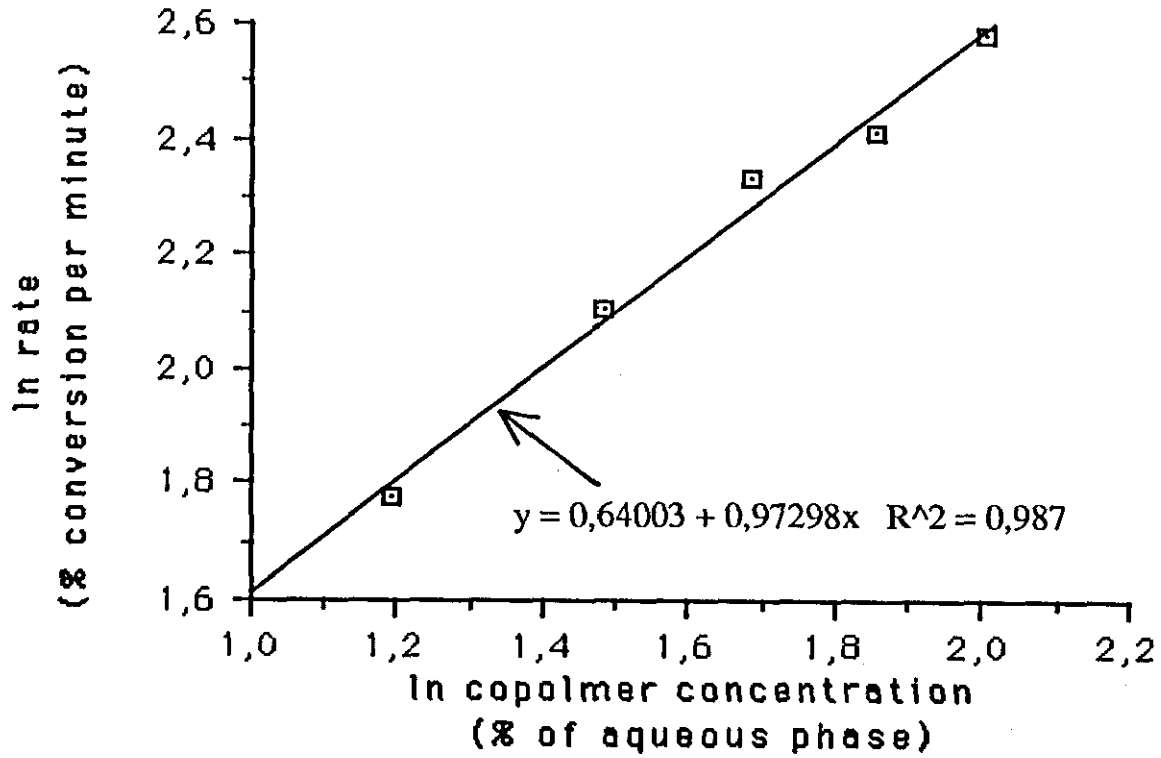

Figure 4.29: Plot of ln (conversion rate) as a function of ln (Copolymer concentration).
Initiation by persulphate / metabisulphite redox, stabilised by copolymer 2000

4.4.3 DSC method of following the polymerisation.

The rate of reaction of polymerisations initiated by the persulphate / metabisulphite redox system was too great for the DSC to be used. The time taken to load a sample into a pan, locate it in the DSC, heat to the reaction temperature and obtain stability in the DSC output signal was significant in terms of the reaction time. The system initiated by 4,4′-azobis(4-cyano-pentanoic acid) was more appropriate for the system. Figure 4.30 shows a DSC trace typical for this system. There were two problems inherent with this technique: Firstly it was shown that the composition of a 10mg sample extracted from a larger sample was not representative of the larger sample. Methyl methacrylate monomer has a lower density than water and as such tends to separate. The bulk sample itself may not be homogeneous and certainly once in the syringe for transfer to the sample pan separation begins to occur. The second problem was the absence of agitation once in the DSC furnace. Without continuous stirring the reaction mixture tends to form two distinct layers one monomer rich and the other water rich. For these reasons the solids method described below was selected as being more appropriate for this system.

4.4.4 Solids content method of following the polymerisation.

Table 4.20 gives details of the formulations of polymerisations performed with the 4,4′-azobis(4-cyano-pentanoic acid) azo initiator system and with the copolymer added via the monomer. The monomer in all cases was methyl methacrylate.

Figure 4.31 shows plots of conversion as a function of time for various concentrations of 4,4′-azobis(4-cyano-pentanoic acid). Figure 4.32 shows

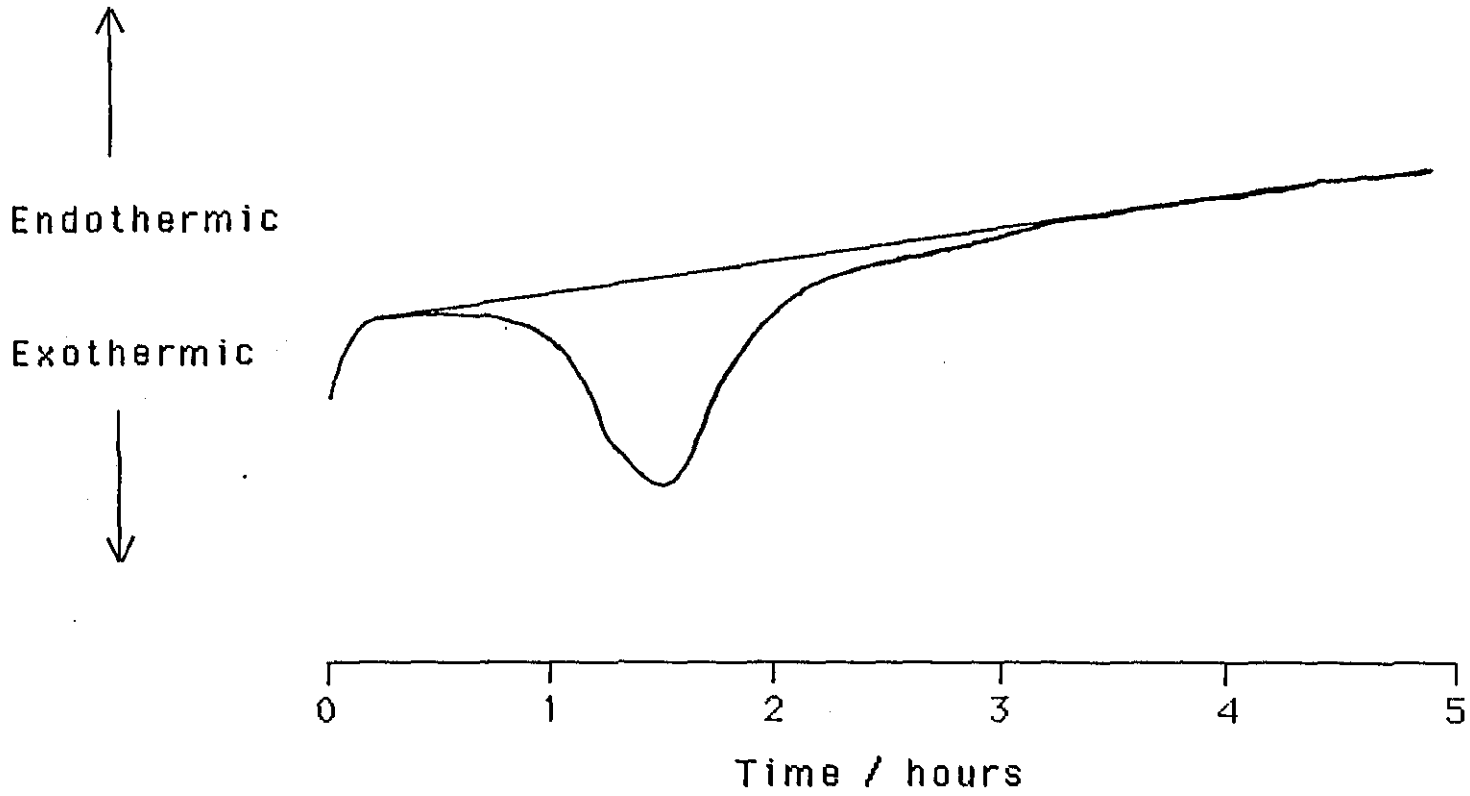

Figure 4.30: Isothermal (70°C) DSC trace showing the exotherm relating to the polymerisation reaction. Polymerisation stabilised by copolymer 2000 initiated by 4,4´azobis(4-cyano-pentanoic acid).

Table 4.20: Formulations for the emulsion polymerisation of methyl methacrylate initiated by 4,4´-azobis(4-cyano-pentanoic acid).

Nr.	Copolymer		4,4´-azobis(4-cyano-pentanoic acid)		Total Water	Monomer	Temperature
21	2000	0.50g	0.25ml	0.5%	12ml	2ml	70°C
22	2000	0.50g	0.50ml	0.5%	12ml	2ml	70°C
23	2000	0.50g	1.00ml	0.5%	12ml	2ml	70°C
24	2000	0.50g	2.00ml	0.5%	12ml	2ml	70°C
25	2000	0.34g	0.50ml	0.5%	12ml	2ml	70°C
26	2000	0.595g	0.50ml	0.5%	12ml	2ml	70°C
27	2000	0.85g	0.50ml	0.5%	12ml	2ml	70°C
28	2000	0.50g	0.25ml	0.5%	12ml	1.5ml	70°C
29	2000	0.50g	0.25ml	0.5%	12ml	2.5ml	70°C

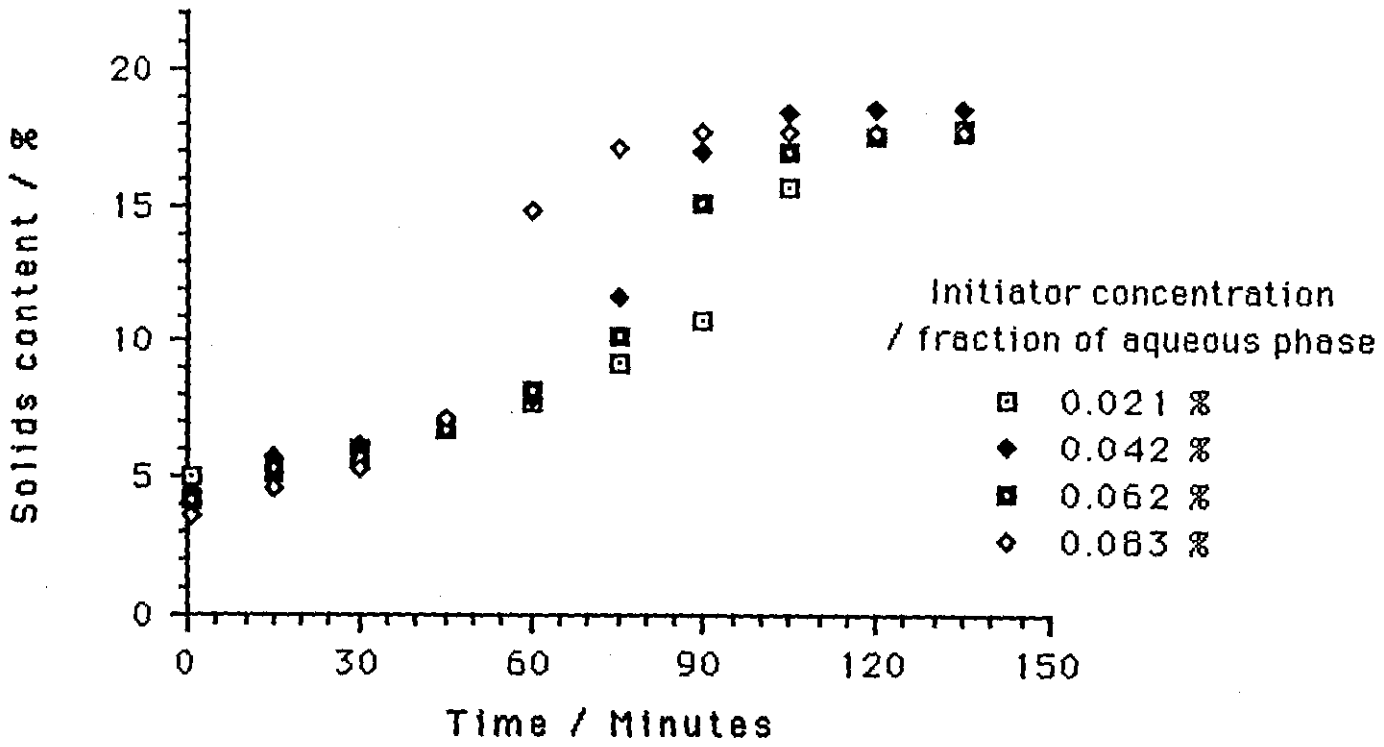

Figure 4.31: Plot of solids content as a function of time for various initiator concentrations.
Polymerisation stabilised by copolymer 2000, initiated by 4,4´-azobis(4-cyano-pentanoic acid)

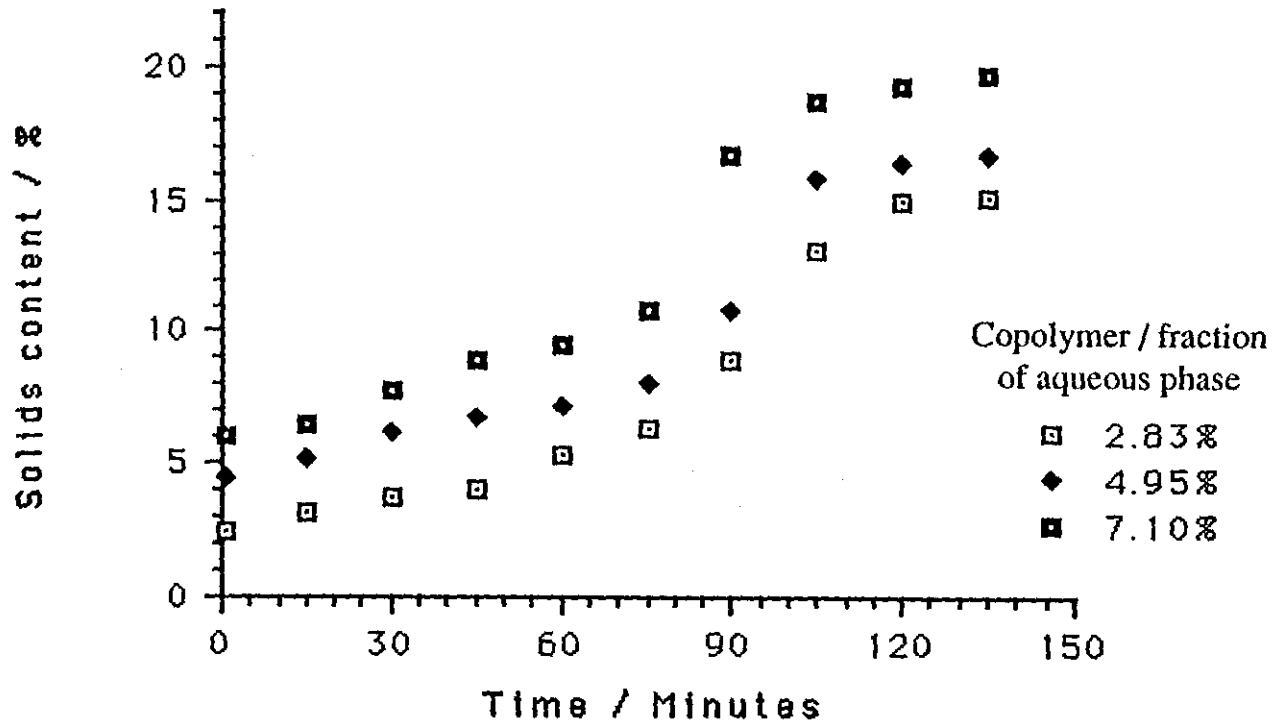

Figure 4.32: Plot of solids content as a function of time for various copolymer concentrations.
Polymerisation stabilised by copolymer 2000, initiated by 4,4´-azobis(4-cyano-pentanoic acid)

plots of conversion as a function of time for various concentrations of copolymer 2000. The polymerisations were performed at a temperature of 343K. Figure 4.33 shows plots of conversion as a function of time for various concentrations of methyl methacrylate monomer.

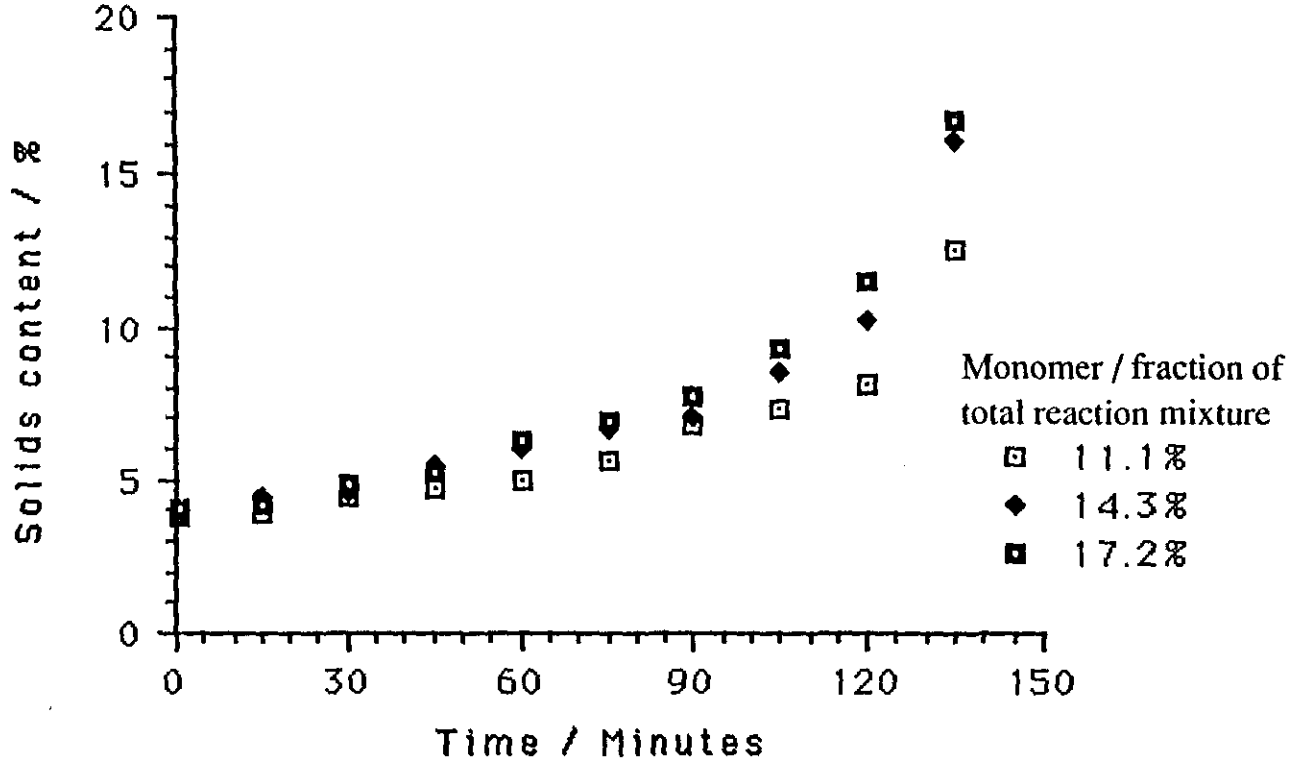

Figure 4.33: Plot of solids content as a function of time for various monomer concentrations.
Polymerisation stabilised by copolymer 2000, initiated by 4,4´-azobis(4-cyano-pentanoic acid)

4.5 CHARACTERISATION OF EMULSION POLYMERS

4.5.1 Transmission Electron Microscopy

Transmission electron micrographs of each product from the emulsion polymerisation experiments were taken. In almost all cases there was observed a degree of agglomeration of particles on the carbon grid. The agglomeration was noted to be two dimensional, ie. all particles were in the plane of the carbon film with no stacking. Increased dilution of the emulsion during sample preparation did improve the separation of the particles but reduced the abundance of particles below practical limits (only two or three particles per picture area). The agglomeration was therefore assumed not to imply flocculation but to have occurred during sample preparation. A typical micrograph is shown in photograph 1.

Figures 4.34 to 4.38 give a graphical summary of the particle size measurements made on the emulsions described in table 4.19, section 4.4.1. All average particle sizes are in μm. The error bars indicate ± the standard deviation of the diameters of the particles measured. Figure 4.34 shows the relationship between final particle size and the concentration of ammonium persulphate (Reactions 1, 2, 3, 4 & 5). Figure 4.35 shows the relationship between particle size and initial copolymer concentration (Reactions 6, 3, 7, 8 & 9). Figure 4.36 shows the relationship between particle diameter and monomer concentration (Reactions 10, 11, 12, 13 & 14). Figure 4.37 shows the relationship between particle diameter and polymerisation temperature (Reactions 15, 3, 11, 16 & 17). Figure 4.38 shows the relationship between particle diameter and the PEO block length (nmr derived) of the copolymer used (Reactions 18, 16, 19 & 20).

Figure 4.39 shows the relationship between particle size and initiator

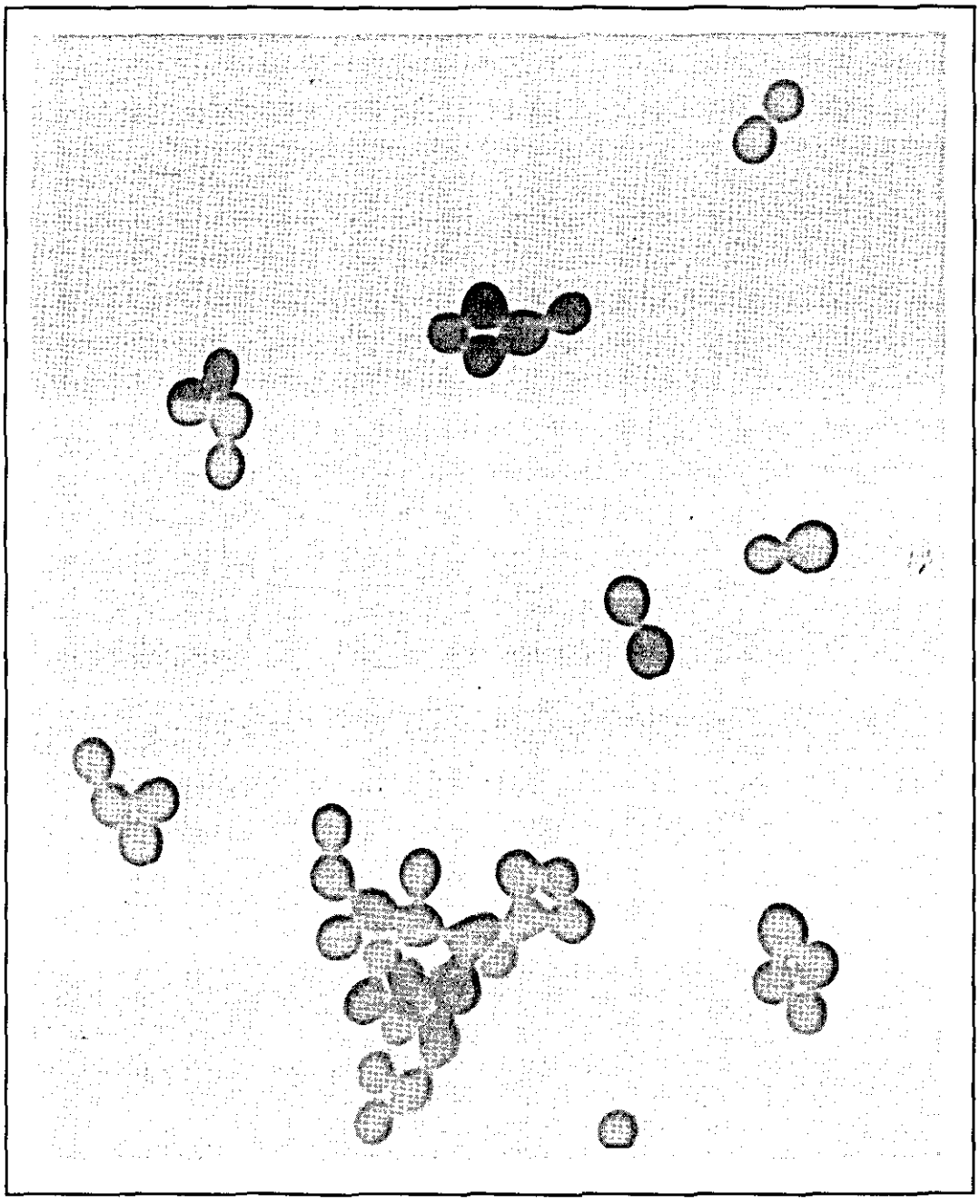

Photograph 4.1: A typical micrograph of emulsion particles. This emulsion polymer was the product of reaction 19 as defined in table 4.19

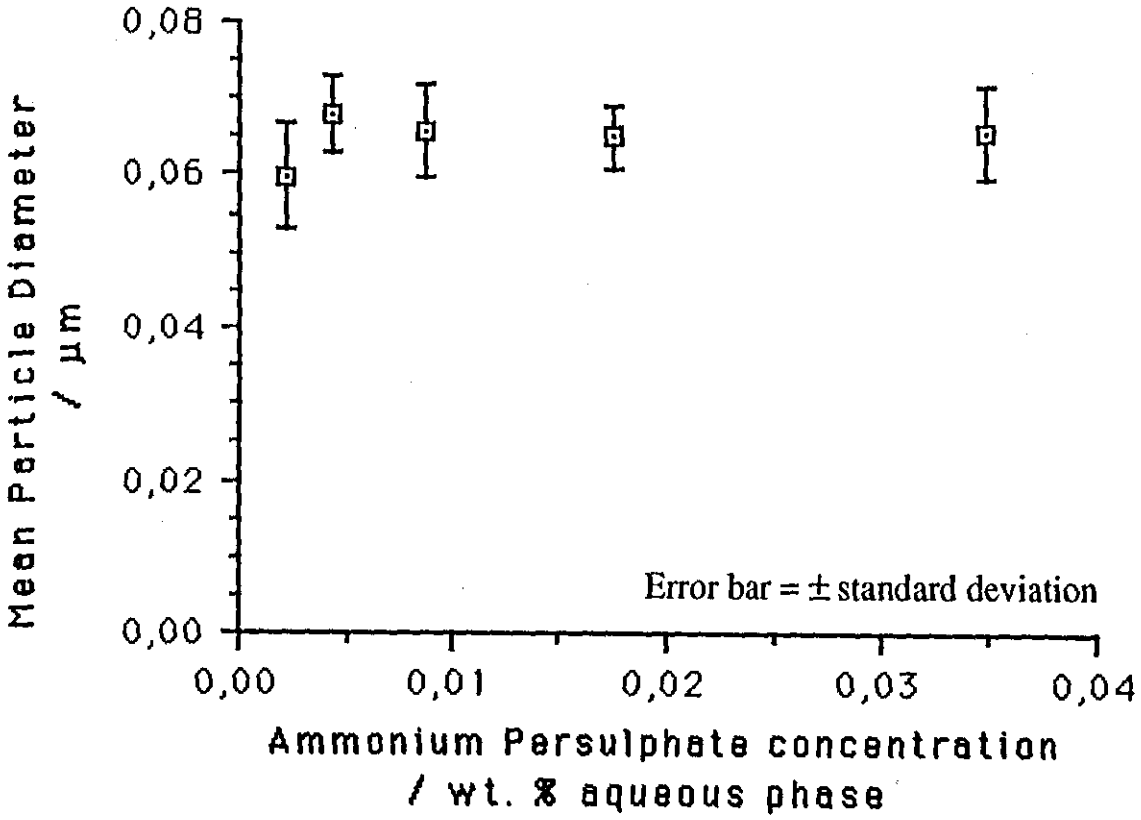

Figure 4.34: Plot of mean particle diameter as a function of ammonium persulphate concentration Initiation by persulphate / metabisulphite redox, stabilised by copolymer 2000.

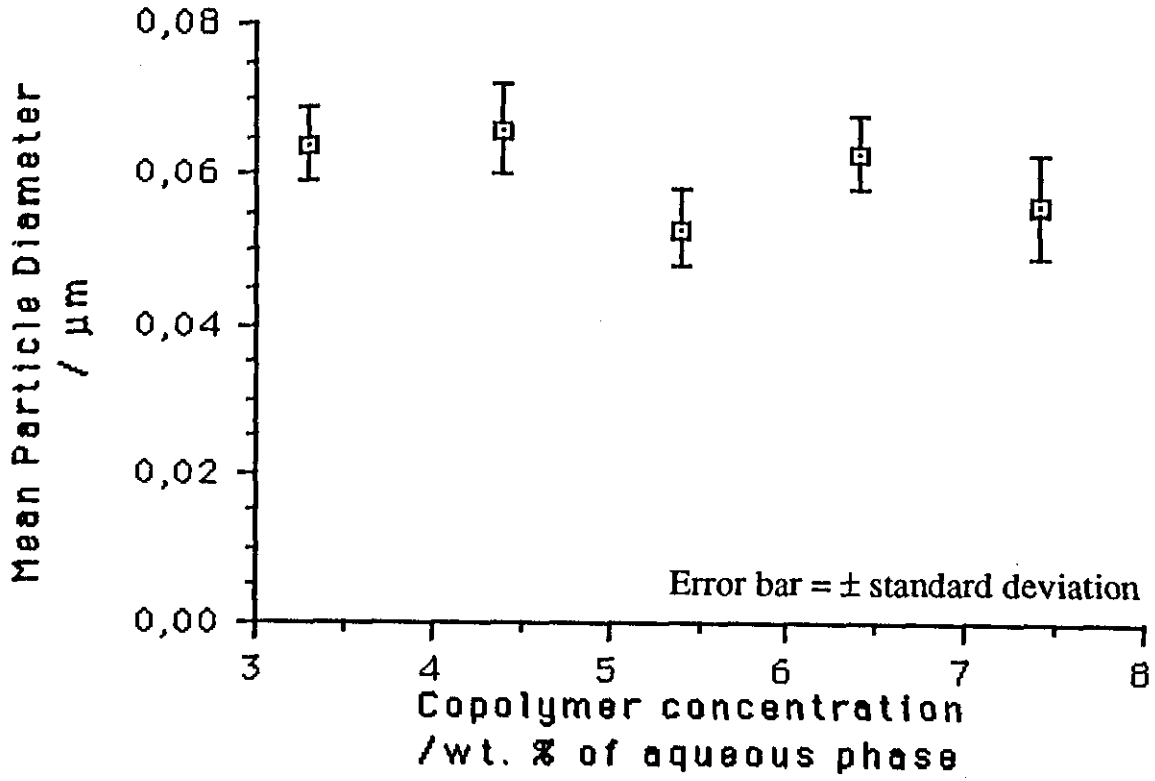

Figure 4.35: Plot of mean particle diameter as a function of copolymer concentration
Initiation by persulphate / metabisulphite redox, stabilised by copolymer 2000

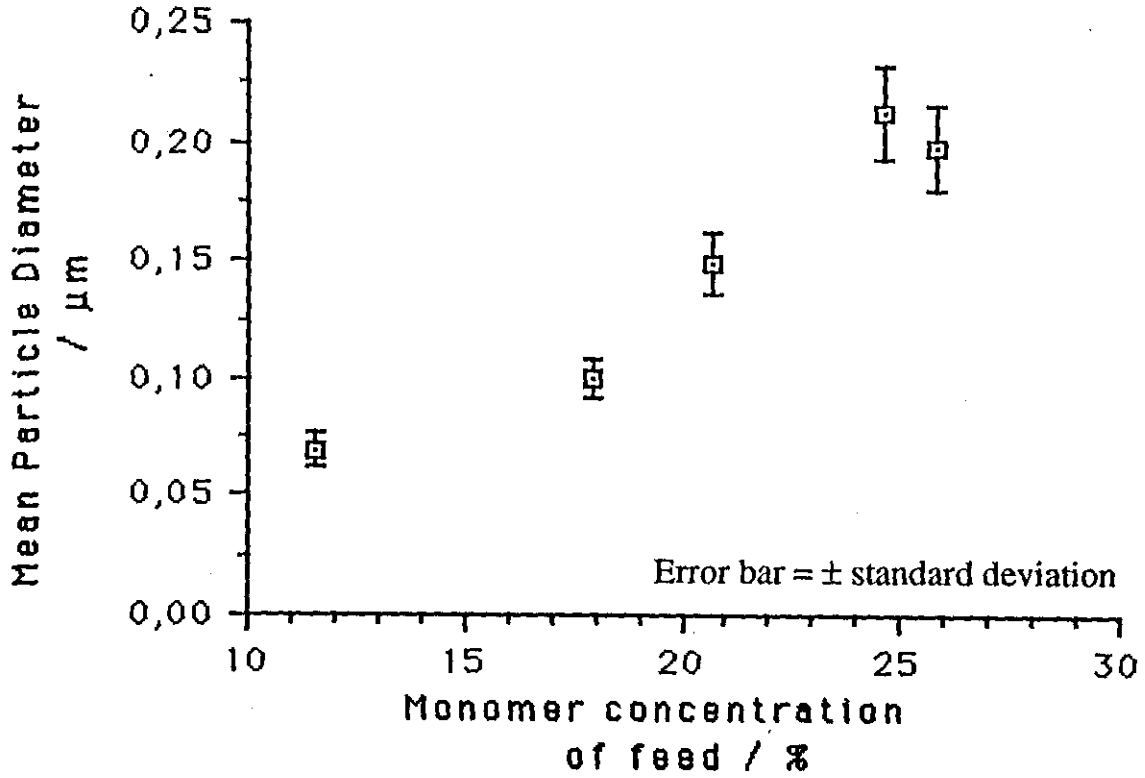

Figure 4.36: Plot of mean particle diameter as a function of monomer concentration.

Initiation by persulphate / metabisulphite redox, stabilised by copolymer 2000

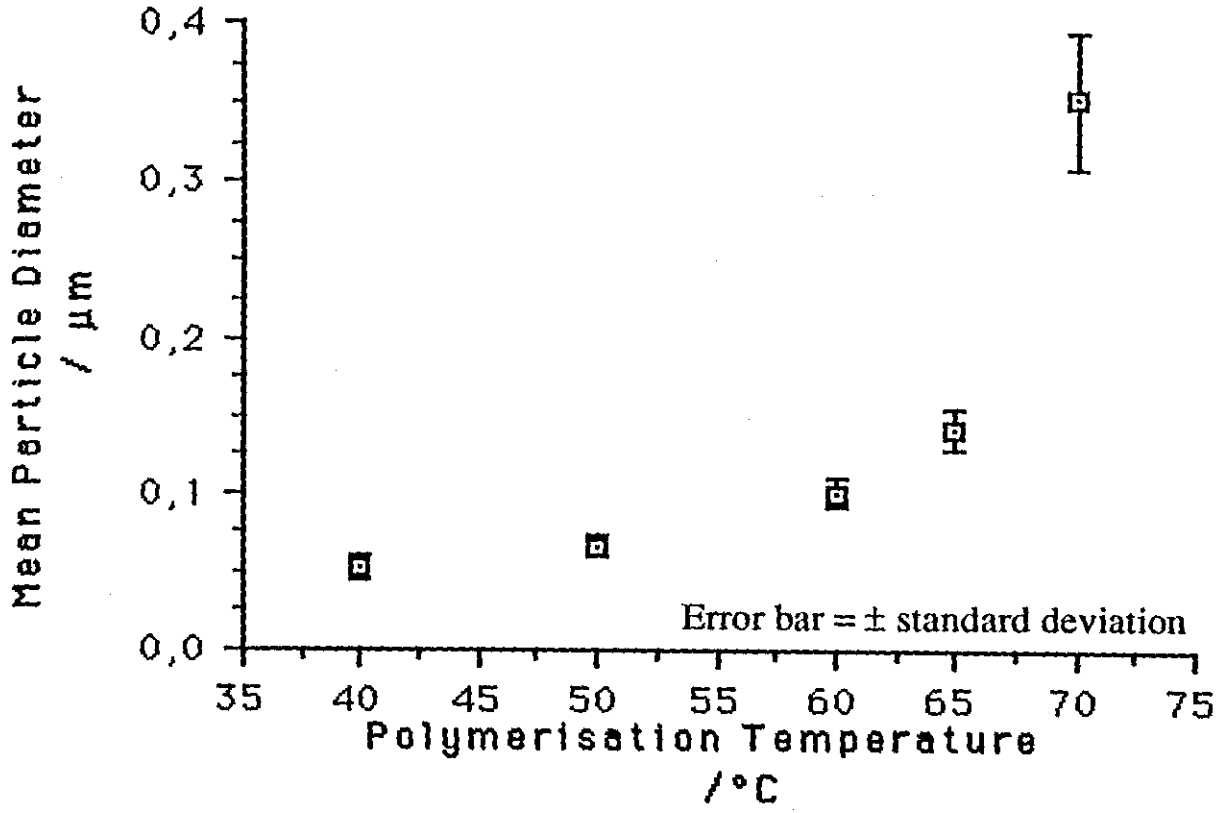

Figure 4.37: Plot of mean particle diameter as a function of polymerisation temperature. Initiation by persulphate / metabisulphite redox, stabilised by copolymer 2000

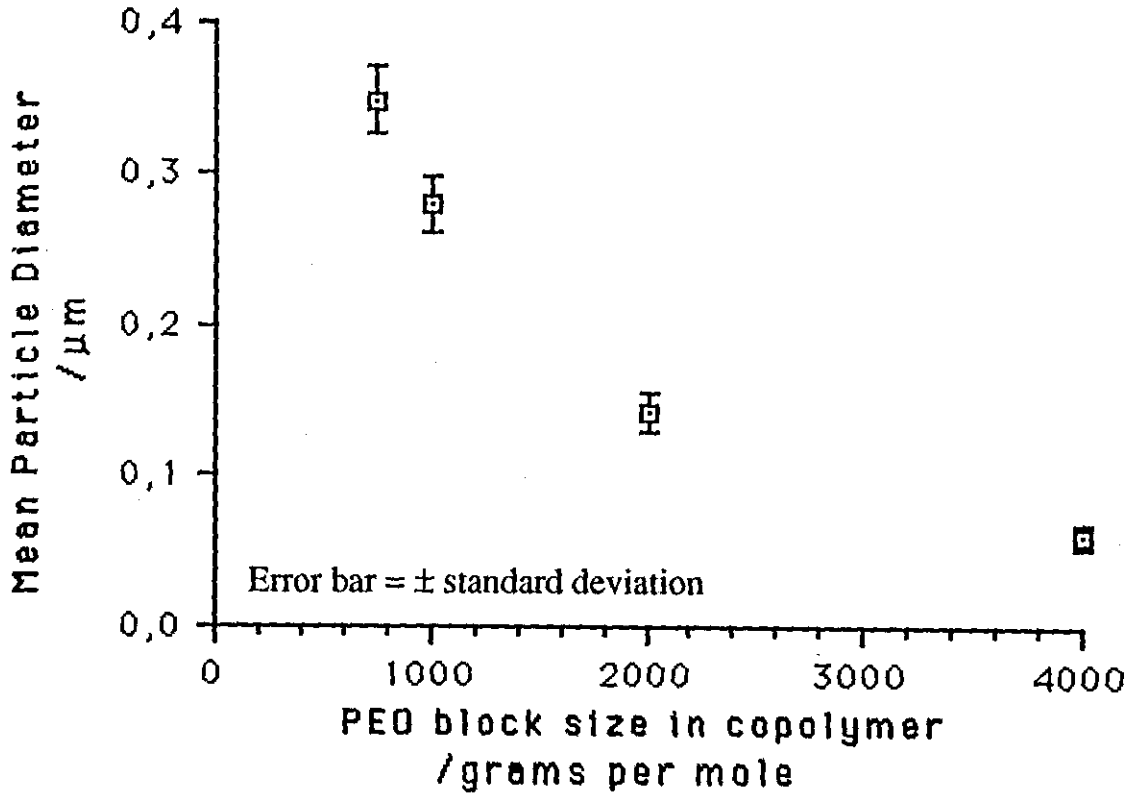

Figure 4.38: Plot of mean particle diameter as a function of PEO block length in the stabilising copolymer Initiation by persulphate metabisulphite redox, temperature 65°C.

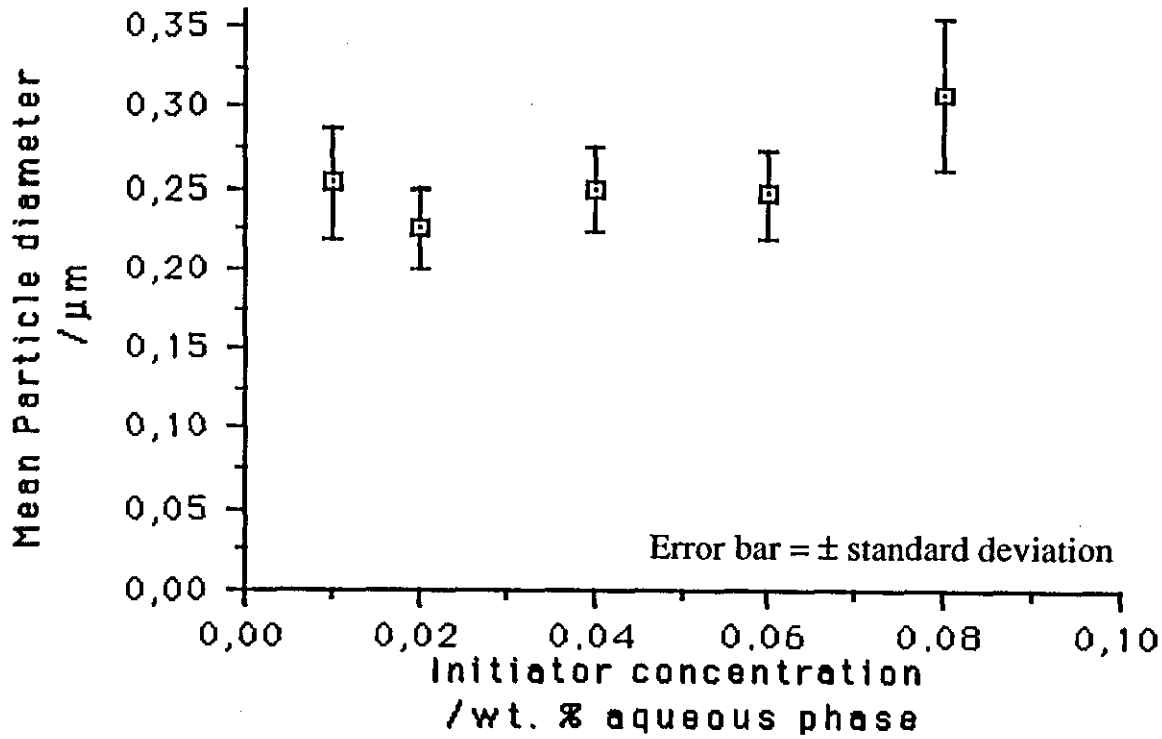

Figure 4.39: Plot of mean particle diameter as a function of initiator concentration
Initiation by 4,4´-azobis(4-cyano-pentanoic acid), stabilised by copolymer 2000.

concentration for polymerisations initiated by 4,4´-azobis(4-cyano-pentanoic acid). (See table 4.20)

4.5.2 Gel Permeation Chromatography

The two samples of emulsion polymers, one ammonium persulphate /sodium metabisulphite redox initiated sample and one 4,4´-azobis(4-cyano-pentanoic acid) initiated sample, were studied by gel permeation chromatography. Chromatograms were very similar in form both containing a low molecular weight fraction and a higher molecular weight fraction. In both cases the low molecular weight fraction corresponds to the copolymer added and presumably the high molecular weight fraction corresponds to the emulsion polymerised material. Table 4.21 shows the computer calculated average molecular weights and figure 4.40 shows the chromatogram from the polymerisation initiated by the ammonium persulphate / sodium metabisulphite redox system.

Table 4.21: GPC results for emulsion polymers

	Persulphate / Metabisulphite	4,4´-azobis (4-cyano-pentanoic acid)
$\overline{M}_n$	6.79×10^3	3.2×10^3
$\overline{M}_w$	7.52×10^5	4.12×10^5
M_p	1.28×10^6	1.50×10^6

These calculated molecular weights account for the polymer in both peaks. $\overline{M}_n$ is dominated by the copolymer content of the sample and $\overline{M}_w$ is affected accordingly. The values for M_p must be considered to give the best indication of the molecular weight of the emulsion polymer.

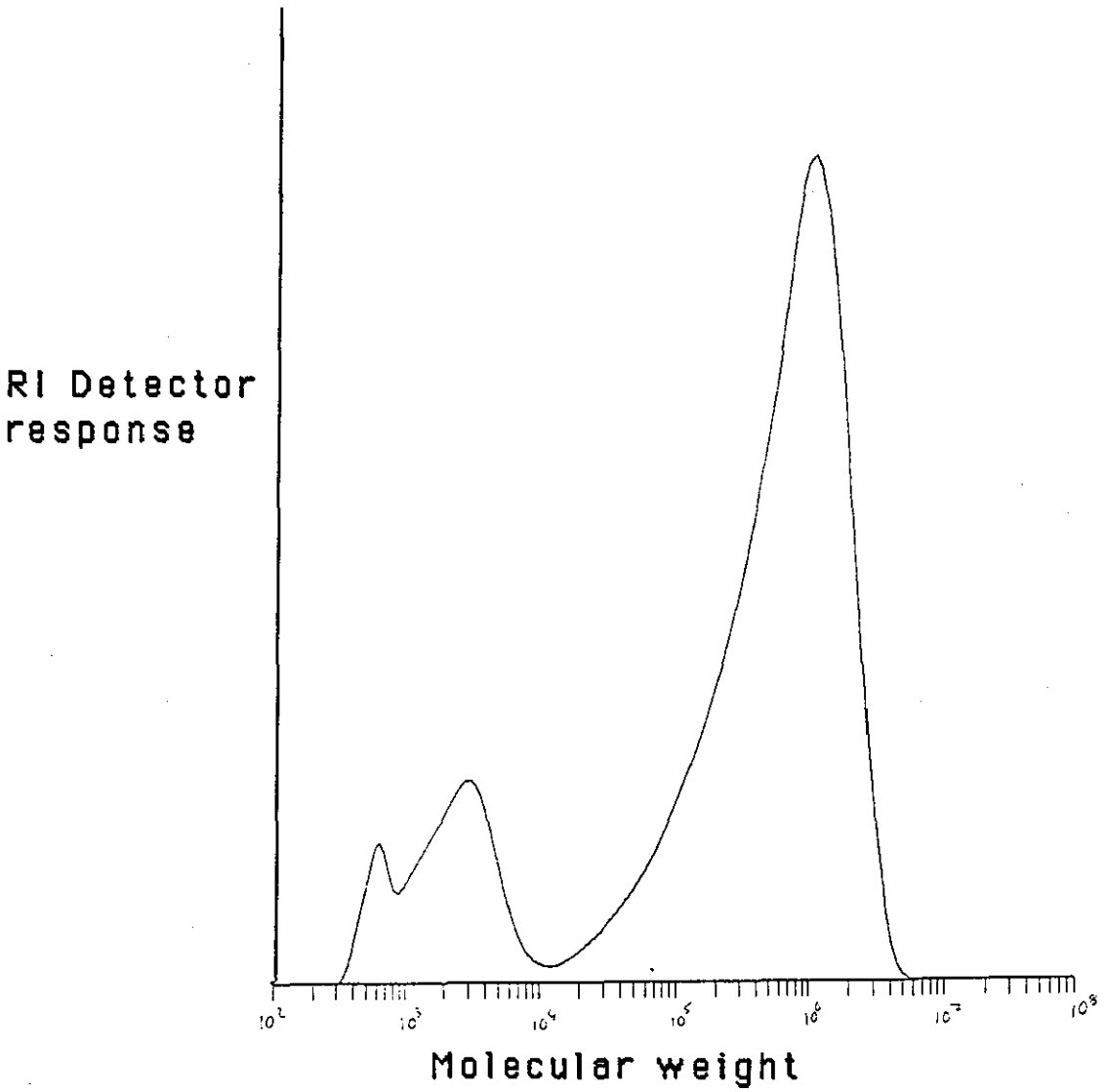

Figure 4.40: Plot of RI detector response as a function of log molecular weight For a polymer initiated by ammonium persulphate / sodium metabisulphite redox and stabilised by copolymer 2000.

4.5.3 Electrophoresis

Electrophoretic mobilities were studied for five selected emulsions. Figures 4.41 and 4.42 show the pH dependence of the mobility for emulsions stabilised by copolymers 1000 and 2000 respectively. Both were initiated by the persulphate / metabisulphite redox system. Both of these emulsions show a mobility over the entire pH range monitored. This mobility indicates that there is an electrostatic contribution to the stability of the emulsions over this range of pH.

Figures 4.43 and 4.44 show the pH dependence of electrophoretic mobility for emulsions stabilised by copolymers 2000 and 4000 respectively. Both were initiated by the water soluble azo initiator 4,4′-azobis-(4-cyano-pentanoic acid). Both emulsions exhibit the same pH dependence of electrophoretic mobility. Between pH=6 and pH=4 the mobility falls to a value close to zero. As a result it can be concluded that these polymers have no electrostatic contribution to their stability at values of pH below 4.

Figure 4.45 shows the pH dependence of electrophoretic mobility for an emulsion stabilised by copolymer 2000 and initiated by the redox initiator system ascorbic acid / potassium permanganate. This emulsion shows a similar behavior to the two azo initiated emulsions above. All three contain carboxylic acid groups which dissociate at pH values above ca. 5. (The pKa value for a carboxylic acid is in the region 4.5-4.9).

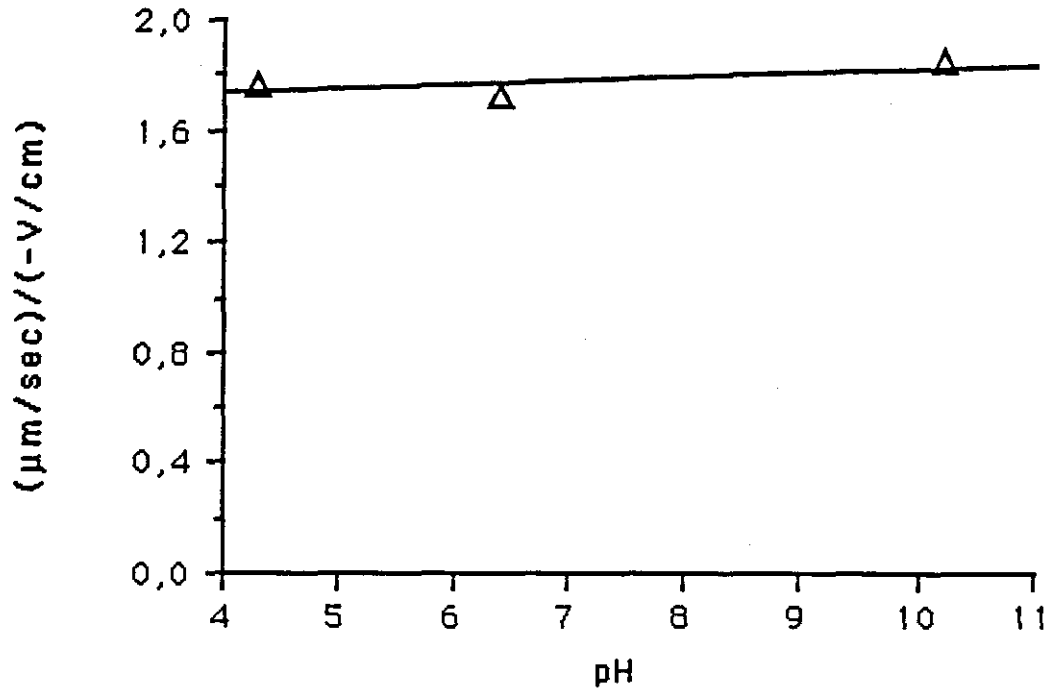

Figure 4.41: Electrophoretic mobility of an emulsion generated with copolymer 1000 with the redox initiator system persulphate / metabisulphite.

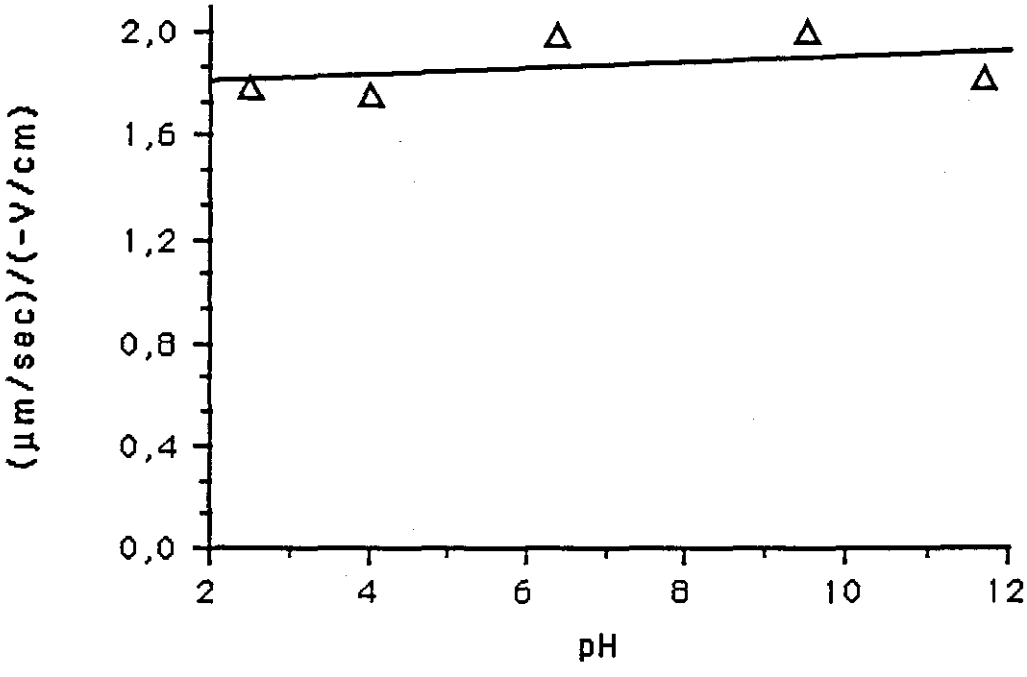

Figure 4.42: Electrophoretic mobility of an emulsion generated with copolymer 2000 with the redox initiator system persulphate / metabisulphite

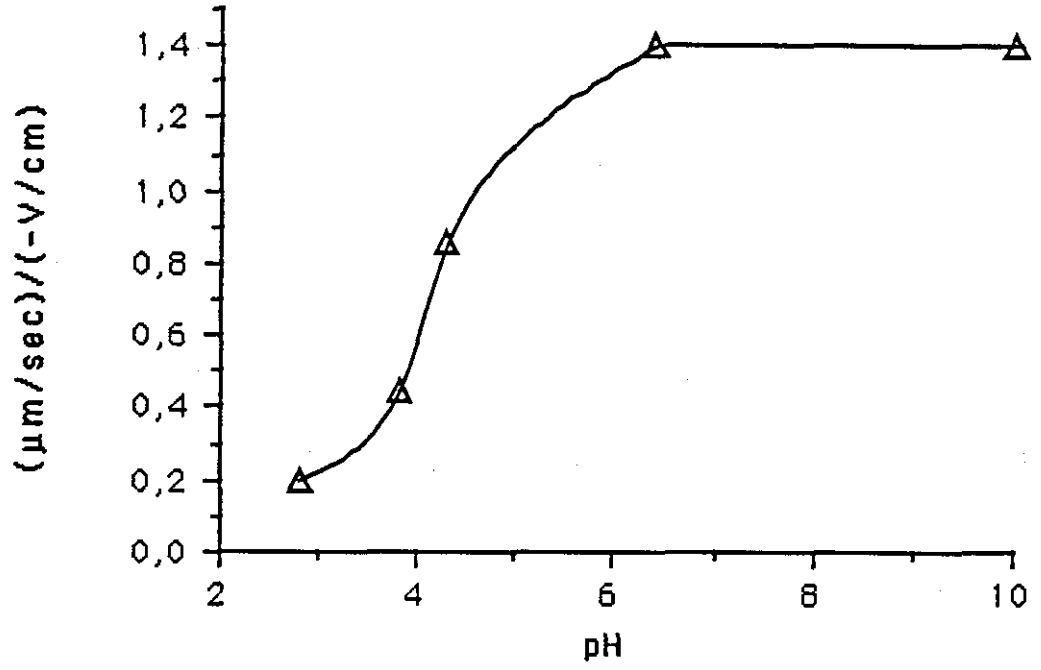

Figure 4.43: Electrophoretic mobility of an emulsion generated with copolymer 2000 with the azo initiator 4,4´-Azobis(4-cyano-pentanoic acid).

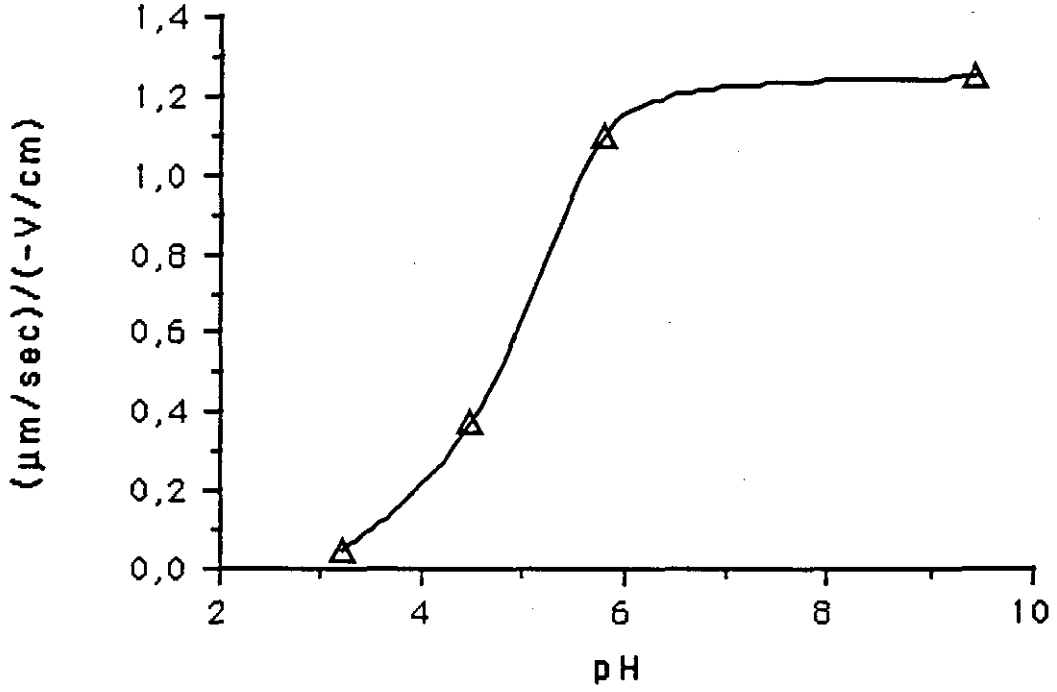

Figure 4.44: Electrophoretic mobility of an emulsion generated with copolymer 4000 with the azo initiator 4,4´-Azobis(4-cyano-pentanoic acid).

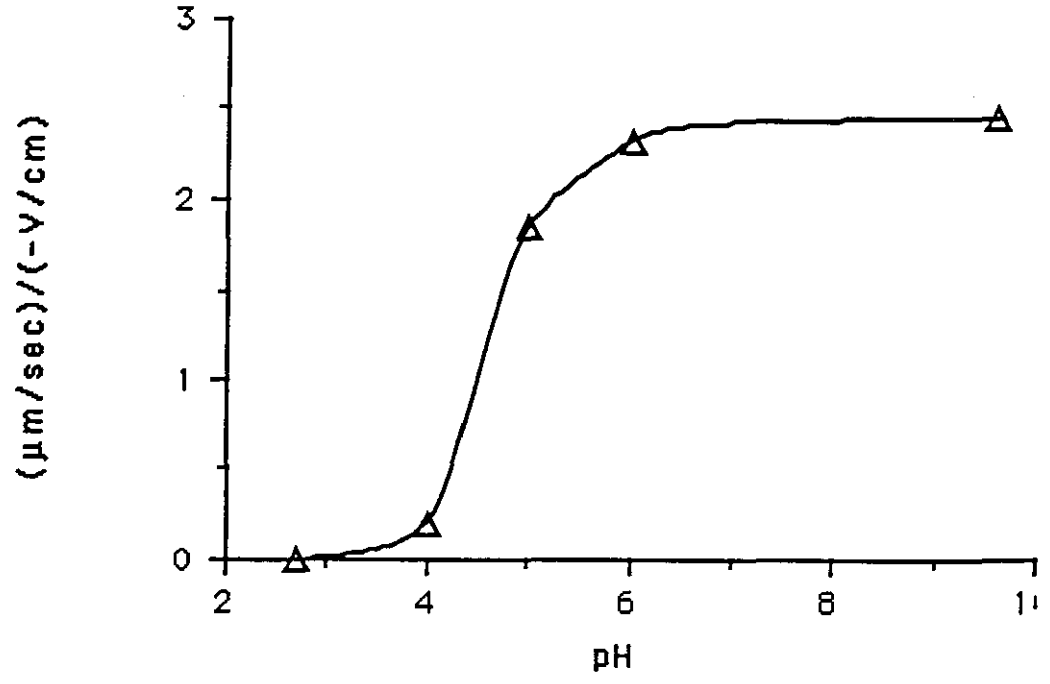

Figure 4.45: Electrophoretic mobility of an emulsion generated with copolymer 2000 with the redox initiator system Ascorbic acid / Potassiumpermanganate.

4.5.4 Stability of emulsions.

Samples of emulsions stabilised with copolymers 2000 and 4000, initiated by 4,4′-azobis-(4-cyano-pentanoic acid) and one stabilised by copolymer 2000, initiated by ascorbic acid $KMnO_4$ were acidified with HCl to pH=2 ±0.5 and stored. After 14 months all three emulsions had settled slightly (clear liquid above the emulsion) but easily redispersed on shaking. After 20 months all three samples had separated and could not be redispersed. It is very possible that these samples had been frozen during the period between 14 and 20 months. (They were stored in an unheated room in Norway- the external temperature during this period fell below -25°C)

4.6 SUBSIDIARY EXPERIMENTS

4.6.1 Monomer Solubility in Water

Figure 4.46 shows the saturation concentration of methyl methacrylate monomer in water as a function of temperature. The location of the minimum in the graph is supported by the fact that on heating to- and cooling to- temperatures around 320K the solution becomes cloudy as monomer comes out of solution.

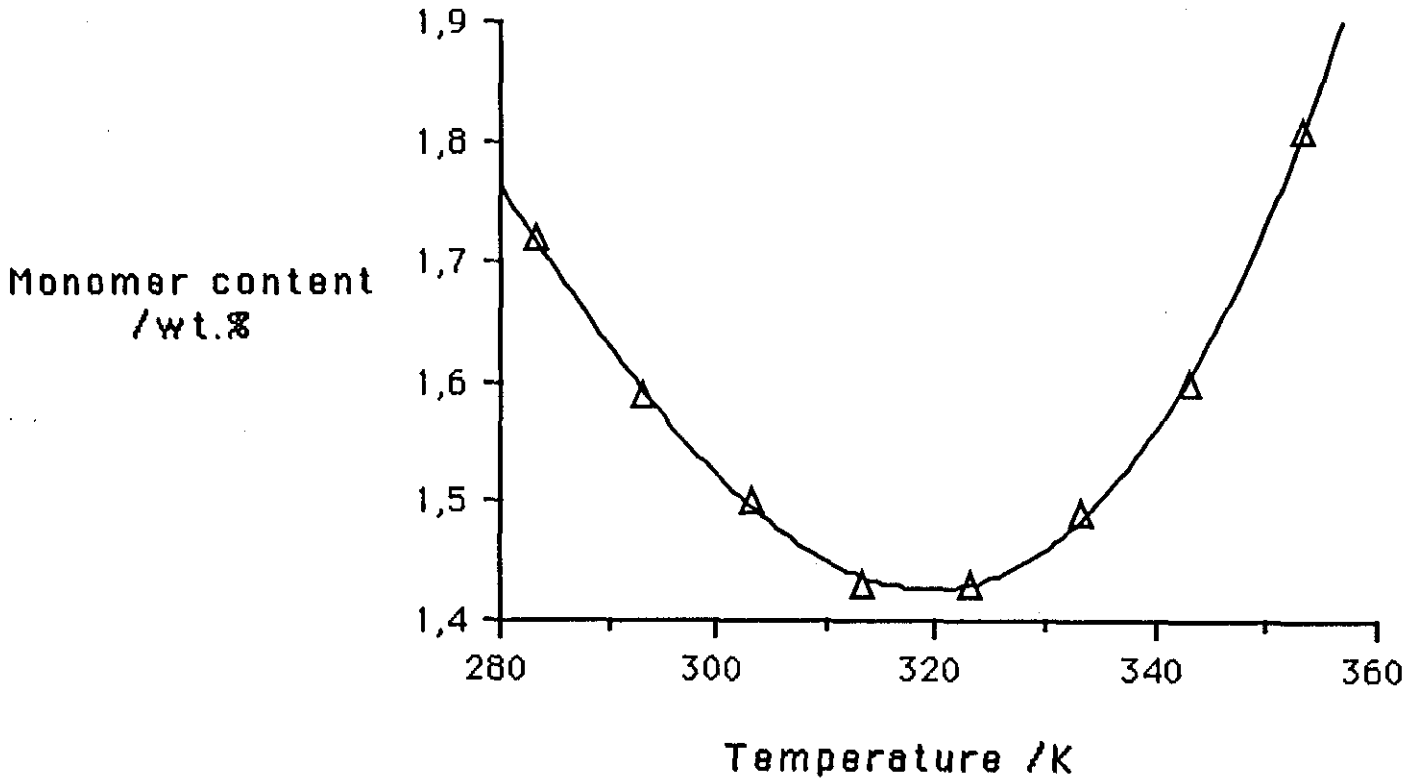

Figure 4.46: Plot of saturation MMA concentration in water against temperature

5. DISCUSSION

5.1 COPOLYMER SYNTHESIS

5.1.1 PMMA synthesis.

The synthesis of carboxyl terminated oligomeric PMMA by free radical polymerisation was performed without complication. The matched chain transfer method with a mercaptan gave very reproducible results. The purification procedures employed served to reduce the polydispersity of the product, with the removal both of the lowest molecular weight molecules and the highest. The polydispersity of the PMMA as measured by GPC was 1.30 in comparison with 2.0 predicted for a free radical polymerisation.

During initial attempts to convert the acid terminated PMMA to the acid chloride products were obtained with colours ranging from yellow to dark brown. Each subsequent synthesis of PMMA yielded a darker colouration. The problem was isolated to being an effect of the thioglycollic acid. It is believed that with time the thioglycollic acid can dimerise presumably eliminating hydrogen.

$$2\,HOOC\text{-}CH_2\text{-}SH \xrightarrow{-H_2} HOOC\text{-}CH_2\text{-}S\text{-}S\text{-}CH_2\text{-}COOH \qquad (5.1)$$

It is postulated that the acid chloride analogue of the compound above yields the colouration.

The problem was finally solved by the use of fresh reagents in addition to the extensive purification processes described in section 3.1.1. The acid chloride utilised for the copolymer synthesis reported was a "water white" solution.

5.1.2 PEO samples.

Results calculated from GPC chromatograms quoted in table 4.3 are given in polystyrene equivalents, ie. the calibration was performed with polystyrene standards and no correction made for the different molecular types. Polystyrene may be considered as a reasonable calibration for PMMA [93], but a correction factor of 0.59 must be applied to the measured values for PEO to adjust for the different polymer chains[94].

Table 5.1: GPC data calculated from RI detector corrected for PEO.

SAMPLE	M_p	$\overline{M}_n$	$\overline{M}_w$	$\overline{M}_w/\overline{M}_n$
PMMA	1405	1237	1605	1.30
PEO 550	507	456	486	1.07
PEO 750	636	517	678	1.32
PEO 1000	786	792	852	1.07
PEO 2000	1578	1566	1644	1.05
PEO 4000	2856	2544	3174	1.25

Values for PEO corrected in accordance with reference 94.

It has been shown that there is a small end group effect related to the methoxy group terminating the PEO chain. The solvated volume for the methoxy terminated molecule is slightly larger than that of the hydroxy terminated molecule even after accounting for the difference in molecular weight. This effect can be seen up to molecular weights of 200-300 g mol^{-1}. The effects however are so small that they will only have a significant effect on the determination of molecular weights for PEO 550.

The molecular weight determination by ^1H nmr was a very elegant method, and for the lower molecular weight PEO samples, this method

could be expected to yield much more precise values for number average molecular weights than GPC. The error associated with the determination of PEO 4000 is the largest of this series. Assuming the integration to be correct to ±0.1 the calculated molecular weight would have an estimated error of ±8%. This is a similar error to that expected in a GPC determination.

Table 5.2: PEO molecular weights by ^{1}H Nuclear Magnetic Resonance compared to GPC results.

SAMPLE	$\bar{M}_n$ ^{1}H nmr	$\bar{M}_n$ GPC
PEO 550	596	456
PEO 750	689	517
PEO 1000	979	792
PEO 2000	2023	1566
PEO 4000	2884	2544

Table 5.2 above gives a direct comparison between results obtained by ^{1}H nmr and GPC. The values yielded by ^{1}H nmr are consistently higher than those from GPC. As the ^{1}H nmr method was a direct method for measuring $\bar{M}_n$ and GPC reliant upon calibration by standard samples the author has most confidence in the ^{1}H nmr results.

5.1.3 Copolymers.

The five (six including copolymer 2000b) copolymer samples were all isolated in good yield. The yield decreased with increasing molecular weight of PEO block length. This may be explained by the purification technique of separation by raising above the cloud point: with the higher molecular weights the cloud point was above 90°C and without doubt the solution had cooled below this temperature before separation was complete thus polymer had commenced returning to solution. The

samples all exhibited a very slight yellow colouration.

In table 5.3, are collected the measured and calculated compositions for the copolymers. `Nominal' refers to the utilisation of the manufacturers molecular weight estimates for the PEO blocks assuming a diblock structure. `Calculated' refers to the value calculated using the ^1H nmr measured molecular weight for the PEO blocks. The remaining columns show the two experimental determinations by the IR method described in section 4.2.2 and the ^1H nmr method from section 4.2.5.

Table 5.3: Copolymer composition as derived by various methods.

PEO in Copolymer	% PEO from				
	Nominal	Calculated	IR 1110 cm^{-1}	IR 1730 cm^{-1}	nmr
550	35	40	32	32	41.8
750	43	43	36	32	44.3
1000	50	52	52	40	63.0
2000	66	69	68	64	74.1
4000	80	76	64	64	76.7

Both of the experimental techniques above consider the relative proportions of the two monomer units and give no indication of their environment, ie. whether they are present as homopolymer or as copolymer. GPC can give a better indication of the degree of success of the linking reaction.

The GPC chromatograms shown as figures 4.3 - 4.7 can be used to give an indication of the copolymer and homopolymer content of the products. Clear shifts towards molecular weights higher than those of the homopolymers can be seen for all copolymer samples. There can be seen

possible homopolymer contamination in copolymer 4000 and to a lesser extent in copolymer 2000. For these two copolymers UV traces were presented in figures 4.8 and 4.9. The UV detector only responds to the PMMA units of the eluting polymer. The UV traces almost match those of the refractive index traces and certainly do not correspond to the chromatogram of the PMMA homopolymer. To summarise, the qualitative interpretation of the GPC chromatograms indicate that the linking reactions were successful and the purification processes adequate.

Quantitative interpretation of the GPC chromatograms is a little difficult as the two blocks forming the copolymer behave differently in the solvent. It has been suggested that the use of a universal calibration based on $\langle r^2 \rangle_0$ is valid for block copolymers[94]. This approach assumes that the molecular size of the diblock copolymer in solution is equal to the sum of the sizes of the two component homopolymer blocks. As long as the weight fractions of the two components and the appropriate shift factors are known corrections may be made for the molecular architecture.

Table 5.4: Copolymer molecular weights as determined by GPC

	PS Equivalent			Shift factor	Corrected		
Copolymer	M_p	$\overline{M}_n$	$\overline{M}_w$		M_p	$\overline{M}_n$	$\overline{M}_w$
550	1720	1600	2110	0.84	1067	1344	1772
750	2020	2010	2700	0.82	1656	1648	2214
1000	2230	2410	3160	0.79	1761	1904	2496
2000	3570	2700	3860	0.72	2570	1944	2779
4000	5470	2690	5480	0.69	3774	1856	3781

The correction factors were calculated utilising the composition data from the ^1H nmr experiments. (See Table 5.3).

The polydispersity index ($\overline{M}_w/\overline{M}_n$) can be used to give an indication of the homopolymer contamination. Copolymers 550, 1000, and 2000 have measured polydispersity indices of about 1.3, approximately the same as the PMMA homopolymer. Copolymer 2000 has a slightly higher index at 1.4 and that of copolymer 4000 at 2.0. These increased values reflect the higher degree of homopolymer contamination.

5.2 COPOLYMERS IN SOLUTION

5.2.1 Visual cloud point.

The cloud point is the temperature at which the polymer solution changes from a homogeneous solution, in this case a micellar solution, to a two phase system where there is a polymer rich phase and a water rich phase. In the early stages of this phase separation the polymer rich phase is present as droplets suspended in the water rich phase. It is these droplets that cause the clouding of the solution. As the temperature is raised further the polymer rich droplets grow larger and tend to collect on the surfaces of the vessel and as a layer on the bottom. Locating the onset of this phase change is dependent upon the sensitivity of the detection system employed and the accuracy of temperature measurement.

The automated system built for this project combined good temperature control and a sensitive method for the determination of absorbance. It was clearly shown that the measured cloud point temperature was dependent upon heating rate. This is a kinetic effect with the rate being determined by the diffusion controlled meeting of micelles. The true phase change temperature corresponds to the cloud temperature when the experiment is performed infinitely slowly. Meeting this criteria is obviously not practical and consequently the compromise of using a heating rate of ca. $0.33°min^{-1}$ was employed. Results obtained for copolymers 1000 and 2000 were very reproducible with an uncertainty of less than 1°. Copolymer 550 had a cloud temperature very close to the freezing point of water; it was not possible to determine any value with the cell. Copolymers 2000 and 4000 both showed cloud point temperatures in excess of 363K (90°C). The original design of the cell did not permit the addition of any insulation. As such it was not possible to heat the cell to these temperatures. If this cell

were to be built again the author would suggest that the heating be supplied electrically and the cell be built with insulated walls.

The visual determination of cloud point temperature can be considered to be second best to the automated cell but it did enable estimates of the cloud points for copolymers 2000 and 4000. The values recorded are higher than for the automated method because of the difficulty of locating the first stages of the clouding with the eye.

Figure 5.1 shows the cloud points determined visually against the PEO block length as determined by ^1H nmr. The shape of this curve is very similar to those displayed by other ethylene oxide adducts[95]. The curve however is located below the simple adducts such as those made from aliphatic acids. This can be explained by the size of the PMMA block when compared with the aliphatic chains. The cloud point is the temperature at which the hydration of the PEO chain can no longer stabilise the solubilisation of the hydrophobic part of the molecule. With increasing size of PEO chain the temperature at which this transition occurs increases. The cloud point for a given molecule is dependent upon its composition and the solvent composition. The presence of electrolytes will alter the hydrate formation and thus the cloud point as will the presence of PEO homopolymer. With a copolymer the polydispersity of the respective blocks will influence the range of temperature at which the clouding occurs.

5.2.2 UV/Vis spectroscopy in mixed solvents.

Methanol is considered as a non-solvent for PMMA[96] but for an oligomeric PMMA with a $\overline{M}_n$ of 910-920 it is a solvent. Both water and alcohols are considered as being solvents for PEO[96]. Addition of methanol to an aqueous micellar solution should increase the solubility of the

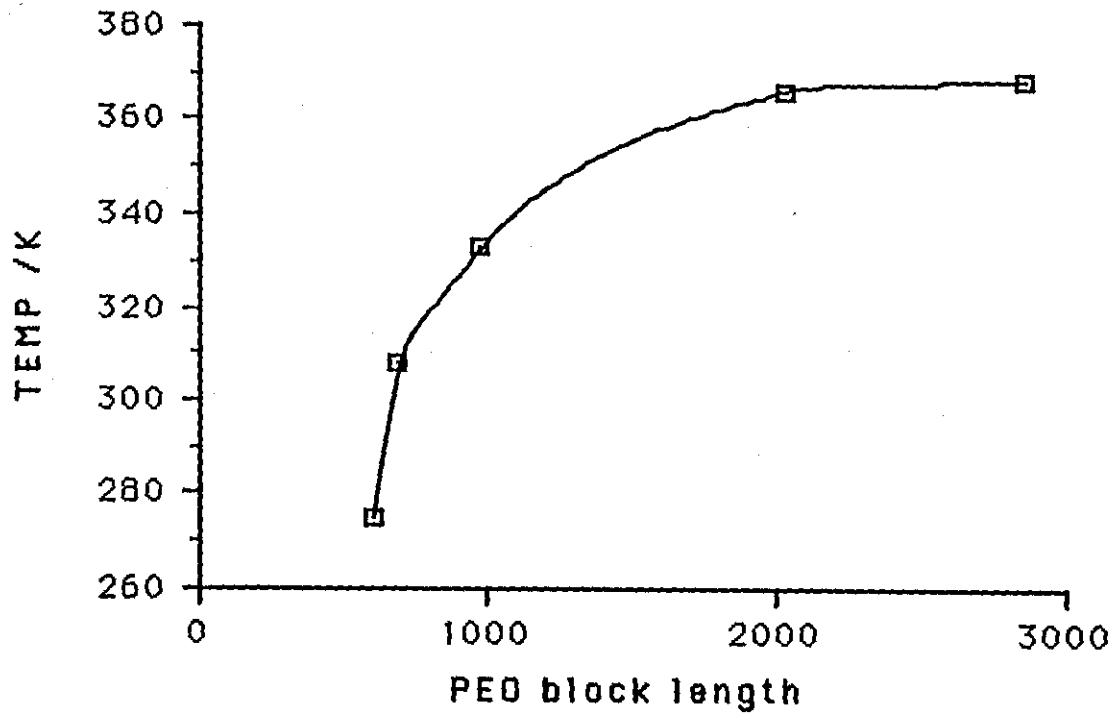

Figure 5.1: Plot of cloud point temperature for copolymers as a function of PEO block molecular weight.

PMMA core but have little effect on the solubility of the PEO block. It would be reasonable to predict that an increase in solvation of the PMMA core would lead to an increase in core size, ultimately resulting in the dissolution of the micelles at very high methanol concentrations. The increase in size would provide an explanation for the absorbance vs. solvent composition plots in figures 4.16 and 4.17. The peaks located between 20 and 50 % water correspond to the solvent composition where the PMMA is becoming more soluble and the particle dimensions have increased to the size where they begin to scatter light. At concentrations of methanol over 80% both components of the copolymer become soluble.

5.2.3 SAXS analysis of copolymers in aqueous solution.

The methods.

Guinier[57,59] established a method for the determination of the radius of gyration of a dispersed phase. The largest errors incurred during the calculation of the radii of gyration (R_g), by this method, occur in the desmearing process. Broadbent, Brown and Dawkins[97] have confirmed experimentally that R_g, as determined by the Guinier method, is not influenced by the presence of a micellar fringe. They determined values for R_g on a micellar system in two dispersion media, one with an electron density different to the soluble component of the copolymer, and one with the dispersion media having an identical electron density to the soluble copolymer block. Both methods gave the same value for R_g. With the second experiment the matched electron densities between the fringe and dispersion media resulted in the data following Porod's law, ie there was no influence of the micellar fringe on the scattering data.

When determining the errors in the determination of fringe thicknesses there are three major points that must be considered. Firstly fluctuations

in electron density in the micelle core will lead to positive deviations from Porod's law. This effect is most significant at temperatures around phase transitions. During this work the temperatures of the samples were at least 40° below the T_g of pure PMMA, ie. far from the expected transition. When approaching the cloud point of the copolymer the situation might be different: The collapse of the PEO fringe could well result in the mixing of the PMMA with the PEO leading to fluctuations in density, hence under estimation of any fringe thickness measurements.

The second consideration is the statistical fluctuation in individual data points. The counting times are limited for practical reasons and as a consequence the errors at the high angular region of the curve greatly restricts use of this high angle data. Roe[98] states thate an error of 1% in the scattering data can lead to unaceptable errors in the determination of σ (and δ).

The third factor is the subtraction of the background scattering data. The empirical equation 5.1 has been used to fit the observed background data[66,67].

$$I_b(s) = a + bs^n \qquad (5.2)$$

with n an even integer. The somewhat arbitary selection of the analytical form for 5.1 can lead to errors in fringe thickness measurements but Roe[98] points out that there is a large degree of latitude in the values of a and b meaning that the fringe thickness values are not very sensitive to the method of background subtraction.

Six methods were outlined in section 2.5.3 for the calculation of micellar fringe dimensions from the interpretation of negative deviations from Porod's law. The methods covered two models for the electron density

profile in the micellar fringe, a linear profile and a sigmoidal profile. Each method was dependent on a mathematical approximation which resulted in a range of values under which it could be considered as accurate. To determine which methods were most appropriate for the system under study, a single sample of each of copolymers 750, 1000, 2000 and 4000 was studied by all six methods. In table 4.8 these calculated results are presented, it should be noted that the parameters δ and σ can be approximately inter-related by the expression: $\delta \approx 12^{0.5}\sigma$ [60]. A summary of the applicability ranges of the various approximations for smeared data is presented in table 5.6 below.

Table 5.6: Range of applicability of various approximations to Porod's law.

Approximation	Applicability	Equation
Linear gradient model		
Vonk	$\delta s < 0.10$	(2.42b)
Exponential	$\delta s < 0.16$ and $0.56 < \delta s < 0.84$	(2.43b)
Sigmoidal gradient model		
Ruland	$\sigma s < 0.014$	(2.50b)
Exponential	$\sigma s < 0.017$	(2.51b)
Bonart & Müller	$\sigma s > 0.29$	(2.54b)
Empirical	$0.009 < \sigma s < 0.72$	(2.55b)

The ranges of applicability above are as a consequence only of the mathematical approximations made in the process of producing relations suited to graphical solution. There is a second limitation that is more difficult to comply with: that is that Porod's law only applies as s tends to ∞. This limit is very restrictive as it is not possible to produce scattering data beyond a certain angle before intensities are too low and the onset of wide angle scattering begins to be observed. The compromise that must be

made is to use as high a value of s as possible then consider the validity of the various approximations.

For these experiments the largest value for `s' was typically 0.01 $Å^{-1}$. considering the data in table 4.8 for the smallest and largest calculated fringe thicknesses the ranges of interest for δs and σs can be calculated. For the linear model this yields $0.16 < \delta s < 0.52$ and for the sigmoidal model $0.05 < \sigma s < 0.21$.

Neither of the two approximations for the linear gradient model are within the limits allowing for a 5% error in the determination of δ. The exponential approximation yields values closest to δ_{real}, but neither are satisfactory.

The empirical solution to the sigmoidal model is the only solution that remains within the 5% error limit for these copolymers. For micellar fringe dimensions slightly larger than exhibited by these copolymers the Bonart and Müller solution would also be applicable, but for these copolymers this solution over-estimates the fringe thickness.

On the basis of this all further discussion will be based on the values determined for the empirical solution to the sigmoidal model. In the results section of this thesis, results for the Vonk solution to the linear model are also presented. These results were selected in preference to the empirical solution on the strength of the discussion relating to the validity of the physical significance behind the approximation to the Maclaurin series (See section 2.5.3).

<u>The copolymers</u>

Referring to the results presented in table 4.8. For the four copolymers

with a fixed PMMA block length and variable PEO block length there would appear to be no distinctive correlation between PEO block length and core size. Measured core sizes range from a R_g of 52Å to 74Å. The experimental error in these determinations is not simple to evaluate but a reasonable estimate could be 10%. Given this estimated error the general trend in the data could be interpreted as an increase in core size with increasing block length, (see figure 5.2).

The interfacial-fringe thickness parameter σ demonstrates a much stronger dependence upon PEO block length. Figure 5.3 shows a plot of σ as a function of PEO block length.

The interfacial fringe thickness parameter σ is not simple to relate to the dimensions of the PEO chains. They are probably better related to the parameter δ, where δ is the distance from the core surface out to the outermost edge of the fringe as shown in figure 2.7. Comparison of the two parameters defining the interfacial thickness for the linear gradient and sigmoidal models as defined in equations 2.35 and 2.36 yields[60]:

$$(K_p s^4)(1-4\pi^2\sigma^2 s^2) \approx (K_p s^4)(1-\pi^2\delta^2 s^2/3) \qquad (5.3)$$

$$\text{ie. } \delta \approx 12^{0.5}\,\sigma \qquad (5.4)$$

Table 5.7 shows the fringe thickness parameters σ and δ along with the dimensions of the PEO component of the copolymer in solution. $\langle r^2\rangle^{0.5}$ is the root-mean-square end-to-end distance of the polymer chain in solution and L_{max} an extended chain length. It has been demonstrated that a short chain polymer ($M < 10^4$ g mol^{-1}) has a similar size in both a good and theta solvent[99]. The characteristic ratio $\langle r^2\rangle / nl^2$ is 4 for PEO in a theta solvent[100], where n is the number of main chain bonds and l^2 is the mean-square bond length. L_{max} is an extended chain length assuming that

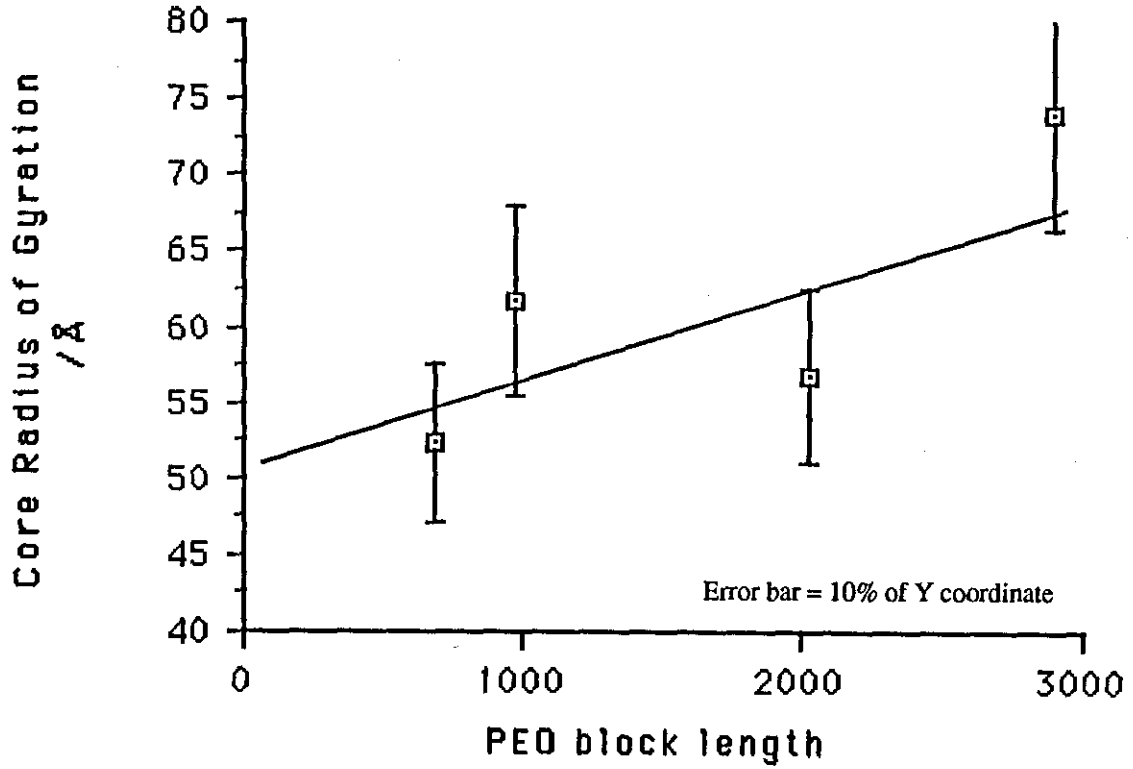

Figure 5.2: Plot of micellar core radius of gyration as a function of PEO block length.

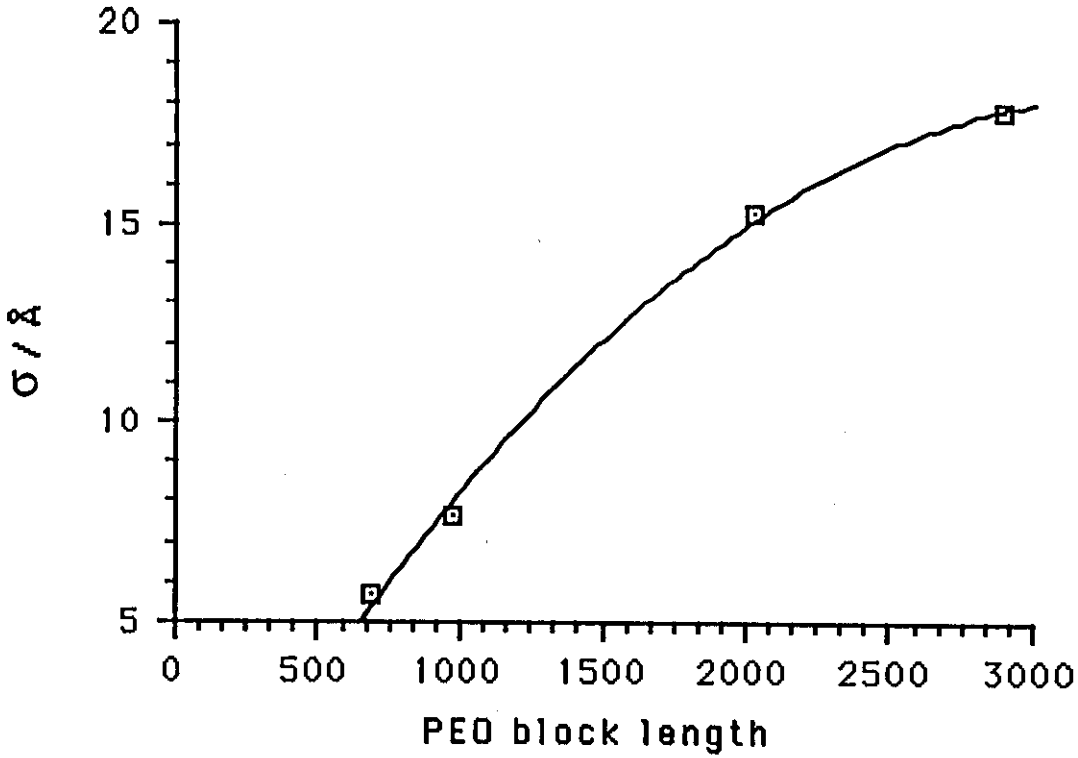

Figure 5.3: Plot of σ (the standard deviation of the Gaussian distribution function describing the micellar fringe) as a function of PEO block length.

a reasonable conformation is that found in the crystal lattice and that sensible bond lengths, bond angles and conformational energies are observed. Thus the conformation of the polymer chain is a helix having repeat units containing 7 monomer units and a repeat distance of 19.3 Å.

Table 5.7 calculated PEO dimensions compared with SAXS results.

copolymer	PEO	$\langle r^2 \rangle^{0.5}$ /Å	L_{max} /Å	σ /Å	δ /Å
750	689	20.6	43	5.7	19.7
1000	979	24.6	61	7.6	26.3
2000	2023	35.3	127	15.3	53.0
4000	2884	42.2	181	17.8	61.7

It would appear that the better model for the conformation of the PEO chain is the unperturbed chain. Certainly the chain is not in the helical conformation.

In figure 5.4, δ is plotted against $\langle r^2 \rangle^{0.5}$ calculated for the PEO block of the copolymer. The curve superimposed on the plot is a second order least squares fit to the data forced to pass through the origin. The origin is the point where there is no PEO chain hence no contribution to the SAXS data.

Following the temperature dependence of the micelle dimensions for a given copolymer, copolymer 1000 was selected for this study as it demonstrates a phase change at around 333K (60°C) a temperature easily obtained within the sample holder of the SAXS camera. The results of this experiment were presented as table 4.10. Up to and including 328K the micelle dimensions remained, within experimental error, constant. At 333K there was observed an apparent increase in core size (R_g increased by

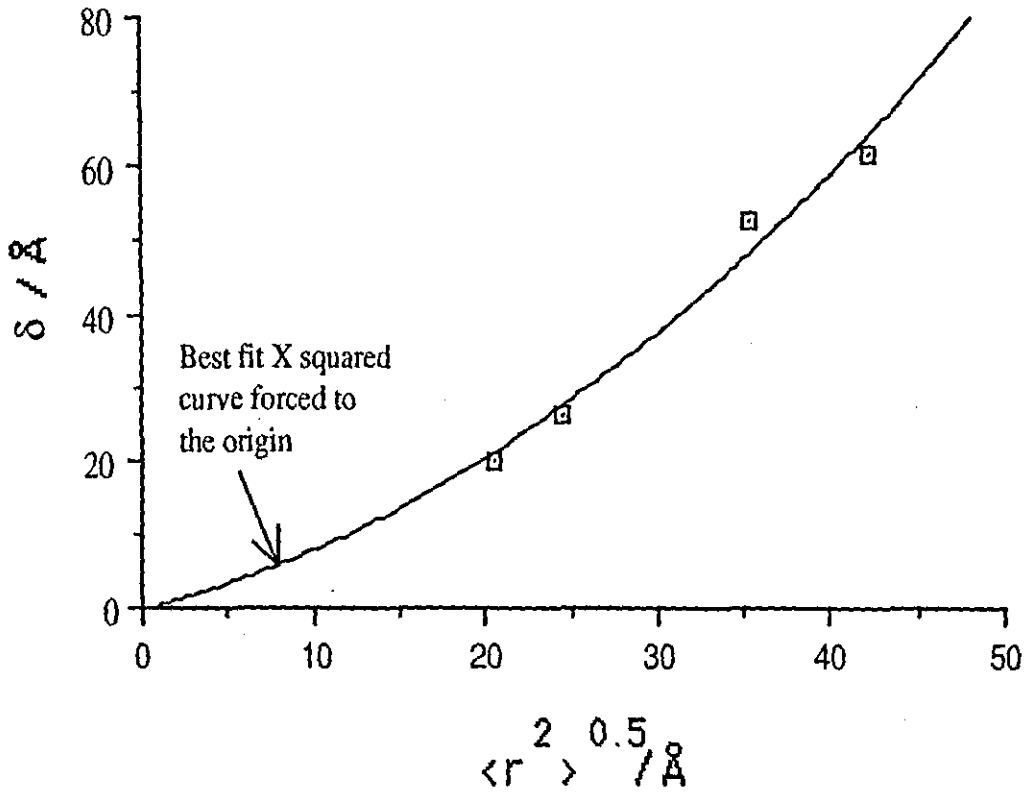

Figure 5.4: Plot of the interface width parameter δ against the root-mean-square end-to-end distance for the PEO chain in solution corresponding to the copolymer.

ca. 12%) and a marked increase in fringe thickness (σ increased by ca. 41%). At 338K the R_g remained the same as measured at 333K but the Porod plot showed a positive deviation, thus could not be used to derive any information related to the micellar fringe dimensions. At 343K it was not possible to establish any dimensions from either the Guinier relation or, as a consequence of negative deviations, from Porod's law. The scattering intensity was noted to be much reduced at temperatures above 333K. The similar experiment with copolymer 2000 covering the temperature range from 293K to 343K showed no major changes in values of either R_g or σ.

For both copolymer 1000 up to the cloud point and copolymer 2000 up to 343K little or no change could be observed from SAXS. Unfortunately for the copolymer 2000 the cloud point temperature of ca. 366K was not accessible by the SAXS experimental setup. Excessive evaporation of solvent could not be prevented. Around the cloud point the copolymer 1000 system became more interesting. The expansion of the core could be explained by either an increase in the number of copolymer molecules in the micelle or by the migration of PEO chains from the aqueous environment into the relatively hydrophobic environment of the micelle core. The increase in apparent micelle fringe thickness is not easy to explain: a decrease in solvation of the PEO chains would cause the polymer chain to contract upon itself. It is possible that the micelle of copolymer 1000 at 333K is not a sphere with a fringe of solvated PEO but is better described as a central core of PMMA with a shell of non-hydrated PEO plus PMMA with the remnants of a hydrated PEO fringe outside this. With this model the scattering from the PMMA domain would be influenced by a smoothing function that would not be well modelled by the sigmoidal model. Above 338K the copolymer produces aggregates too large to be studied by SAXS.

Table 4.14 shows the results of a similar experiment where aqueous

solutions of copolymer 2000 were studied as a function of temperature; this time however the aqueous phase was saturated with MMA monomer. This situation is a more realistic environment for the copolymer at the beginning of a polymerisation. This system is complicated as a result of the solubility behaviour of MMA monomer in water as a function of temperature. Figure 4.45 shows this solubility profile over the relevant range of temperature. The solubility goes through a minimum at about 320K. Figure 5.5 shows a comparison of the data obtained for copolymer 2000 with and without added MMA monomer. At 294K the R_g of the core was recorded as 66.9Å in comparison with 56.7Å for the same copolymer without the monomer. An increased core size was observed at temperatures up to 313K but above this the micelles appeared to have similar dimensions to the un-swelled counterparts. The implication of this is that at the temperature used in the polymerisation experiments under conditions where monomer is present but not in excess the micelles contain surprisingly little monomer. In addition the core size of the micelles reach the minimum value at approximately the same temperature as the solubility of the monomer in water was observed to be at a minimum.

The mode of addition of monomer to the aqueous phase was shown to be critical with respect to the behaviour of the subsequent polymerisation. This is discussed in detail in section 5.3.1. Dissolution of copolymer 2000 directly in water produced a cloudy solution implying that it contained particles as large as the wavelength of visible light. SAXS analysis of this solution revealed a core R_g slightly larger than the corresponding result for the same copolymer added via methanol (see tables 4.18 and 4.14 respectively). More notable was the value of the interfacial-fringe thickness parameter σ: this value at 7.4Å is approximately 1/3 of the corresponding result for the same copolymer added via methanol. This may be interpreted in two ways: the fringe may be smaller; or, as a

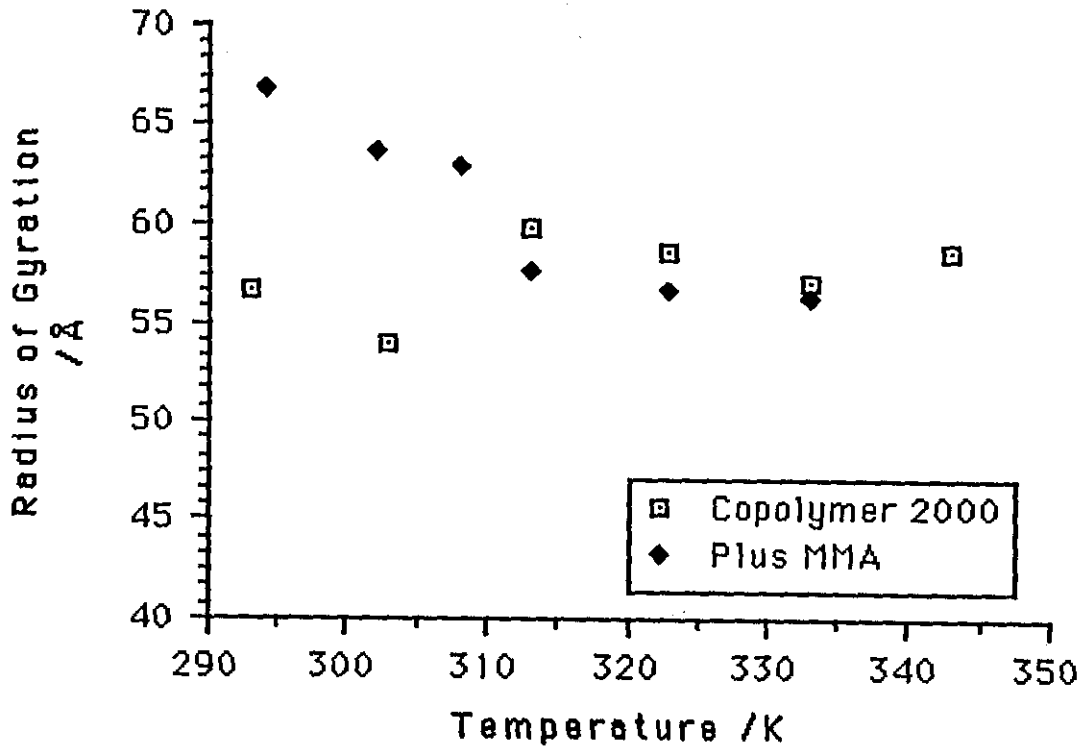

Figure 5.5: Comparison between radii of gyration for copolymer 2000 with and without added MMA. Plot of radius of gyration as a function of temperature.

consequence of phase mixing, the Porod plot is subject both to a negative deviation from the fringe thickness and simultaneously a positive deviation as a result of an inhomogeneous particle core. The net result being an apparent low value for σ. When the copolymer was added to the aqueous phase after first being dissolved in MMA the core R_g was again large (swollen with monomer) and the value calculated for σ was comparable to that of the micellar solution produced via methanol with added monomer.

5.3 POLYMERISATION OF METHYL METHACRYLATE USING COPOLYMER STABILISERS

5.3.1 Mode of addition of copolymer.

The mode of addition of copolymer to the reaction system appears critical to its function. The dissolution of the copolymer directly in water would appear to leave the copolymer in a different form when compared with the two indirect methods of addition. Addition of the copolymer via methanol followed by the removal of the methanol by distillation appears to produce exactly the same results as dissolving the copolymer in the monomer phase. Addition of the copolymer via methanol followed by boiling and subsequent cooling gives the same result as the direct addition. This solution and the direct addition solution are both cloudy in appearance whereas the methanol derived solution is relatively clear. It would appear that the cloud point behaviour of these copolymers is not reversible as has been observed for the simpler PEO adducts[95]. Reversibility of the aggregation may be thermodynamically favored but, within the time scale of the experiments, may not occur as a result of the kinetics of the PEO-co-PMMA system. If this theory is correct the behaviour of a graft copolymer of PEO on PMMA, where the molecular weight of the PMMA backbone would be much higher, would be expected to show a more exaggerated effect.

5.3.2 Methods of following the polymerisation.

Three methods have been employed during this study to follow the polymerisation of MMA monomer with the aid of copolymers as stabilisers: a crude Differential Thermal Analysis (DTA) method; Differential Scanning Calorimetry (DSC); and a solids method.

Considering the DSC method first, DSC was used to produce very clear plots of energy released as a function of time for polymerisations initiated by 4,4′-azobis(4-cyano-pentanoic acid). Unfortunately it was not possible to provide agitation of the sample within the sample pan during the 3-4 hours of the experiment. Considering the density differences between MMA and water it is unreasonable to expect the sample to remain homogeneous during this time period. It is most likely that the monomer formed a "cream" on the surface or the water. As a consequence the data derived from this method cannot be considered as giving a true picture of the larger scale experiment.

The method of following the temperature difference (ΔT) between the reaction vessel and the thermostatically controlled water bath enabled the rapid reactions initiated by the persulphate / metabisulphite redox to be followed. As was discussed in section 4.4.2, the method can only be used to estimate the reaction rate when the first derivative of the rate is zero. This yields a value for the polymerisation rate that can be utilised to estimate the order of reaction with respect to various components.

The solids method for monitoring the conversion of monomer to polymer directly is the most appropriate method of following the slower polymerisations. If the time period required to extract a sample from the reaction vessel and quench the reaction can be made much smaller than the period between samples the conversion can be followed very closely. This criteria could easily be met for the 4,4′-azobis(4-cyano-pentanoic acid) initiated systems with reaction times extending over hours.

5.3.3 Ammonium persulphate / Sodium Metabisulphite redox.

In aqueous solution in the absence of metabisulphite ions the persulphate ion can decompose thermally to yield free radicals. The reaction in neutral

and basic conditions has been shown to follow the following mechanism[101,102].

$$S_2O_8^{2-} \longrightarrow 2SO_4^{\cdot-} \quad (5.5)$$

$$2SO_4^{\cdot-} + 2H_2O \longrightarrow 2HSO_4^- + 2HO^{\cdot} \quad (5.6)$$

$$2HO^{\cdot} \longrightarrow H_2O + 1/2O_2 \quad (5.7)$$

The flux of free radicals is modest: the persulphate decomposition has a half life of 1030 hours at 40°C and 38.5 hours at 60°C [102]. When metabisulphite ions are present the following additional reactions can take place increasing the rate of free radical generation.

$$S_2O_5^{2-} + H_2O \longrightarrow 2HSO_3^- \quad (5.8)$$

$$S_2O_8^{2-} + HSO_3^- \longrightarrow SO_4^{2-} + SO_4^{\cdot-} + HSO_3^{\cdot} \quad (5.9)$$

$$SO_4^{\cdot-} + HSO_3^- \longrightarrow SO_4^{2-} + HSO_3^{\cdot} \quad (5.10)$$

The metabisulphite acts as a source of bisulphite ions (by hydrolysis). The bisulphite ions can then react to form both the sulphate radical ion and the bisulphite radical. The sulphate radical ion can initiate polymerisation or react with a second bisulphite ion to yield a bisulphite radical. Assuming the rate of polymer initiation to be the same for both radicals, then the number of polymer chains initiated by bisulphite radicals should be greater than those initiated by sulphate radical ions.

All reaction profiles showed three distinctive stages: an initial stage where the rate of polymerisation was increasing, a second, brief stage where the polymerisation rate was approximately constant, and a final third stage

where the rate increased for a short period followed by a decrease to zero rate. The first stage is presumably the period in which the number of loci is defined, the second stage is the steady growth stage and the final stage marks the end of the existence of free droplets of monomer and is complete when the last monomer is used up. The acceleration during the third stage is related to the decrease in k_t as the viscosity within the particles increases. This is the well-known "gel-effect" associated with the names Norrish[78], Schulz[79] and Trommsdorff[80].

In experiments 1 to 5 as defined in table 4.19 the concentration of ammonium persulphate was varied over the range 9.5×10^{-5} to 1.5×10^{-3} mol l^{-1} . The other components were maintained at constant levels with the metabisulphite at a concentration of 9.6×10^{-3} mol l^{-1}. After hydrolysis this metabisulphite could be considered to yield a concentration of bisulphite ions twice that of the initial metabisulphite concentration. Taking a simplification of the rate determining step in the production of radicals to be:

$$S_2O_8^{2-} + HSO_3^- \longrightarrow SO_4^{2-} + 2R^{\cdot} \qquad (5.11)$$

where R. takes into account the products of equations 5.5 and 5.6. Assuming the reaction to be first order with respect to the loss of persulphate and bisulphite ions, the rate of free radical generation can be expressed as:

$$\frac{dR^{\cdot}}{dt} = k\,[S_2O_8^{2-}]^{0.5}\,[HSO_3^-]^{0.5} \qquad (5.12)$$

Figure 4.27 showed a plot of ln conversion rate as a function of $\ln\{[S_2O_8^{2-}]\,[S_2O_5^{2-}]\}^{0.5}$. The gradient of the least squares fit to this line is 3/5. This is in exact agreement with the experimental results of Hay and co

workers[103]. The results of Hay were obtained from studies of the emulsion polymerisation of vinylidene chloride with sodium lauryl sulphate as the surfactant. In these experiments they maintained the ratio of ammonium persulphate to sodium metabisulphite constant. When displaying results they plotted log (conversion rate) against log (persulphate concentration) and obtain a slope of 3/5. If their "X" axis is converted to $\ln\{[S_2O_8^{2-}]\,[S_2O_5^{2-}]\}^{0.5}$, an identical slope is obtained.

The particle size of the resultant polymers showed no significant trend. Within experimental error the particle size was independent of initiator concentration.

The Smith-Ewart theory suggests that the steady rate of polymerisation should be of the order 2/5 with respect to the initial initiator concentration. For the above to hold Smith and Ewart require that, during the period of locus formation, ρ (the rate of entry of radicals into micelles and loci in unit volume) is proportional to the rate of generation of free radicals. This will be so if the period of locus formation is short relative to the half life of the initiator. Also for this to hold the initiator decomposition must be first order with respect to its own concentration. The persulphate / metabisulphite system is not first order with respect to initiator concentration and no determination has been made of the half life of the system or the time scale of the period of locus formation.

The Smith - Ewart model suggests that the reaction rate is determined by the number of polymerisation loci. If the number of particles is fixed, as is indicated by the final particle size measurements, then the polymerisation rates should have been independent of initiator concentration. This data must be considered as being inconsistent with the Smith - Ewart model.

Figure 4.29 shows the relationship between ln (reaction rate) and ln (copolymer concentration). The slope of this graph is essentially one implying that the rate is proportional to the copolymer concentration over the range of concentrations studied.

The particle size of the final polymer showed a small tendency to decrease with increasing copolymer concentration.

The Smith-Ewart theory suggests that the steady rate of polymerisation should be of the order 3/5 with respect to the micelle generating substance. This is not in agreement with the reported order of 1.0 above. The value 3/5 is derived assuming that the number of polymerisation loci is constant at this stage of the reaction. In this instance the quantity of copolymer (micelle generating substance) is very high and possibly the number of loci is not constant.

The effect of an increase in initial monomer concentration was to increase the final particle size. The relationship was not however that the particle volume was proportional to the monomer concentration as would be predicted if the total number of particles remained constant. Figure 5.6 shows the same data as is presented in figure 4.36 but with the diameter data converted to volume. The curve superimposed on the data is an exponential curve and is far from linear.

The apparent discrepancy may well be explained in terms of the availability of the copolymer during the early part of the reaction. The copolymer is soluble in both the MMA monomer and in water. When the two alternative solvents, water and monomer, are present there must be a partition of the copolymer between the two phases. The greater the volume of monomer the smaller the quantity of copolymer that will be in the aqueous phase during the early stages of the reaction. The copolymer

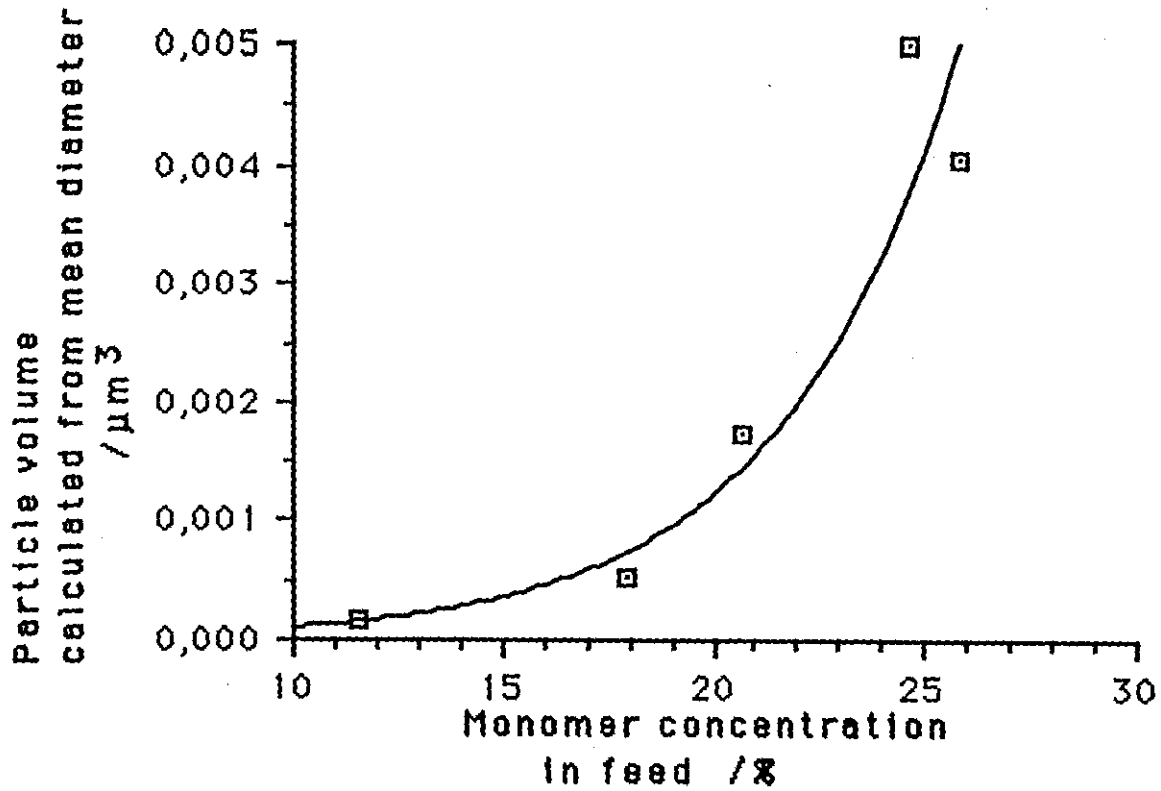

Figure 5.6: Plot of particle volume as a function of initial monomer concentration

in the monomer will become available later in the reaction as the monomer transfers from the droplets to the growing polymer particles.

Figure 4.37 showed the influence of polymerisation temperature on the final particle size. With increasing temperature there was noted an increase in particle diameter. The increase in particle size may be attributed to a number of causes. Firstly, the partition of copolymer between the monomer and aqueous phase discussed above will move towards copolymer being dissolved in the monomer. With increasing temperature the solubility of the PEO part of the copolymer in water decreases making it more favourable for the copolymer to be in the monomer. Secondly, as a result of the decrease in hydration of the PEO the surface area of a particle that can be stabilised by a PEO chain of a given molecular weight will decrease with increasing temperature. This decrease in stabilisation potential of each copolymer chain means that the surface area to volume ratio for the emulsion must decrease. To accommodate this requirement the number of particles is reduced and the average size increased.

The effect of altering the PEO block length in the copolymer on the resultant emulsion particle size was shown in figure 4.38. An increase in block length increases the surface area that can be stabilised by each molecule but, at the same time, decreases the number of copolymer molecules per unit mass of copolymer.

Table 5.8 summarises calculations designed to estimate the relative potential for the four copolymers to stabilise an emulsion. The calculations consider the unperturbed dimensions of the PEO chain in water. The radius of gyration is calculated from the root-mean-square end-to-end distance given in table 5.7 and this value squared is considered as proportional to the surface area stabilised by an individual chain. The total

area for 1g of copolymer considers the stabilised area to be equal to that of the circle of radius equal to the radius of gyration.

Table 5.8 Estimation of surface area stabilised by 1g of copolymer.

Copolymer	$\bar{M}_n$ PEO	$\langle r^2\rangle^{0.5}$	$\langle S^2\rangle^{0.5}$	$\pi\langle S^2\rangle$	Moles / g	Area /g
750	689	20.6Å	8.4Å	222Å^2	6.22×10^{-4}	831m^2
1000	979	24.6Å	10.0Å	314Å^2	5.27×10^{-4}	996m^2
2000	2023	35.3Å	14.4Å	652Å^2	3.40×10^{-4}	1335m^2
4000	2884	42.2Å	17.2Å	932Å^2	2.63×10^{-4}	1476m^2

$\langle r^2\rangle^{0.5}$ is the root mean squared end to end distance for the PEO chain, $\langle S^2\rangle^{0.5}$ is the root mean squared radius of gyration, and $\pi\langle S^2\rangle$ is the estimate of the surface area that the chain can cover, hence provide steric stabilisation for. The total area per gram accounts for the PMMA contribution to the molecular mass

A plot of this calculated area against the experimentally obtained total surface area (figure 5.7) is far from linear. The copolymer 4000 produces polymer particles far smaller than would be expected on this basis (or conversely copolymer 750 produces particles larger than expected). The stage of the polymerisation critical to defining the ultimate particle number, and hence size, is stage I as defined by Smith and Ewart. During this stage the partition of copolymer between water and monomer will be different for each copolymer as the relative water solubility of the copolymer increases with increasing PEO content. There will be a greater proportion of copolymer 4000 in the aqueous phase than for the lower molecular weight copolymers. The mobility of copolymer will also be a function of PEO chain length the smaller copolymers, as a result of solubility, being less able to transfer from micelles to growing particles. A particle with less than its required stabilisation will be more liable to

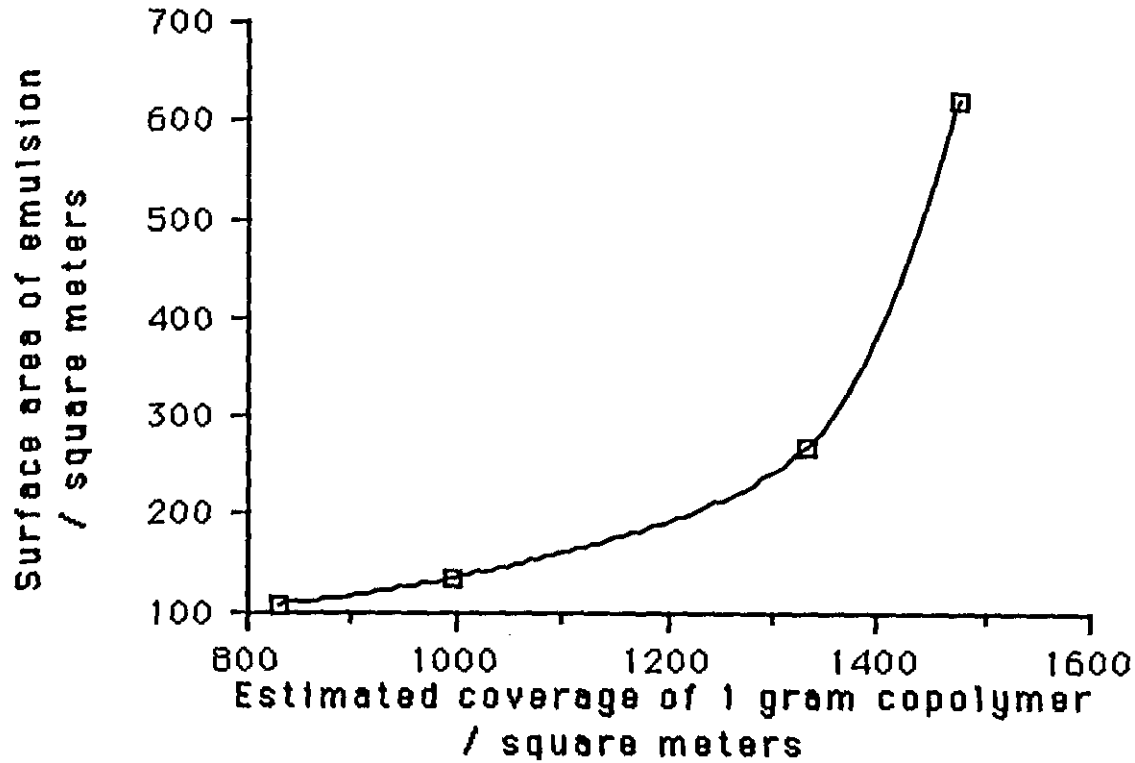

Figure 5.7: A comparison of the total surface area of emulsions produced with various copolymers to the estimated potential coverage of these copolymers.

aggregate with other particles than a fully covered particle. This will directly lead to a reduction in the number of particles.

5.3.4 Ascorbic acid / potassium permanganate redox initiator.

Organic acid / potassium permanganate redox systems have been used by many workers to yield free radicals in aqueous systems. Acids used include ascorbic acid[104], lactic acid[105], malic acid[106] and oxalic acid[107].

The ascorbic acid system involves a two part mechanism[104]. The initial step is an oxidation of the ascorbic acid into threonic acid and oxalic acid (Equation 5.13).

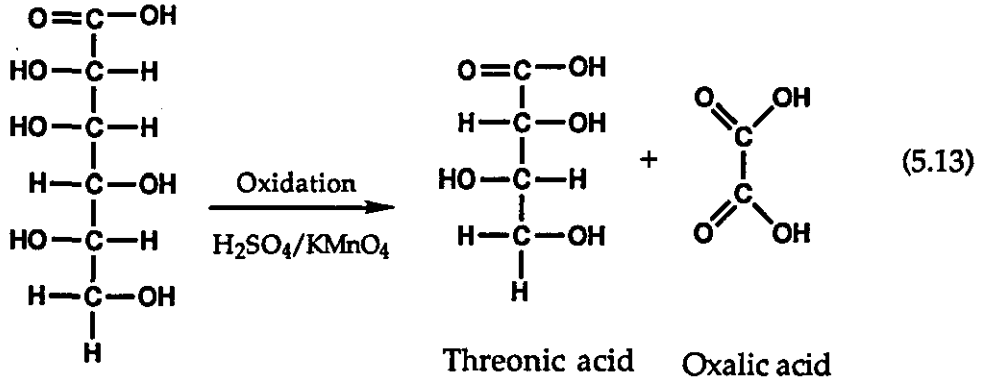

Ascorbic acid
Hydrated form

Threonic acid

Oxalic acid

(5.13)

The oxalic acid is then further oxidised as shown in equations 5.14-5.19. Reactions 5.14, 5.17 and 5.19 result in the production of free radicals and equations 5.15 and 5.18 destroy the free radicals generated. Thus the two initiating species are $\cdot COO^-$ and $\cdot C_2O_4^-$.

$$Mn^{4+} + C_2O_4^{2-} \xrightarrow{\text{measureable}} Mn^{3+} + CO_2 + \cdot COO^- \quad (5.14)$$

$$Mn^{4+} + \cdot COO^- \xrightarrow{\text{rapid}} Mn^{3+} + CO_2 \quad (5.15)$$

$$Mn^{3+} + 2C_2O_4^{2-} \xrightarrow{\text{rapid}} Mn(C_2O_4)_2^- \quad (5.16)$$

$$Mn^{3+} + C_2O_4^{2-} \xrightarrow{\text{measureable}} Mn^{2+} + CO_2 + \cdot COO^- \quad (5.17)$$

$$Mn^{3+} + \cdot COO^- \xrightarrow{\text{rapid}} Mn^{2+} + CO_2 \quad (5.18)$$

$$Mn^{3+} + C_2O_4^{2-} \longrightarrow Mn^{2+} + \cdot C_2O_4^- \quad (5.19)$$

Clearly end groups derived from either of these two radical ions will, at high pH, confer some degree of charge stabilisation to the growing polymer particle. But below approximately pH 4 the acid groups will no longer dissociate leaving the polymer particle with no charge stabilisation.

Polymerisations performed with this redox were not monitored for conversion vs. time but were performed with the intention of monitoring latex stability in acid conditions.

5.3.5 4,4′-Azobis(4-cyano-pentanoic acid) initiator.

4,4′-Azobis(4-cyano-pentanoic acid) can be considered as a water soluble analogue of azobisisobutyronitrile. Its decomposition rate is first order with respect to its own concentration and the decomposition is little affected by the environment[72]. The decomposition occurs under the influence of temperature alone. Nitrogen is eliminated leaving two free radical species.

The polymerisations performed show again three distinctive stages but not exactly the same as the persulphate / metabisulphite system. Approximately the first hour of the polymerisation shows a slow acceleration in the rate of polymerisation. During the next 30 minutes there is observed a period of rapid polymerisation. The third period is

marked by a slowing down in the reaction rate. An increase in initiator concentration results in the period of rapid polymerisation occurring at an earlier stage; a reduction in concentration delays this stage. The level of copolymer has a similar effect with an increased concentration resulting in an earlier onset of rapid polymerisation. Sufficient polymerisations were not performed to enable the determination of the dependence of the polymerisation rate on these parameters.

As was observed with the persulphate / metabisulphite system there was little or no effect of initiator concentration on the the final size of the polymer particles. This underlines that the parameters that define the final number of polymerisation loci for these systems are not dominated by the initiator concentration.

5.4 STERICALLY STABILISED PARTICLES?

5.4.1 Electrophoretic mobility

The determination of the electrophoretic mobility gave an indication of the presence of an ionic contribution to the colloidal stability and showed how this contribution varied with pH.

All emulsions generated with the persulphate / metabisulphite system showed an electrophoretic mobility over the pH range measured (pH = 2 to 12). This implies that the stability of these emulsions cannot be solely attributed to the copolymer. Emulsions generated with the 4,4′-azobis(4-cyano-pentanoic acid) initiator system exhibited a mobility at high pH but in acidic conditions, below the pKa of the acid, the mobility fell to zero. The system initiated by the ascorbic acid / potassium permanganate redox system showed a similar profile with no mobility evident at low pH. Thus for the 4,4′-azobis(4-cyano-pentanoic acid) system and the ascorbic acid / potassium permanganate redox system at pH 4 and less all colloidal stability must be as a result of the PMMA/PEO copolymer.

5.4.2 Emulsion stability

All emulsions reported in this thesis were stable over short time periods (days). The polymers generated with the aid of copolymer 750 tended to sediment if left for extended periods without agitation. All emulsions with the higher copolymers showed stability over extended time periods.

The three acidified samples described in section 4.5.4 demonstrated that the copolymer 2000 alone can confer stability to the emulsions. Ionic groups do contribute to the stability at higher pH and in the case of the persulphate / metabisulphite system there is a contribution over the entire pH range.

6. CONCLUSIONS

6.1 COPOLYMER SYNTHESIS

The method of synthesis of the PMMA component of the copolymer produced a polymer / oligomer with a much lower polydispersity than might have been predicted when first considering the technique employed. The free radical polymerisation could, at best, be expected to give a polydispersity of 2.0 but the purification steps employed were very efficient at removing both high and low molecular weight material from the polymer. The resultant polymer with a number average molecular weight of 908 g mol^{-1} and a polydispersity index of 1.30 was more than satisfactory. The second batch of PMMA produced by repeating the procedure was, within the expected error for the measurement technique, the same as the first.

The method of coupling the PMMA to the PEO was relatively efficient for the lower molecular weight PEO samples but yields were considerably reduced for the PEO 2000 and 4000 samples. Yields would be expected to improve with an extension in the reaction time and/or the better removal of HCl from the reaction flask. (See the comments relating to the addition of a base and catalysis in chapter 7)

The purification of the copolymers was, as shown by GPC, better for the lower molecular weight block copolymers. The copolymer made with PEO 4000 was significantly contaminated with homopolymer.

6.2 COPOLYMERS IN SOLUTION

The copolymers produced exhibited cloud points in the range <275K for copolymer 550 up to 368K for copolymer 4000. Of the copolymers only copolymer 550 had a cloud point so low that it was not possible to study micelle formation in water.

SAXS has been used successfully to show that copolymers 750, 1000, 2000 and 4000 all have a core - shell micelle structure below their respective cloud points. The data handling technique of Guinier[57,59] has been used to calculate radii of gyration of the micellar cores and the empirical method of Koberstein, Morra and Stein[60] has been used to interpret negative deviations from Porod's law[61,62,63] in terms of fringe thicknesses. This empirical method was selected in favour of five alternative methods on the basis of the applicability of each method for estimating fringe thicknesses of the size measured for these copolymers. The variations in these two parameters have been studied for the four copolymers as a function of copolymer molecular weight, copolymer concentration, temperature, method of copolymer addition to water and the presence of methyl methacrylate monomer.

Copolymer molecular weight.

Only variations in the molecular weight of the hydrophilic PEO block have been studied here. There maybe a slight tendency for the radius of gyration of the core to increase with increasing PEO block length. There is, however, a much more pronounced tendency relating to the measured fringe thickness. The fringe thickness increases with increasing PEO block length. Considering the calculated chain lengths for two extremes of conformation, a helix and an unperturbed chain, the better model for the

chains in the micelles is the unperturbed model.

Copolymer concentration.

No significant changes in micellar dimensions were observed as a function of copolymer concentration up to concentrations of 10 wt.%. At these high concentrations the SAXS curves showed maxima assumed to be interference peaks caused by structure of the micelles in solution, ie. some form of close packing of the micelles.

Temperature.

Copolymer 2000 showed no significant change in micellar dimensions over the temperature range 293 to 343K. Copolymer 1000 showed no significant changes in micellar dimensions up to 328K but showed an increase in both the radius of gyration of the core and the measured fringe thickness at the cloud point (333K). At temperatures above 333K the SAXS curves could not be explained by a core-shell model. SAXS has been shown to be a very interesting tool for the study of this transition.

Method of copolymer addition to water.

The method of addition of the copolymer to water was shown to be critical in determining the success of an emulsion polymerisation; therefore, this was studied carefully. The addition of the copolymer 2000 via a solvent for both blocks of the copolymer followed by the careful removal of this solvent resulted in strong scattering and micelles that could be described by a core-shell model. Direct addition to water produced much lower scattering intensities and interpretation of the obtained scattering showed the radius of gyration of the core to be similar to the alternative method of addition but the fringe thickness was recorded as being only one third as thick. This measurement could be real or this result could be an indication

that there are positive deviations from Porod's law superimposed on the negative deviations caused by the interfacial fringe. Given this uncertainty in interpretation it is still clear that the two methods of addition give the copolymer different structures in solution.

The presence of methyl methacrylate monomer.

Copolymer 2000, first dissolved in methyl methacrylate monomer and then added to water, produced micelles with similar measured dimensions as micelles generated via the methanol method, with methyl methacrylate added to the water after the generation of the micelles. The intensity of the X-ray scattering curves are similar. Both show a larger value for the core radius of gyration and fringe thickness when compared to the monomer free micelle. Increasing the temperature from 293 to 233K reduces both the measured core size and the fringe thickness to values similar to the micelles without monomer present. It is interesting to note that the solubility of the monomer in the water is also falling as the temperature increases.

SAXS therefore shows that there should be no difference between adding the copolymer via methanol with subsequent removal of the methanol and addition of the copolymer via the monomer. There should, however, be a difference if the copolymer is added directly to the water.

6.3 COPOLYMERS AS STABILISERS IN EMULSION POLYMERISATION

In contrast to the earlier work at ICI with graft copolymers of PEO on PMMA it has been shown that AB block copolymers of PMMA and PEO can be used to stabilise the emulsion polymerisation of methyl methacrylate. Stable emulsions have been obtained with copolymers with a PMMA block length of 910 g mol^{-1} and PEO block lengths of 690, 980, 2020 and 2880 g mol^{-1}. The best stability was observed from the copolymers with nominal PEO block lengths of 1000 and 2000. Emulsions have been shown to be stable at low values of pH over periods in excess of 1 year. At these pH levels the emulsions show no electrophoretic mobility; therefore, there is no electrostatic contribution to their stability.

It has been shown that the mode of addition of the copolymer to the reaction mixture is critical to the outcome of polymerisation. Copolymer added directly to water will not stabilise an emulsion polymerisation. Copolymer added to water via methanol, a solvent for both components of the copolymer, followed by the careful removal of the methanol will stabilise a subsequent polymerisation and copolymer dissolved in methyl methacrylate monomer before addition to water will also stabilise a polymerisation.

It is believed that the principle difference between an AB block copolymer and a graft copolymer during an emulsion polymerisation is the ability of copolymer chains to transfer from non-active micelles via the aqueous phase to the surface of growing polymer particles. It is not as easy for a bulky graft molecule to disentangle itself from a micelle and pass into the aqueous phase as it is for a linear molecule of much lower molecular weight. It is also possible that graft copolymer on the surface of a growing polymer particle has a greater tendency to be buried as the particle grows.

A study of the kinetics of the polymerisation shows that Smith-Ewart theory[71] does not form a good description of the polymerisation of methyl methacrylate with these copolymers as stabilisers. Smith-Ewart theory predicts steady reaction rates proportional to initiator to the power 2/5 and micelle forming agent to the power 3/5. For this system it has been observed that the reaction rate is proportional to the initiator concentration to the power 3/5 and directly proportional to the copolymer concentration.

7 SUGGESTIONS FOR FUTURE WORK

This project has established a synthetic technique for producing well characterised AB block copolymers of PMMA and PEO. One series of copolymers has been produced maintaining the PMMA block length as a constant.

The first important extension to this work would be to synthesise copolymers with variations in PMMA block length. The synthesis technique would probably be appropriate for a PMMA block of twice the molecular weight but with higher molecular weights the purification technique for the homopolymer would need revision. Problems would also be encountered during the purification of lower molecular weight PMMA as a result of changes in solubility. Yields from the esterification step could probably be improved by performing the reaction in the presence of a base. Addition of a stoichiometric quantity of pyridine and a catalytic quantity of 4-dimethylaminopyridine would form appropriate conditions[108]. Higher molecular weight copolymers would probably be more efficiently produced anionically.

The second interesting extension would be to produce tri-block copolymers PEO-b-PMMA-b-PEO. It would be interesting to compare the copolymer 2000 described in this thesis with both a 2000-1000-2000 (PEO-PMMA-PEO) and a 2000-2000-2000. Important questions relating to the break-up of micelles and transfer of copolymer between non-active micelles and growing polymer particles might be answered with a study of these compounds. These compounds could be generated anionically by initiating the polymerisation of methyl methacrylate with the sodium salt of α-hydroxy-ω-methoxy PEO in the presence of dicyclohexyl-18-crown-6[16], followed by coupling with dichlorodimethoxysilane[19]. The alternative

would be to produce an α,ω-carboxy-PMMA then couple via the esterification reaction described in this thesis to an α-hydroxy-ω-methoxy PEO. The synthesis of the α,ω-carboxy-PMMA can be performed by a number of techniques. For the selection of a synthetic route a recent review of telechelic oligomers by Ebdon might be useful [109].

A detailed study of the micellar environment by nmr would be interesting. A comparison of the relaxation times for both atoms in the PMMA blocks and in the PEO blocks with those of the homo-polymers, in both the solid state and in solution, would confirm the structure of the micelle. It would be very interesting to discover how much of the PEO is contained within the core of the micelle and how much forms the solvated fringe structure.

It would be interesting to extend the study of these copolymers to mixed solvent systems, namely alcohol / water mixtures. The solvation of the copolymer will increase with increasing alcohol content in the water, the extreme being where the copolymer is to be found as discrete molecules and not micelles. This could be studied in terms of emulsion polymerisation or by SAXS. In fact some preliminary SAXS work has been performed on solutions of copolymer 2000 in methanol / water mixtures but has not been reported here.

8. REFERENCES

1 B. Vincent., Advances in Coll. and Interface Sci., **4**, 193, (1974).

2 D.W. Osmond, F.A. Waite,.Cpt. 2 "Dispersion polymerisation in organic media" K.E. Barrett Ed. Wiley, London. (1975).

3 D.H. Napper., J. Coll. Interface Sci **58**, 390, (1977).

4 G. Taylor., PhD. Thesis Loughborough University (1977).

5 S.A. Shakir., PhD. Thesis Loughborough University (1987).

6 G. Maghami., Post doctoral work Loughborough (1984)

7 W.D. Harkins., J. Chem. Phys., **13**, 381, (1945).

8 W.D. Harkins., J. Chem. Phys., **14**, 47, (1946).

9 W.D. Harkins., J. Am. Chem. Soc., **69**, 1428, (1947).

10 W.D. Harkins., J. Polym. Sci., **5**, 217, (1950).

11 J.C. Saam, D.J. Gordon, S. Lindsey., Macromolecules **3**, 1, (1970).

12 W.G. Davies, D.P. Jones., IEC Prod. Res. Dev. **10**, 168, (1971).

13 J.G. Zilliox, J.E. Rovers, S. Bywater., Macromolecules **8**, 573, (1975).

14 A. Marsiat, Y. Gallot., Makromol. Chem. 176, 1641, (1975).

15 J.V. Dawkins, G. Taylor., Polymer **20**, 599, (1979).

16 T. Suzuki, Y. Murakami, Y. Tsuji, Y. Takegami., J. Polym. Sci. Polym. Letters Ed. **14**, 675, (1976).

17 M. Morton., Anionic polymerisation, Principles and Practice, Accademic Press, New York (1983).

18 P. Dreyfus, L.J. Fetters, Rubber Chem. Technol., **153**, 728, (1980).

19 H.F. Mark, N.M. Bikales, C.G. Overberger, G. Menges (Eds.) Encyclopedia of polymer science. 2nd Ed. Wiley Interscience, New York. **2**, 1, (1990).

20 ICI British Patent 1 096 912 (1963).

21 T. Otsu, M. Yoshida., Makromol. Chem. Rap. Com. **3**, 127 (1982).

22 J.P. Kennedy., J Macromol. Sci. Chem. Ed., **13**, 695 (1979).

23 J. Ebdon., Lancaster University. Personal communication (Unpublished results). (1989).

24 T. Otsu, A. Kuriyama., Polymer Bulletin **11**, 135 (1984).

25 T. Otsu, T. Ogawa, T. Yamamoto., Macromolecules **19**, 2087 (1986).

26 K. Redford, G. Clark. Senter for Industriforskning, Oslo, Norway. Paper in preparation. (1991).

27 R.J. Ceresa, W.F. Watson., British Patent 832 193 (1955).

28 H. Fujiwara, K. Goto., Polymer Bulletin **23**, 27, (1990).

29 C.H. Bamford, A.D. Jenkins., Nature 176, 78, (1955).

30 A.S. Gomes, F.M. Coutinho, J.R. Marinho., J. Polym. Sci. Letters. **25**, 237, (1987).

31 T. Graczyk, V. Hornof., J. Polym. Sci. Polym. Chem. Ed., **26**, 2019, (1988)

32 Mino, Kaizerman.,J. Polym. Sci., **122**, 242, (1958).

33 W.H. Keesom., Physik. Z., **22**, 129, (1921).

34 P. Debye., Physik. Z., **21**, 178, (1920).

35 F. London., Physik. Z., **63**, 245, (1930).

36 H.C. Hamaker., Rec. Trav. Chim., **55**, 1015, (1936)

37 H.C. Hamaker., Rec. Trav. Chim., **56**, 3727, (1937).

38 E.J. Vervey, J.T. Overbeek., "Theory of the stability of lyophobic colloids" Elsevier, Amsterdam. (1948).

39 H.B. Casimir, D. Polder., Phys. Rev. **73**, 360, (1948).

40 E.M. Lifshitz., J. Exper. Theor. Phys. USSR, **29**, 94, (1955)

41 E.M. Lifshitz., Soviet Physics, JETP, **2**, 73, (1956).

42 S. Derjaguin, L. Landau., Acta Phys. Chem., 14, 633, (1941).

43 D.H. Napper., Polymeric stabilisation of colloid dispersions, Academic Press, London (1983).

44 E.W. Fischer., Kolloid-Z., **160**, 120, (1958).

45 R.H. Ottewill, T. Walker., Kolloid Z., **227**, 108 (1968).

46 P.J. Flory, W.R. Krigbaum., J. Chem. Phys., **18**, 1086, (1950).

47 D.H. Napper., Trans, Faraday Soc., **64**, 1701, (1968).

48 D.H. Napper., J. Coll. Interface Sci., **29**, 168, (1969).

49 A. Doroszkowski, R. Lambourne., J. Polym. Sci. C, **34**, 253, (1971).

50 A. Doroszkowski, R. Lambourne., J. Coll. Interface Sci., **43**, 97, (1973).

51 P.J. Flory., J. Chem. Phys. **10**, 51, (1942).

52 F.A. Waite., ICI Paints division, unpublished work. (1971).

53 H. Lange., Kolloid Z. **131**, 96, (1962).

54 C. Tanford., The hydrophobic effect, 2nd Ed. Wiley, New York (1990).

55 J. Israelachvili, Surfactants in Solution . K.L. Mittal, P. Bothorel. (Eds.) Pleunum Press, London. 4, 3 (1986).

56 C. Price, E.K.M. Chan, A.L. Hud, R.B. Stubbersfield., Polymer Commn. **27**, 196, (1986).

57 A. Guinier, G. Fournet., Small-angle scattering of X-rays, Wiley, New York (1955)

58 A. Dijkstra, G. Kortleve, C.G. Vonk., Kolloid Z. **210**, 121, (1966).

59 A. Guinier., Ann. Phys. (Paris), 12, 161, (1939).

60 J.T. Koberstein, B. Morra, R.S. Stein., J. Appl. Cryst. **13**, 34, (1980).

61 G. Porod., Kolloid Z. **124**, 83, (1951).

62 G. Porod., Kolloid Z. **125**, 51, (1952).

63 G. Porod., Kolloid Z. **125**, 109, (1952).

64 W. Ruland.,J. Appl. Cryst. **4**, 70, (1971).

65 J. Rathje, W. Ruland., Coll. Polym. Sci. **254**, 358, (1976).

66 C.G. Vonk., J. Appl. Cryst. **6**, 81, (1973)

67 A. Todo, T. Hashimoto, H. Kawai., J. Appl. Cryst. **11**, 558, (1978).

68 R.W. Hendricks, P.W. Schmidt., Acta Phys. Austriaca, **26**, 97, (1967).

69 R.W. Hendricks, P.W. Schmidt., Acta Phys. Austriaca, **37**, 20, (1973).

70 R. Bonart, E.H. Müller., J. Macromol. Sci. Phys. Ed. **10**, 177, (1974).

71 W.V. Smith, R.H. Ewart., J. Chem. Phys., 16, 592, (1948).

72 D.C. Blackley., "Emulsion polymerisation" Appl. Sci. Pub., London (1975).

73 M. Morton, S. Kaizerman, M.W. Altier., J. Coll. Sci. **9**, 300, (1954).

74 F. Li-In-On, B. Vincent, F.A. Waite., Amer. Chem. Soc. Symp. Ser. **9**, 165, (1975).

75 C. Cowell, F. Li-In-On, B. Vincent., J. Chem. Soc., Faraday Trans. **74**, 337, (1978).

76 B. Vincent, P.F. Luckham, F.A. Waite., J. Colloid Interface Sci. **73**, 508, (1980).

77 W.S. Zimmt., J. Appl. Polym. Sci., **1**, 323, (1959).

78 R.G.W. Norrish, R.R. Smith., Nature **150**, 336, (1942).

79 G.V. Schultz, G. Harborth., Makromol. Chem. **1**, 106, (1947).

80 E. Trommsdorff, H. Köhle, P. Lagally., Makromol. Chem. **1**, 169, (1947).

81 D. Gershberg., A. Inst. Chem. Eng. Symposium series **3** (1965).

82 P.L. Lee, H.M. Longbottom., J. Appl. Polym. Sci.**14**, 1377, (1970).

83 B. Emelie, C. Pichot, J. Guillot., Makromol. Chem., Suppl. **10/11**, 43, (1985)

84 M.W. Thompson, F.A. Waite, British Patent 1096912 (1967)

85 F.A. Waite, J. Oil Col. Chem. Assoc. **54**, 342 (1971)

86 T. Corner, Adv. Polym. Sci. **62**, 95 (1984)

87 J.M. Goldwasser, H.G. Adolph, Polym. Eng. Sci. **26**, 1510 (1986)

88 F.P. Warner, Ph.D. Thesis Loughborough University (1975).

89 C.G. Vonk, Software kindly made available to Loughborough University.

90 W.I. Bengough, H.W. Melville., Proc. Roy. Soc. A **225**, 330, (1954).

91 W.I. Bengough, H.W. Melville., Proc. Roy. Soc. A **230**, 429, (1955).

92 A. Doroszkowski., Personal communication (1991)

93 J.V. Dawkins., J. Macromol. Sci. -Phys. B **2**, 623, (1968).

94 J.V. Dawkins, M.J. Guest, G.M. Jeffs., J. Liq. Chromatogr. **7**, 1739, (1984).

95 N. Schönfeldt., Surface active ethylene oxide aducts. Pergamon Press, London (1969).

96 J. Brandrup, E.H. Immergut. (Eds.), Polymer Handbook 3rd Ed. Wiley, New York. (1989).

97 G. Broadbent, D.S. Brown, J.V. Dawkins., Polymer Comm. **28**, 282, (1987).

98 R.J. Roe., J. Appl. Cryst. **15**, 182, (1982).

99 V. Bianchi, A. Peterlin., J. Polym. Sci., Part A2, 6,, 1759, (1968).

100 P.J. Flory., Statistical mechanics of chain molecules, Wiley Interscience, New York (1969).

101 P.D. Bartlett, J.D. Cotman Jr., J. Am. Chem. Soc. **71**. 1419, (1949).

102 I.M. Kolthoff, I.K. Miller., J. Am. Chem. Soc. **73**, 3055, (1951).

103 P.M. Hay, J.C. Light, L. Maker, R.W. Murray, A.T. Santonicola, O.J. Sweeting, J.G. Wepsic., J. Appl. Polym. Sci. **5**, 23, (1961).

104 J.S. Shukla, D.C. Misra., J. Polym. Sci. Polym. Chem. Ed., **11**, 751, (1973).

105 G.S. Misra, U.D.N. Bajpai., J. Macromol. Sci. Chem. Ed., **13**, 1135, (1979).

106 G.S. Misra, J.J. Rebello., Makromol. Chem., **176**, 2203, (1975).

107 G.S. Misra, J.S. Shukla, H. Narin., Makromol. Chem., **119**, 74, (1968).

108 V.G. Höfle, W. Steglich, H. Vorbrüggen., Angew. Chem. 90, 602, (1978).

109 J.R. Ebdon., "New methods of polymer synthesis", Blackie, Glasgow (1991).